AD-A154 827 VIBRATIONALLY ENHANCED DISSOCIATION OF DIATOMIC MOLECULES(U) CHEMICAL DYNAMICS CORP COLUMBUS OH B C GARRETT ET AL. MAY 85 CDTR-85-1 AFWAL-TR-85-2020 1/3

UNCLASSIFIED F33615-82-C-2241 F/G 7/4 NL

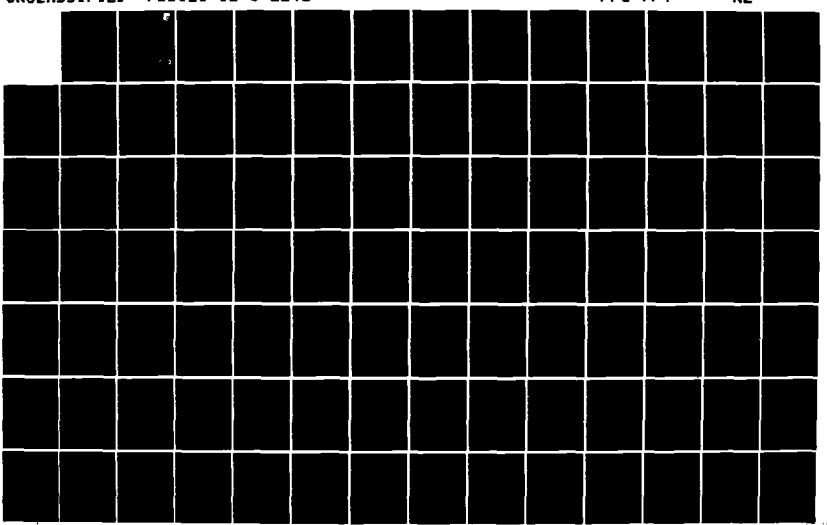

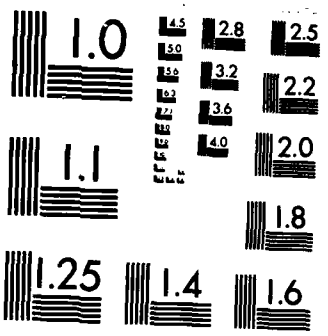

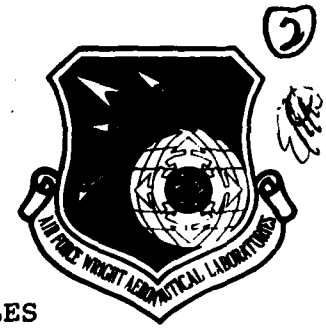

AFWAL-TR-85-2020

VIBRATIONALLY ENHANCED DISSOCIATION OF DIATOMIC MOLECULES

Bruce C. Garrett
Lynn T. Redmon
Michael J. Redmon

CHEMICAL DYNAMICS CORPORATION
1550 WEST HENDERSON ROAD
COLUMBUS, OHIO 43220

MAY 1985

FINAL REPORT FOR PERIOD SEPTEMBER 1982 - SEPTEMBER 1984

APPROVED FOR PUBLIC RELEASE; DISTRIBUTION UNLIMITED.

AERO PROPULSION LABORATORY
AIR FORCE WRIGHT AERONAUTICAL LABORATORIES
AIR FORCE SYSTEMS COMMAND
WRIGHT-PATTERSON AIR FORCE BASE, OHIO 45433

NOTICE

When Government drawings, specifications, or other data are used for any purpose other than in connection with a definitely related Government procurement operation, the United States Government thereby incurs no responsibility nor any obligation whatsoever; and the fact that the government may have formulated, furnished, or in any way supplied the said drawings, specifications, or other data, is not to be regarded by implication or otherwise as in any manner licensing the holder or any other person or corporation, or conveying any rights or permission to manufacture use, or sell any patented invention that may in any way be related thereto.

This report has been reviewed by the Office of Public Affairs (ASD/PA) and is releasable to the National Technical Information Service (NTIS). At NTIS, it will be available to the general public, including foreign nations.

This technical report has been reviewed and is approved for publication.

LT PETER HAALAND
Project Scientist

ROBERT L. KERR, Chief
Energy Conversion Branch
Aerospace Power Division
Aero Propulsion Laboratory

FOR THE COMMANDER

JAMES D. REAMS, Chief
Aerospace Power Division
Aero Propulsion Laboratory

"If your address has changed, if you wish to be removed from our mailing list, or if the addressee is no longer employed by your organization please notify AFWAL/POOC, *W-PAFB, OH 45433 to help us maintain a current mailing list".*

Copies of this report should not be returned unless return is required by security considerations, contractual obligations, or notice on a specific document.

UNCLASSIFIED

SECURITY CLASSIFICATION OF THIS PAGE (When Data Entered)

REPORT DOCUMENTATION PAGE		READ INSTRUCTIONS BEFORE COMPLETING FORM
1. REPORT NUMBER AFWAL-TR-85-2020	2. GOVT ACCESSION NO.	3. RECIPIENT'S CATALOG NUMBER
4. TITLE (and Subtitle) VIBRATIONALLY ENHANCED DISSOCIATION OF DIATOMIC MOLECULES		5. TYPE OF REPORT & PERIOD COVERED Final 20 Sept 82 - 19 Sept 84 6. PERFORMING ORG. REPORT NUMBER CDTR-85-1
7. AUTHOR(s) Bruce C. Garrett Lynn T. Redmon Michael J. Redmon		8. CONTRACT OR GRANT NUMBER(s) F33615-82-C-2241
9. PERFORMING ORGANIZATION NAME AND ADDRESS Chemical Dynamics Corporation 1550 West Henderson Road Columbus, Ohio 43220		10. PROGRAM ELEMENT, PROJECT, TASK AREA & WORK UNIT NUMBERS P.E. 61102F 2301 52 92
11. CONTROLLING OFFICE NAME AND ADDRESS Aero Propulsion Laboratory, (AFWAL/POOC-3) Air Force Wright Aeronautical Laboratories Wright Patterson AFB, Ohio 45433		12. REPORT DATE May 1935 13. NUMBER OF PAGES 187
14. MONITORING AGENCY NAME & ADDRESS(if different from Controlling Office)		15. SECURITY CLASS. (of this report) Unclassified 15a. DECLASSIFICATION/DOWNGRADING SCHEDULE

16. DISTRIBUTION STATEMENT (of this Report)

Approved for public release; distribution unlimited.

17. DISTRIBUTION STATEMENT (of the abstract entered in Block 20, if different from Report)

18. SUPPLEMENTARY NOTES

Accession For	
NTIS GRA&I	X
DTIC TAB	☐
Unannounced	☐
Justification	
By	
Distribution/	
Availability Codes	
Dist	Avail and/or Special
A/1	

19. KEY WORDS (Continue on reverse side if necessary and identify by block number)

Cross sections, excited states, excitations, electron impact, dissociation, vibrational enhancement, rotational enhancement, impact parameter method.

20. ABSTRACT (Continue on reverse side if necessary and identify by block number)

The impact parameter method for electron impact excitation of diatomic molecules has been extended to treat dissociation and to include the effects of vibrational and rotational excitation. The method was found to agree well with previous theoretical calculations of excitation and dissociation cross sections for H_2. The agreement with experimental cross sections is poorer but consistant with our understanding of the processes. The

DD FORM 1 JAN 73 1473 EDITION OF 1 NOV 65 IS OBSOLETE

UNCLASSIFIED

SECURITY CLASSIFICATION OF THIS PAGE (When Data Entered)

20. ABSTRACT Cont.

method has been applied to electron impact excitation and dissociation of O_2^{π}, S_2^{π}, HCℓ, and HgBr through optically allowed transitions. Vibrational excitation of the molecule can significantly affect the cross sections for these processes, either increasing or decreasing the cross sections by as much as 2 orders of magnitude, whereas, rotational excitation has a much smaller effect on the cross sections.

FOREWORD

This technical report describes research performed under Project 2301, "Vibrationally Enhanced Dissociation of Diatomic Molecules", by Chemical Dynamics Corporation, during the period 20 September 1982 to 19 September 1984. The authors acknowledge helpful discussions with project monitors Capt. Greg Schneider and Lt. Peter Haaland, and Dr. Alan Garscadden of the Air Force Wright Aeronautical Laboratories, and Dr. C. William McCurdy of Ohio State University.

TABLE OF CONTENTS

LIST OF ILLUSTRATIONS

LIST OF TABLES

SECTION I

INTRODUCTION

The major goal of the research described in this report is the calculation of electron-impact dissociation cross sections for vibrationally and rotationally excited diatomic molecules. Dissociation by electron impact to form neutral species is an important process in gas-phase electric discharges and can significantly affect the efficiency of laser plasmas. Although large populations of rotationally and vibrationally excited species exist in plasmas, little is known either experimentally or theoretically about the dependence of electron-impact dissociation cross sections upon the initial rovibrational state of the diatomic molecule. The cross sections reported here are important to the basic understanding of the dissociation process as well as for input to modelling studies of gas-phase electric discharges.

The first task was the selection and verification of a theoretical method that was capable of reasonably accurate predictions of cross sections for dissociation by electron impact at relatively low collision energies. Several methods have been previously applied to electron-impact excitation and dissociation, but none of these have studied the effects of changing the initial rotational and vibrational state upon the cross sections. From these methods, the impact parameter method was selected as the one best suited to our needs. We extended it to treat dissociation and to include the effects of vibrational and rotational motion. The method was verified by application to transitions in the H_2 molecule for which experimental results were available for comparison.

The impact parameter method was then applied to transitions in the O_2, S_2, HCl, and HgBr molecules for electron translational energies in the range from threshold to 25 eV. First, a survey was made of the dependence of the

cross sections on initial vibrational state. For these studies the rotational degrees of freedom were treated as being degenerate. Cross sections were computed for initial vibrational states $v_i = 0$, 1, and 2 for O_2 and HCl and for $v_i = 0$ to 4 for S_2 and HgBr. Then a survey was made of the dependence of the cross sections on initial rotational state for various initial vibrational states. Cross sections were computed for a distribution of initial rotational states characterized by temperatures of 0, 300, 400, 600, and 1000 K.

The results of the calculations are summarized in Section II. This section also provides a summary of the general trends observed in our studies and assesses the general applicability of the calculations. The Appendices contains manuscripts prepared for publication, which give more detailed descriptions of the methods employed, the calculations, and the results. Appendix A describes the impact parameter method, our extensions to it, and the application of the method to electronic transitions in the H_2 molecule. Appendix B describes the electronic structure calculations for O_2 and S_2, and Appendix C presents the dynamical calculations on these molecules. Appendix D provides a test of some of the methods by comparing our calculation of oscillator strengths with experimental ones for the well-studied Schumann-Runge transition in O_2. Appendix E and F present our calculations on the HCl and HgBr molecules, respectively. Finally, flowcharts of the computer programs developed for the impact parameter method are provided.

SECTION II

SUMMARY OF WORK PERFORMED

1. The Impact Parameter Method

The impact parameter (IP) method for diatomic molecules as originally formulated by Hazi is extended to treat dissociation and to include the effects of vibrational and rotational excitation. In its extended form, the expression for the state-to-state cross section retains the simple form obtained by Hazi; the cross section is the product of a structural factor S_{if}, which depends upon the electronic properties of the diatomic molecules, and a dynamical factor $D_{if}(E)$, which depends upon the translational energy E of the incident electron and the transition energy E. This expression has a form similar to that for the photodissociation cross section except that the dynamical factor replaces the factor depending on the frequency of the radiation and the symmetry dependence in the structural factor is different. In both cases the structural factor is proportional to the absolute oscillator strength, which can be obtained directly from spectroscopic data or from calculations based upon potential energy curves and the transition dipole moment. The dynamical factor is easily evaluated in terms of modified Struve and Bessel functions.

In the IP method, nuclear motion is treated within the adiabatic approximation and the motion of the incident electron is treated as a straight-line classical trajectory. The probability of an electronic transition for a fixed nuclear geometry and initial impact parameter is given by time-dependent perturbation theory, where the molecular electrons are perturbed by the incident electron. In this method only the repulsive interactions

treated; exchange interactions are neglected. The coulomb repulsion term expanded in a multipole series and approximated by its asymptotic form. s assumes that the major contributions to the cross section come from large act parameters. Cross sections are obtained by averaging the probabilities r molecular orientations, nuclear separation, and initial impact parameters. onzero value b_0 is used as the lower limit in the integration over impact ameter to avoid divergence of the cross section. The minimum impact ameter is fitted so that the IP cross sections match those of the Born roximation at very high translational energies.

Thus the IP method is a semiempirical theory designed to have the correct h energy behavior. Hazi and coworkers have shown that it also gives a ter prediction of cross sections at low energies than plane-wave methods h as the Born approximation. Because of the neglect of electronic exchange ween the incident and molecular electrons, the IP method is limited to dies of electronic transitions which are optically allowed and it becomes s accurate at threshold energies.

In principle, the IP cross sections can be evaluated using experimental a to obtain the structural factor. However, in most of the cases that studied, this data is incomplete and does not include information about ational-state dependence. Therefore, all of our structural factors are culated from potential energy curves and dipole transition moment curves. best available potential data are used: RKR (Rydberg-Klein-Rees) points n available, otherwise the most accurate ab initio points. The transition ole moments are taken from ab initio calculations since they are hard to ract from experimental data. As a check on the accuracy of this input a, we compare our computed oscillator strengths with experimental ones n they are available.

le I. Test of the Treatment of Small Impact Parameters in the IP Method.

ystem	$b_0(a_0)$	$\tilde{b}_0(a_0)$	E_{tr}(eV)	$P(b_0,E)$	$P(\tilde{b}_0,E)$	$\frac{\tilde{\sigma}^{IP}}{\sigma^{IP}}$	$\frac{\Delta\sigma^{IP}_{b_0}}{\tilde{\sigma}^{IP}} \times 100\%$
X→B)	1.74	3.20	10	0.14	0.024	0.78	43
			20	0.23	0.039	0.73	52
			50	0.12	0.029	0.87	40
X→Π)	0.466	0.353	12	0.020	0.052	1.82	30
			20	0.016	0.051	1.50	21
			50	0.006	0.027	1.34	16
X→E)	0.261	0.534	12	2.05	0.37	0.81	33
			20	1.32	0.31	0.90	26
			50	0.52	0.13	0.92	19
X→B)	1.84	3.44	10	0.56	0.104	0.77	48
			20	0.32	0.078	0.87	39
			50	0.13	0.036	0.92	29
X→Π)	4.3(-16)	5.2(-16)	10	3(28)	2(28)	0.99	0
			20	1(28)	1(28)	1.00	0
			50	6(27)	4(27)	1.00	0
$X\rightarrow 2^3\Sigma_u^-$)	4.58	6.99	10	0.004	0.001	0.90	51
			20	0.007	0.001	0.77	63
			50	0.006	0.002	0.96	53
ι(X→A)	2.74	4.98	8	0.025	0.003	0.61	52
			20	0.019	0.004	0.81	48
			50	0.009	0.002	0.90	37
3r(X→A)	1.79	3.47	8	0.03	0.006	0.79	44
			20	0.014	0.004	0.89	33
			50	0.006	0.002	0.92	25

$$\tilde{\sigma}^{IP}_{b_0} = \pi \tilde{b}_0^2 \, P(\tilde{b}_0, E) \tag{4}$$

the $\tilde{b}_0$ is adjusted to make $\tilde{\sigma}^{IP}(E)$ agree with the BA cross section at high energies. A measure of the importance of the region between b = 0 and $\tilde{b}_0$ is then given by the ratio of $\tilde{\sigma}^{IP}_{b_0}$ to $\tilde{\sigma}^{IP}$ and the ratio between $\tilde{\sigma}^{IP}_{b_0}$ and σ^{IP} gives an estimate of the error in $\sigma^{IP}(E)$ from the method of treating low impact parameters. In Table I we present these two ratios at three energies for several of the electronic transitions considered in this report. Also included in the table are the two minimum impact parameters b_0 and $\tilde{b}_0$ and the values of the opacity functions at these values of the impact parameter. The largest difference between σ^{IP} and $\tilde{\sigma}^{IP}_{b_0}$ is for the X to Π transition in O_2, but they differ by only 80%. The contribution to $\tilde{\sigma}^{IP}$ from low impact parameters is typically between 20% and 60%, the lower values associated with small $\tilde{b}_0$'s . The first-order perturbation approximation is most valid when the opacity functions are much less than one. Thus the IP method should be better justified for systems in which $P(\tilde{b}_0, E)$ is small such as the X to Π transition in O_2, the X to $2^3\Sigma_u^-$ transition in S_2, the X to A transition in HCl, and the X to A transition in HgBr. The X to Π transition in S_2 is clearly a case where the approximations break down.

The energetic threshold energy for dissociation (the lowest energy at which dissociation is allowed) can be accurately computed to within 0.01 to 0.1 eV for all but the HgBr system using known spectroscopic data. The dynamical threshold energy is defined in this work as the lowest energy at which the cross section becomes 0.01 times its maximum value. The dynamical threshold is determined mostly by the lowest transition energy at which the overlap between the initial and final nuclear wavefunctions becomes appreciable.

unction is interpreted as the probability of electronic excitation for a ranslational energy E and impact parameter b. The integral cross section s related to the opacity function by

$$\sigma(E) = 2\pi \int_0^\infty db\ b\ P(b,E) \tag{1}$$

nd the opacity function is bounded by one. However, in the IP method P(b,E) iverges for small b. To avoid divergence of the integral cross section, n the p·esent work the lower limit of integration in equation (1) is replaced y b_0

$$\sigma^{IP}(E) = 2\pi \int_{b_0}^\infty db\ b\ P^{IP}(b,E) \tag{2}$$

Contributions to σ(E) are excluded from regions where the approximations of the theory break down and where exchange effects become important. b_0 is chosen so that the cross section from the IP method is the same as that from the BA method at very high energy. To test the effects of this method for selecting b_0 and to estimate the possible contribution to $\sigma^{IP}(E)$ from b =) to b_0 an alternative treatment of the low b region is tested. Instead of using equation (2) which assumes the contributions to (E) from b between 0 and b_0 are negligible, the probability is assumed to be constant for this range of impact parameters and the cross section is approximated by

$$\tilde{\sigma}^{IP}(E) = \tilde{\sigma}^{IP}_{b_0} + 2\pi \int_{b_0}^\infty db\ b\ P^{IP}(b,E) \tag{3}$$

here

5. Error Estimates

It is difficult to obtain quantitative estimates of the probable errors in the IP method. The method contains several approximations and the validity of each of these approximations is dependent upon the specific electronic transition being studied. To help understand the order of magnitude of the errors expected we compare the IP method with the Born approximation for which the limitations are better understood.

Both methods separate nuclear and electronic motion by the Born-Oppenheimer (fixed-nuclei) approximation and this approximation is very well justified. Both are first-order perturbation treatments and, therefore, assume that probabilities for electronic excitation for fixed impact parameter (or orbital angular momentum) are much less than unity. Furthermore, both methods only treat the perturbation potential as a coulombic repulsion term and neglect the electron exchange interaction. As pointed out by Inokuti[1] these approximations are valid when the translational energy of the incident electron is much larger than the orbital energies of the molecular electrons. Approximating the orbital energies by the lowest ionization potential for the diatomic molecules studied here, the translational energy must be much greater than from 9 to 13 eV. Although this condition is not met for energies below 100-1000 eV, the BA and IP methods can predict accurate integral cross sections to much lower energies. Typically BA cross sections are factors of 2 to 5 times too large in the medium energy range below 50 eV.[2]

The limit at which the above validity criterion is met can also be reached by increasing the orbital angular momentum (ℓ) or the impact parameter (b). Thus at large ℓ or b, the BA and IP expressions for the opacity function P(b,E) and for the large-angle differential cross section become valid. The opacity

section is seen as the rotational temperature is raised from 0 to finite temperatures. This is a symmetry effect resulting from the lack of a j = 0 state for electronic states.

The impact parameter method as described in this report is applicable to any optically allowed transition in diatomic molecules. The applications presented here have been to dipole allowed transitions, but the methods can be extended to treat higher multipole transitions.

4. General Trends

The cross sections are most strongly influenced by the overlap of the initial vibrational wavefunction with the final wavefunction for nuclear motion and the magnitude of the transition dipole moment. Transitions with poor Franck-Condon overlaps for $v_i = 0$ will generally have a large enhancement with increasing v_i whereas transitions with large Franck-Condon overlaps for $v_i = 0$ will generally have little dependence upon v_i or will decrease with increasing v_i.

In general, the effect of changing initial rotational states is much smaller than the effect of increasing the vibrational state. Within the IP method, only transitions in which the rotational quantum number j changes by ±1 are allowed. Therefore, increasing j_i does not change the transition energy appreciably and the threshold energy for excitation changes only slightly. The main effect of increasing j_i is to increase the effective potential by the centrifugal term $j(j+1)/2\mu R^2$. The increase in the potential is large for smaller R, so the potential well and the vibrational wavefunction for a given level v_i are shifted to large internuclear distances and changed in shape slightly. However, changing j_i is a small perturbation on the wavefunction compared to changing v_i.

The two exceptions to this behavior that we observed were for the X-E transition in O_2, the X-$2^3\Sigma_u^-$ transition in S_2, and X-Π transitions in general. For small j_i the X-E excitation of O_2 is predominately to quasibound states of the local well; however, as j_i (and thereby j_f) are increased the local well in the E-state potential becomes more shallow. Eventually it disappears whereupon the excitation becomes dissociative. Thus the dissociative cross sections are enhanced by a factor of 2 as the rotational temperature is raised from 0 to 300 K. For X-Π transitions a factor of 2 decrease in the cross

The X-to-A dissociation cross sections have an interesting dependence upon rotational temperature T_{rot}. Upon increasing T_{rot} from 0 to 300 K the cross sections decrease by about a factor of 2. Increasing T_{rot} to 1000 K decreases the cross sections further, but by less than 10%. This behavior was also observed in calculations for $v = 0$, 1, and 2.

D. HgBr

The $A^2\Pi$, $B^2\Sigma^+$, and $C^2\Pi$ states of HgBr are the three lowest excited electronic states which have optically allowed transitions to the $X^2\Sigma^+$ electronic state. The main route for electron-impact dissociation of the X state is through the A state; for all v_i considered the contributions to the dissociation cross section from the B and C states are less than 10^{-24} cm^2. The X-to-A dissociation cross sections have very little dependence upon the initial vibrational state v_i. Therefore, the overall dissociation cross sections will not be vibrationally enhanced.

The X-to-A dissociation cross sections have the same rotational-temperature dependence as the X-to-A transition in HCl. As T_{rot} is increased from 0 to 300 K the cross sections decrease by about a factor of 2, and as T_{rot} is increased to 1000 K the cross sections decrease further, but by less than 1%. We also observe this behavior for $v = 3$ and 4. Thus we see a negligible dependence of the dissociation cross section on temperature for this system.

with rotational temperature, particularly for $\nu_i>0$. The X-B dissociation cross section for $\nu_i = 0$ decreases by 25% as the rotational temperature is increased from 0 K to 1000 K. For $\nu_i = 1$ the cross section increases by 5% over this temperature range, while for $\nu_i = 2$ and $\nu_i = 3$ the increase is 11%. For $\nu_i = 4$ the increase is 8%. The X-Π cross section has a negligible temperature dependence regardless of initial vibrational state.

The X-$2^3\Sigma_u^-$ cross section for $\nu_i = 0$ increases by a factor of 1.6 from 0 K to 300 K, with negligible change for further increase in temperature. For $\nu_i = 3$ the 0 K to 300 K change is a factor of 4, with the cross section then showing a decrease of 15% by 1000 K. For $\nu_i = 4$, the 0 K to 300 K increase is by a factor of 8, with a subsequent decrease by 26% as the temperature is raised to 1000 K.

C. HCl

The main route for electron-impact dissociation of the $X^1\Sigma^+$ state of HCl is through the $A^1\Pi$ state. The A state is the lowest state accessible by an optical transition from the ground electronic state. The next two states allowed are the $2^1\Sigma^+$ and $C^1\Pi$ states. Each has a broad well so that the energy at the ground-state equilibrium geometry is below the respective dissociation limits. Therefore, excitation to bound levels will be preferred over dissociation. Furthermore, since these dissociation limits are both approximately 15 eV above the X-state minimum, the threshold for dissociative excitation through these states will be much higher than that of the A state.

The X-to-A dissociation cross sections are slightly enhanced near threshold and for energies above 10 eV with increasing ν_i. From 12 to 20 eV the $\nu_i = 1$ cross sections are about 15% larger than those for $\nu_i = 0$, and the $\nu_i = 2$ cross sections are about 10% higher than those for $\nu_i = 1$.

B. S_2

S_2 is isoelectronic with O_2 so the three analogous excited electronic states were considered for this system: $B^3\Sigma_u^-$, $B'^3\Pi_u$, and $2^3\Sigma_u^-$. The avoided crossings seen in the O_2 system are not present here except for the $2^3\Sigma_u^-$ state, which has a local minimum in its potential energy curve. Cross sections for dissociation of the $X^3\Sigma_g^-$ electronic state through the B state are 2 to 4 orders of magnitude smaller than those for transitions to bound vibrational states. Increasing the initial vibrational level greatly enhances the cross sections for dissociation but has little effect upon the bound-state cross sections. For example, at 20 eV, changing ν_i from 0 to 1 decreases the bound-state cross section by only a few percent and increases the dissociative cross section by a factor of 14.7. Increasing ν_i up to 4 increases the dissociation cross section by three orders of magnitude relative to $\nu_i = 0$.

The Π state is repulsive, and for $\nu_i = 0$ the X-to-Π transition is the dominant route for dissociation. This cross section reaches a peak of 4.6×10^{-17} cm^2 at an energy of 6.5 eV and falls off rapidly to a value of 2×10^{-17} cm^2 at 20 eV. The cross sections are enhanced slightly upon increasing ν_i; at 6.5 eV the increase is only 25% in going from $\nu_i = 0$ to 4.

The contributions to the dissociative cross section from the X-to-$2^3\Sigma_u^-$ transition are harder to assess because of the existance of predissociating quasibound states in the local well of the $2^3\Sigma_u^-$ state. Although the dissociation cross sections for this transition show a large enhancement with increasing ν_i (over 4 orders of magnitude from $\nu_i = 0$ to 4), it will still be less than about 3×10^{-19} cm^2 for $\nu_i = 4$.

The dependence of the dissociation cross section on rotational temperature for S_2 is similar to O_2 in that the X-B and X-Π transitions show little effect, regardless of ν_i, while the $2^3\Sigma_u^-$ cross section shows a significant increase

for v_i = 0 or 1, but it should provide between 20 to 30% of the dissociative cross section for v_i = 2 for energies above about 12 eV. For v_i = 0 and 1 the total dissociative cross section rises from a threshold near 7 eV to about 8×10^{-17} cm^2 at 20 eV, and for v_i = 2 it rises to maximum of almost 11×10^{-17} cm^2 at 20 eV.

No appreciable change is predicted for the X-to-B dissociation cross section for v_i = 0, 1, or 2 as the rotational temperature is increased from 0 to 1000 K. The largest changes (about +6%) occur for near-threshold energies, and at 20 eV the changes are less than 1%. The X-to-B bound-state cross sections decrease as the rotational temperature is increased; typically by 7-8% as T_{rot} is increased from 0 to 300 K and by 25% as it is increased from 0 to 1000 K.

For the X-Π transition the threshold v_i = 0 cross section increases by 4% from 0 K to 300 K, with no further change to 1000 K. For v_i = 1, the cross section decreases by 4% between 0 K and 300 K, and decreases an additional 2% by 1000 K. At higher energies the decrease between 0 K and 300 K is 7%, with an additional 2% decrease by 1000 K. Thus the cross section for this transition is not very sensitive to rotational temperature.

The X-to-E dissociation cross sections show the largest change as the rotational temperature is increased. At energies near threshold the v_i = 0 cross section increases by factors of 2 and 2.1 upon increasing the temperature from 0 to 300 K, and from 300 K to 1000 K, respectively. At higher energies the increases are factors of 1.65 and 1.75 for the same changes in temperature. The v_i = 1 threshold cross section decreases by 0.8 in going from 0 K to 300 K, with no further change observed in increasing the temperature to 1000 K. At higher energies the behavior is similar, except that the factor reduces to 0.6. For v_i = 2, the threshold cross section increases by 1.3 between 0 K and 300 K, with no further change in going to higher temperature.

3. Dynamical Calculations

A. O_2

Three excited electronic states were considered for this system: $B^3\Sigma_u^-$, $1^3\Pi_u$, and $E^3\Sigma_u^-$. The presence of a (diabatic) Rydberg state of the same symmetry causes the potential curves for each of these states to have shoulders or local minima resulting from one or more avoided crossings near the equilibrium geometry of the ground electronic state. Avoided crossings also cause rapid changes in the transition dipole moment and affect the shapes of the excitation and dissociation cross sections curves as a function of translational energy.

Cross sections for dissociative transitions from the ground electronic state $X^3\Sigma_g^-$ through the B state are 2 to 4 orders of magnitude larger than those for transitions to bound vibrational levels of the B state. Increasing the initial vibrational level greatly enhances the cross sections for excitation to bound states but has little effect upon the dissociative cross sections. For example, at 20 eV, changing v_i from 0 to 1 increases the bound-state cross section by a factor of 10.1 and increasing v_i from 1 to 2 increases it by a factor of 4.2. At the same energy the dissociative cross section decreases by only 19% upon increasing v_i from 0 to 2.

The Π state is mostly repulsive, and the dissociative cross sections for the X-to-Π transition are 50 to 70 times smaller than the dissociation cross sections for X-to-B transitions. The X-to-Π cross sections show only a moderate enhancement with increasing v_i.

The contributions to the dissociative cross section from the X-to-E transition are harder to assess because of the existence of predissociating quasibound states in the local well of the E state. Our estimate is that the E state will not contribute significantly to the total dissociative cross section

be higher, but the various states can be treated equally since the orbitals can be optimized for each state. Because they are optimized especially for the configuration space used, the potential energy curves are smoother and probably more accurate.

2. Ab Initio Electronic Structure Calculations

Ab initio electronic structure calculations are performed to provide input for the impact parameter calculations. Although RKR potential data are available for many of the s ates of interest, they do not provide global descriptions of the curves. In particular, the repulsive parts of the potentials, which are critical for calculations of dissociative cross sections, must be obtained from *ab initio* calculations. Although the transition dipole moment for the equilibrium geometry can be estimated from spectroscopic data by using the Franck-Condon approximation, accurate calculations of oscillator strengths and electron-impact cross sections require the transition dipole moment as a function of R. Therefore, it must be obtained from *ab initio* calculations. Finally, the electronic wavefunctions and transition dipole density matrix are required as input to the Born calculations used in determining b_0. These are also provided by *ab initio* calculations.

We have used the most accurate *ab initio* data available. Some data has been taken from the literature to augment or replace our own calculations. The method we have employed is the multiconfigurational self-consistent field (MCSCF) method. It is well suited for the description of ground and excited states of diatomic molecules. MCSCF is a state-of-the-art method "beyond" Hartree-Fock; i.e., it treats electron correlation. The method not only optimizes the eigenvectors (i.e., the configuration coefficients) as does the configuration interaction (CI) method, it also optimizes the orbitals from which the configurations are constructed. Thus for a given basis set and configuration space, it provides the optimum result. Although, for a given effort in computer time, the configuration space of an MCSCF calculation is usually smaller than that of a CI calculation, we expect to obtain potential energy curves of a higher quality. The total energies obtained will generally

To assess the accuracy of the computed cross sections, we compare our results with experimental and other theoretical cross sections for the $X^1\Sigma_g^+$-to-$B^1\Sigma_u^+$ and X-to-$B'^1\Sigma_u^+$ transitions in H_2. Cross sections for transitions to bound vibrational states are calculated in addition to those for dissociative transitions. The experimental and previous theoretical results do not include treatment of vibrational and rotational effects. Therefore, we compare cross sections in which the rotational degrees of freedom are treated as degenerate and excitation is from the ground vibrational state. In general the agreement of our cross sections with those from previous theoretical calculations is very good.

The experimental cross sections for the X-to-B transition to bound states are smaller than the theoretical ones by about a factor of 2. Most of this discrepancy can be attributed to problems with resolving the measured signal at small scattering angles.

The theoretical cross sections for direct dissociation to produce H(2s) via the X-to-B' transition are smaller than the experimental cross sections by factors of 3 to 4. However, the experiment measures the total H(2s) formed; it can not distinguish products of direct dissociation through the B' state from products of excitation through other electronic states or indirect processes, such as cascading from higher electronic states. The agreement of the IP method with other theoretical methods is very encouraging, and the comparisions with experiment are consistent with our understanding of the processes.

Table 2. Threshold Energies (in eV) Predicted by the IP Method.

System	v_i	Energetic Threshold	Dynamic Threshold
$O_2(X \rightarrow B)$	0	7.083	7.3-7.4
	1	6.890	6.9-7.0
	2	6.700	6.8-6.9
$O_2(X \rightarrow PI)$	0	5.116	9.4-9.5
	1	4.923	8.7-8.8
	2	4.733	8.0-8.1
$O_2(X \rightarrow E)$	0	7.083	11.4-11.5
	1	6.890	11.2-11.3
	2	6.700	11.0-11.1
$S_2(X \rightarrow B)$	0	5.567	<5.6
	1	5.476	<5.6
	2	5.386	<5.4
	3	5.300	<5.4
	4	5.212	<5.4
$S_2(X \rightarrow PI)$	0	4.421	~5.6
	1	4.330	5.4-5.5
	2	4.240	5.2-5.3
	3	4.153	5.0-5.1
	4	4.066	4.9-5.0
$S_2(X \rightarrow 2^3\Sigma_u^-)$	0	5.567	8.0-8.1
	1	5.476	7.9-8.0
	2	5.386	7.8-7.9
	3	5.300	7.7-7.8
	4	5.212	7.6-7.7
$HC\ell(X \rightarrow A)$	0	4.279	7.0-7.1
	1	3.921	6.2-6.3
	2	3.576	5.4-5.5
$HgBr(X \rightarrow A)$	0	0.468	1.1-1.2
	1	0.450	1.0-1.1
	2	0.432	1.0-1.1
	3	0.414	0.8-0.9
	4	0.396	0.8-0.9

This depends strongly upon the initial and final state potential energy curves and the transition dipole moment between the two states but only weakly upon the interaction of the incident electron with the target molecule. The dynamical threshold energies are probably accurate to within 0.1-0.5 eV for all but the HgBr system. The energetic and dynamical threshold energies are shown in Table 2. The dynamical threshold will be most accurate for systems in which the energetic and dynamical thresholds are close, such as the X to B transition in O_2 and S_2. The behavior of the IP and BA cross sections for energies very near threshold is not accurate for electronic transitions. These cross sections can be in error by an order of magnitude or more because the approximations in the theories break down, exchange interactions become more important, and important resonance effects are neglected.

Although the absolute magnitudes of the integral cross sections may be in error by as much as an order of magnitude for the lowest energies, predictions of the dependence of the cross sections upon initial vibrational and rotational states should be reliable. The change in cross sections as a function of the initial vibrational and rotational state is controlled by the change in overlap between the initial and final wavefunctions for nuclear motion. Thus it is the structural factor determined by the potential energy curves and dipole transition matrix elements which determines the vibrational and rotational dependence of the cross sections and not the dynamics of the interaction between the incident electron and the target molecule. Also the change in the dynamical threshold energies with initial vibrational state should be accurate to within 0.1-0.5 eV.

More accurate dynamical methods are required to obtain accurate absolute cross sections near threshold. The first-order perturbation treatment of the collision actually becomes valid at very low translational energies for nonzero impact parameters. To see this consider the effective potential felt

by the incident electron at long range. This potential is the sum of the (positive) centrifugal term and a multipole expansion whose leading term is a (negative) quadrupole. The potential is negative at small distances then increases to a maximum. The value of the potential at the maximum and the distance increase with increasing impact parameter. If the electron energy is small enough the centrifugal barrier will prohibit the electron from penetrating to close distances and the first order perturbation approximation to the interaction will be valid. For electronic excitations this criterion can only be met in the exit channel and this approach will not be useful. However, the BA or IP methods could be used to accurately predict the threshold behavior of the cross sections for rotational and vibrational excitation cross sections which are dominated by scattering at nonzero impact parameter.

The only methods capable of predicting accurate cross sections at threshold energies are those based upon an accurate quantum mechanical treatment of the scattering system. These include close-coupling calculations and the distorted wave Born method which is very similar to a two-state close-coupling calculation. The major limitation in the distorted wave method is the improper treatment of resonance behavior which is very important at low energies. The limitations in the close-coupling calculations are associated with numerical difficulties in the calculations. The major difficulties are the accurate inclusion of exchange interactions, the related difficulty of including electron-capture states in the expansion of the total wavefunction, and the convergence of the cross sections with respect to the number of channels. Local approximations to the electron exchange terms have been developed and have been shown to be extremely easy to use and also very accurate for energies above 10 to 20 eV. These methods have not been adequately tested for low energies but may be accurate to within about a factor of two in the cross section for threshold energies. This could be easily tested for some atomic

cases for which accurate quantum scattering calculations have been performed down to very low energies. Once a local approximation to the exchange is included, electron-capture states can be routinely added to the basis without further complications and resonance features can be accurately described. Cross sections are known to converge slowly with increasing basis set size. Rather than using large basis sets, accurate calculations can be obtained using small basis sets in which the electronic wavefunctions for the target molecule are allowed to distort as the incident electron approaches. These polarization effects have been effectively included in calculations of elastic, and vibrationally and rotationally inelastic cross sections, but have not been used in calculations of electronic excitations.

In summary, the IP cross sections for electron-impact dissociation for energies a few eV above threshold are probably accurate to within factors of 2 to 5 for most of the transitions studied here. The major exception is the X-to-Π transition in S_2 which may be in error by an order of magnitude or more. The cross sections are qualitative at best for energies near threshold. For these energies resonances can drastically alter the shape of cross sections and they are not included in the IP method. The effect of increasing the initial vibrational state should be well predicted and the threshold energies and their dependence upon initial vibrational state should be accurate to within 0.1 to 0.5 eV.

6. Comparison with Other Dissociation Processes

A. H_2

Dissociative attachment (DA) is the predominant dissociation mechanism in H_2 below 5 eV. The process is understood to involve resonant excitation of low lying electronic states of H_2^-, which subsequently dissociate into H and H^-. A strong dependence of the cross section on molecular vibration has been theoretically predicted[3] and experimentally verified[4,5]. Theoretical prediction of a large rotational enhancement[6] was not observed in experiments[7].

The DA process has also been studied experimentally in both H_2 and D_2 by Allan and Wong[8], who investigated with refined techniques the effect of both molecular vibrational and rotational energy on the dissociation cross section. They concluded that there is a strong vibrational effect in which the threshold cross section increases by four orders of magnitude for vibrational excitation from $v = 0$ to $v = 4$. They determined that the rotational energy dependence is much smaller, and is described well by the resonance model calculations of Wadehra and Bardsley[9-11]. The cross section increases by approximately a factor of five from $j = 0$ to $j = 7$. Thus as a function of total internal energy, initial vibration is much more effective than rotation in increasing the efficiency of dissociation by this mechanism. However, a more detailed analysis[11] indicates that it is the total amount of available internal energy that determines the dissociation rate, and that rotational energy is efficient provided the molecules are sufficiently rotationally hot.

The resonance dominated dissociative attachment process, important below 5 eV, rapidly diminishes above that energy to values below 10^{-21} cm^2. Above 15 eV, a major channel is direct dissociation to neutral species. This process is the thrust of the research discussed in this report. As for DA, the direct dissoci-

ation process is enhanced by vibrational energy, but to a lesser extent. A factor of four increase in the cross section is found in going from $v = 0$ to $v = 4$. In contrast to DA, there is a negligable effect due to rotational energy. The threshold energies decrease by the vibrational state energy change in going to higher V. Since we are already at fairly high energies (above 20 eV) these increments represent small changes in total energy.

B. O_2

The effect of initial vibrational energy upon the dissociation of O_2 by electron attachment has been studied both experimentally[4,5] and theoretically[12]. In the following figure the DA cross sections are shown for thermal distributions of vibrational states at 300 and 1400 K. The cross sections shown are those calculated by O'Malley, which agree very well with experiment. At 300 K over 99% of the O_2 molecules are in their ground vibrational state and at 1400 K approximately 80% are in $v_i = 0$ and 16% are in $v_i = 1$. Therefore, the 300 K DA cross sections are dominated by dissociation from $v_i = 0$, whereas the DA cross sections for 1400 K are the averages of cross section for a few vibrational states. Vibrational excitation of the O_2 molecule gives a large enhancement of the cross section at threshold energies. The cross section curves are shifted to lower energies by about 1 eV as v_i is increased from 0 to 1.[12] This is reflected in a shift of the cross section curve at 1400 K to lower energies relative to 300 K.

For comparison, impact parameter cross sections for direct dissociation through the B state are also shown for $v_i = 0$, 1, and 2. The IP cross sections are shifted to lower energies by an energy approximately equal to the vibrational energy spacing in O_2 (about 0.2 eV) as v_i is increased from 0 to 1. The different behavior in these cross sections compared to the DA ones at threshold arises from a difference

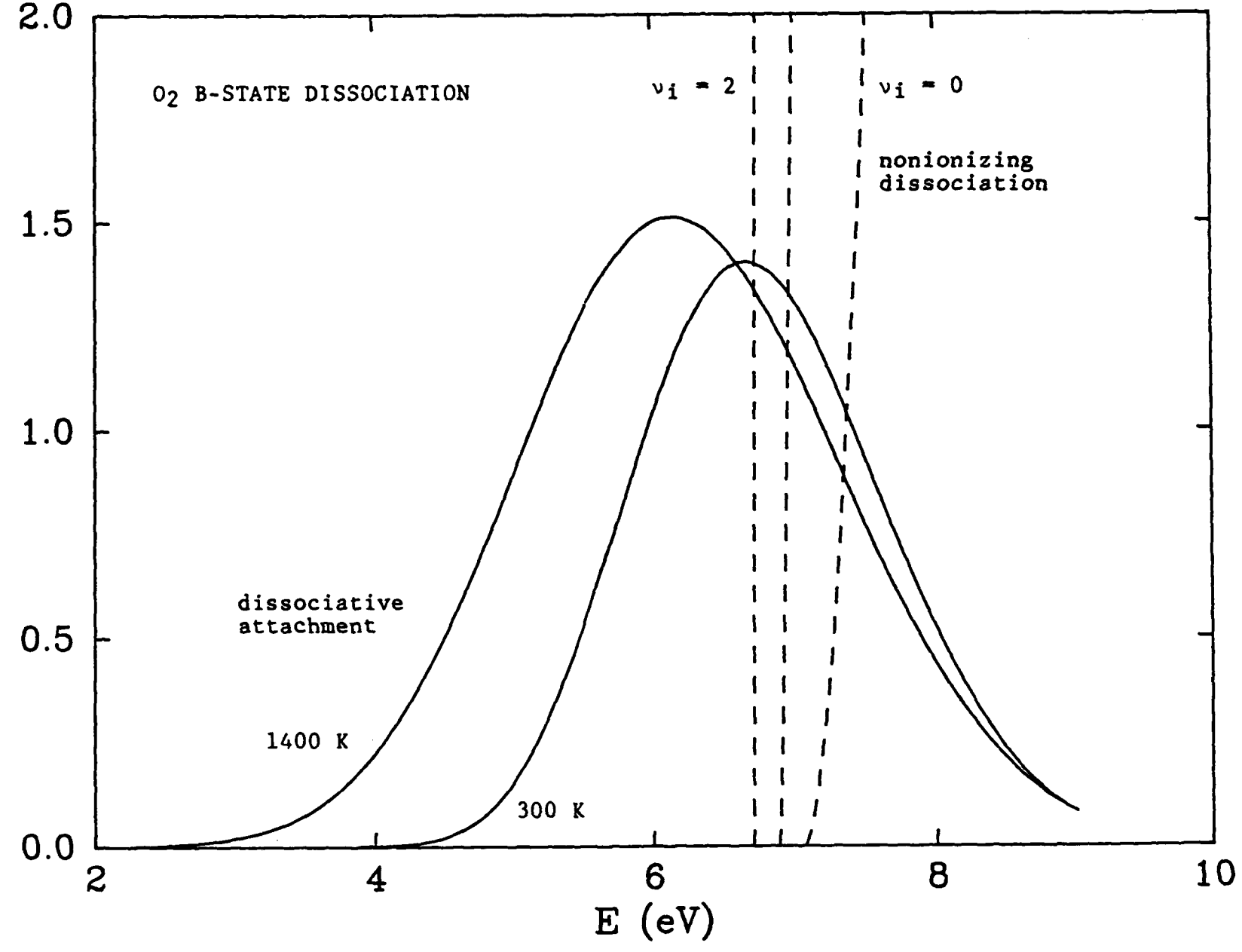
O_2 B-STATE DISSOCIATION
$\nu_i = 2$
$\nu_i = 0$
nonionizing dissociation
dissociative attachment
1400 K
300 K
Cross Section ($10^{-18}cm^2$)
E (eV)
2.0
1.5
1.0
0.5
0.0
2
4
6
8
10

Figure 1

in the mechanisms for the two processes. The nonionizing dissociation process occurs by excitation from the vibrational level of the ground electronic state to the continuum of the B state with an energetic threshold of about 6.7 eV for $\nu_i = 0$. The IP cross sections at threshold energies are controlled by the overlap between the continuum wavefunction and the initial vibrational wavefunction. In this case, the overlap does not depend strongly upon the initial vibrational energy level, there being only a slight enhancement of the $\nu_i = 1$ and 2 cross sections over those for $\nu_i = 0$ at threshold energies. Therefore, for the nonionizing process the thresholds decrease by approximately the vibrational energy level spacing as ν_i increases. The dissociative attachment of O_2 is postulated to occur through the $^2\Pi_u$ state of O_2^- with a threshold of 3.6 eV for $\nu_i = 0$. The cross section for this process is believed to be quite high ($\sim 10^{-16}$ cm^2) and the magnitude of the DA cross section is determined by the competition between autoionization to form neutral O_2 and dissociation to form $O + O^-$. The major effect in this process is the change in the probability of survival in the ionic state as the vibrational state is changed. Because this enters through an exponential factor in the cross section it is seen to have a much more drastic effect upon the DA cross sections than a simple shift to lower energies by the vibrational energy level spacing.

O'Malley has shown that the effect of rotational excitation is minor compared to the vibrational effect for the DA cross section[12]. This agrees with the conclusion we have drawn for the direct dissociation process.

We note that the effect of including exchange effects will change the shapes of the cross section for the direct dissociation process at threshold energies. However, the mechanism of direct excitation will be dominated by the overlaps of the initital and final wavefunctions and the qualitative trends seen in the IP calculations are still expected. The effect of resonances near threshold are more complicated and can alter even the qualitative nature of the predictions.

HCl

The dependence of the dissociative attachment cross section for HCl has been studied by Allan and Wong[13]. The mechanism for this process is similar to that discussed for O_2. Electron attachment is postulated to occur to form the lowest $^2\Sigma^+$ state of HCl^- which has a threshold for dissociation only 0.6 eV above the ground vibrational state of the ground electronic state of neutral HCl. The vibrational energy level spacing of HCl is about 0.35 eV; therefore, by $v_i = 2$ the DA cross sections are nonzero down to zero translational energy. A dramatic enhancement of the DA cross section is seen as the temperature is raised from 300 to 1000 K. For 1000 K the DA cross sections extend down to zero energy even though the relative population of $v_i = 2$ to $v_i = 0$ is 0.03%. As in the case of dissociative attachment for O_2, for HCl the cross sections for electron attachment to HCl are very high at low energies and roughly independent of initial vibrational state. The DA cross sections are then determined by the competition between dissociation and autoionization to form neutral species. The survival factor (probability of not autoionizing) is strongly dependent upon the vibrational state and enters the DA cross section through an exponential factor.

The structure seen in the DA cross sections for HCl are not caused by the DA process itself but by the competition of dissociative attachment with vibrational excitation of HCl. At energies at which excited vibrational states of neutral HCl become accessible, the vibrational excitation cross sections become very large and caused a dip in the DA cross sections.

The impact parameter cross section for dissociation of HCl through the A state are shown in Appendix E. Near threshold the effect of increasing the initial vibrational level is quite dramatic. This is because the overlap of the initial and final wavefunctions for energies near threshold is very sensitive to v_i. Also, the structure seen in the cross section near threshold is a reflection of the

structure in this overlap caused by the nodes in the excited state wavefunctions for the initial electronic state. The origin of this structure is very different from that for the structure in the DA cross sections.

As mentioned in the previous section, the IP method is not valid near threshold but the dependence of the cross sections upon vibrational energy level should be reliably predicted. However, near threshold resonance effects can be important and can significantly alter these predictions.

7. Recommendations

The cross sections presented in this report are suitable for kinetic modelling of electron dissociation processes in plasmas at energies above threshold. Since electron-impact excitation and dissociation of molecules plays an important role in laser plasmas, plasma switches, and general gas-phase electric discharges, it is important to develop theoretical methods that are reliable near threshold. We have examined possible approaches, and conclude that a more rigorous treatment using discrete variable methods is promising and should be pursued.

Extensions of the impact parameter method to treat polyatomic molecules is possible by using wavepacket methods or the eikonal approximation. Both methods have been successfully applied to photodissociation.[14,15] Since selective vibrational excitation of the parent polyatomic molecule can lead to changes in the ratio of product fragments, this process should be investigated as a possible means to rapidly switch a gas discharge.

REFERENCES

M. Inokuti, Rev. Mod. Phys. 43, 297 (1971).

S. Trajmar, D. C. Cartwright in Electron-Molecule Interactions and Their Applications, Vol. 1, p. 156, ed. L. G. Christophorou, Academic Press (1984).

Yu. N. Demkov, Phys. Rev. Lett. 15, 235 (1965).

W. R. Henderson, W. L. Fite, and R. T. Brackmann, Phys. Rev. 183, 157 (1969).

D. Spence and G. J. Schulz, Phys. Rev. 188, 280 (1969).

J. C. Y. Chen and J. L. Peacher, Phys. Rev. 163, 103 (1967).

D. Spence and G. J. Schulz, J. Chem. Phys. 54, 5424 (1971).

M. Allan and S. F. Wong, Phys. Rev. Lett. 41, 1791 (1978).

J. M. Wadehra and J. N. Bardsley, Phys. Rev. Lett. 41, 1795 (1978).

J. N. Bardsley and J. M. Wadehra, Phys. Rev. A. 20, 1398 (1979).

J. M. Wadehra, Phys. Rev. A 29, 106 (1984).

T. F. O'Malley, Phys. Rev. 155, 59 (1967).

M. Allan and S. F. Wong, J. Chem. Phys. 74, 1687 (1981).

S.-Y. Lee and E. J. Heller, J. Chem. Phys. 76, 3035 (1982).

P. K. Swaminathan and D. A. Micha, Int. J. Quantum Chem. S 17, 192 (1983).

APPENDIX A

An improved impact parameter method for electronic excitation and dissociation of diatomic molecules by electron impact

Michael J. Redmon, Bruce C. Garrett,

Lynn T. Redmon, and C. W. McCurdy*

Chemical Dynamics Corporation
1550 West Henderson Road
Columbus, OH 43220

* Permanent address: Department of Chemistry, Ohio State University, Columbus, Ohio 43210

The impact parameter method for electron impact excitation of diatomic ecules is reformulated to explicitly treat molecular vibration and rotation to permit the study of molecular dissociation. Applications are made optically allowed transitions involving the X $^1\Sigma_g^+$, B $^1\Sigma_u^+$ and B' $^1\Sigma_u^+$ states H_2. The resulting cross sections are compared to other theoretical culations and to experimental data. This method is applicable to heavy tomic molecules and is expected to be useful in studying trends in ctronic excitation and dissociation cross sections associated with iations in internal energy.

$$\chi^{\alpha_f}_{\varepsilon \ell_f}(R) \xrightarrow[R\to\infty]{} CkR[j_{\ell_f}(kR) - \tan(\eta) n_{\ell_f}(kR)] \tag{35}$$

ere

$$k = (2\mu_{AB}/\hbar)[\varepsilon - V_{\alpha_f}(R=\infty)] \tag{36}$$

$_f$ and n_{ℓ_f} are regular and irregular Ricatti-Bessel functions,[42] respectively, is the phase shift, and C is a constant obtained by normalizing the wave-ıction to unit density per unit energy.[12] The transition energy ΔE [Eq. ɔ)] is replaced by

$$\Delta E = \varepsilon - \varepsilon^{\alpha_i}_{v_i j_i} \tag{37}$$

d the final expression for the averaged cross section is

$$\sigma^{\alpha_i \alpha_f}_{v_i}(E, T_{rot}) = \left[Q^{\alpha_i}_{v_i}(T_{rot})\right]^{-1} \left\{ \sum_{j_i=0}^{j_i^{max}} d_{j_i} (2j_i+1) \exp(-\varepsilon^{\alpha_i}_{v_i j_i}/k_B T_{rot}) \right.$$

$$\left. \times \sum_{\ell_f} \int_{\varepsilon_{min}}^{\varepsilon_{max}} d\varepsilon \ \sigma^{\alpha_i \alpha_f}_{v_i j_i \varepsilon \ell_f}(E) \right\} \tag{38}$$

ere, in analogy to Eq. (28),

$$\sigma^{\alpha_i \alpha_f}_{v_i j_i \varepsilon \ell_f}(E) = S^{\alpha_f \alpha_i}_{\varepsilon \ell_f v_i j_i} D^{\alpha_f \alpha_i}_{\varepsilon \ell_f v_i j_i}(E) \tag{39}$$

this case, the final rotational angular momentum quantum number is terpreted as the orbital angular momentum quantum number ℓ_f of the separating oms. We refer to the cross section defined by Eq. (38) as the IPVRD cross

Invoking the Franck-Condon approximation in Eq. (12) and assuming the vibrational states are degenerate we obtain[30]

$$\sigma_{if}(E,T_{rot}) \xrightarrow[T_{rot}\to 0]{} \frac{m_e^2 e^2}{3\hbar^4} (2-\delta_{\Lambda_f,0}) [M_{\alpha_f\alpha_i}(R_{eq})]^2 D^{\alpha_f\alpha_i}(E) \qquad (32)$$

where we assume the sum over the Franck-Condon factors is unity (this is true only if continuum states are also included in the "sum"). This expression thus represents excitation to both bound and dissociative states. We call the cross section denoted by Eq. (29) the IPVR cross section, the one given by Eq. (31) the IPV cross section, and the one given by Eq. (32) the IP cross section. The last is the form obtained by Hazi.[30]

B. Bound-to-Continuum Transitions

Next we consider the modification necessary for dissociative transitions. In this case we no longer have a vibrational quantum number for the final state; instead we have the continuum energy ε. Thus we replace all occurrences of the quantum number v_f by ε in the preceeding equations. The wavefunctions for the continuum states are solutions to the equation

$$[-(\hbar^2/2\mu_{AB})d^2/dR^2 + V_{\alpha_f}(R) + \hbar^2\ell_f(\ell_f+1)/2\mu_{AB}R^2)]\ \chi^{\alpha_f}_{\varepsilon\ell_f}(R) = \varepsilon\chi^{\alpha_f}_{\varepsilon\ell_f} \qquad (33)$$

subject to scattering boundary conditions, i.e.,

$$\chi^{\alpha_f}_{\varepsilon\ell_f}(R) \xrightarrow[R\to 0]{} 0 \qquad (34)$$

$$\sigma_{v_i}^{\alpha_i\alpha_f}(E,T_{rot}) = \left[Q_{v_i}^{\alpha_i}(T_{rot})\right]^{-1}\left\{\sum_{j_i=0}^{j_i^{max}} d_{j_i}\,(2j_i+1)\,\exp(-\varepsilon_{v_i j_i}^{\alpha_i}/k_B T_{rot})\right.$$

$$\left.\times \sum_{v_f=0}^{v_f^{max}} \sum_{j_f} \sigma_{v_i j_i v_f j_f}^{\alpha_i\alpha_f}(E)\right\} \qquad (29)$$

where $Q_{v_i}^{\alpha_i}(T_{rot})$ is the rotational partition function for vibronic state $\alpha_i v_i$

$$Q_{v_i}^{\alpha_i}(T_{rot}) = \sum_{j_i=0}^{j_i^{max}} d_{j_i}\,(2j_i+1)\,\exp(-\varepsilon_{v_i j_i}^{\alpha_i}/k_B T_{rot}) \qquad (30)$$

k_B is Boltzmann's constant, and v_f^{max} is the vibrational quantum number of the highest bound state of the final electronic state. The nuclear spin degeneracy factor d_{j_i} is unity except for certain classes of homonuclear diatomics (see Table 1). j_i^{max} is selected by practical consideration.

The sum over final rotational states has nonzero contributions only for j_f equal to j_i-1 or j_i+1, ($j_f \geq 0$). In the low temperature limit, only the j_i=0 and j_f=1 states contribute to $\sigma_{v_i}^{\alpha_i\alpha_f}(E,T_{rot})$. Then the sums over the Clebsch-Gordan coefficients in Eq. (19) can be evaluated to give a factor of 1/9 and the cross section Eq. (29) reduces to

$$\sigma_{v_i}^{\alpha_i\alpha_f}(E,T) \xrightarrow[T_{rot}\to 0]{} \sum_{v_f=0}^{v_f^{max}} \frac{m_e^2 e^2}{3\hbar^4}\,(2-\delta_{\Lambda_f,0})\,[M_{v_f v_i}^{\alpha_f\alpha_i}]^2\,D_{v_f v_i}^{\alpha_f\alpha_i} \qquad (31)$$

where

$$m_e u_i^2 = E \tag{22}$$

$$m_e u_f^2 = E - \Delta E \tag{23}$$

$$\gamma_i = \ell_o \, \Delta E / m_e u_i^2 \tag{24}$$

$$\gamma_f = \ell_o \, \Delta E / m_e u_f^2 \tag{25}$$

$$\bar{\gamma} = 2\ell_o \, \Delta E / m_e (u_i^2 + u_f^2) \tag{26}$$

E is the relative translational energy of the incident electron, m is the electron mass, ℓ_o is the minimum value of the incident electronic orbital angular momentum quantum number, u_i (u_f) is the initial (final) electron speed, and the transition energy ΔE is defined by

$$\Delta E = \epsilon^{\alpha_f}_{v_f j_f} - \epsilon^{\alpha_i}_{v_i j_i} \tag{27}$$

The dependence of the dynamical factor on molecular vibrational and rotational quantum numbers is only through the transition energy.

The cross section is expressed as the product of the structural factor for the molecule, given by Eq. (19), and the dynamical factor for the electron, given by Eq. (21):

$$\sigma^{\alpha_i \alpha_f}_{v_i j_i v_f j_f}(E) = S^{\alpha_f \alpha_i}_{v_f j_f v_i j_i} \; D^{\alpha_f \alpha_i}_{v_f j_f v_i j_i}(E) \tag{28}$$

A. Bound-to-Bound Transitions

The cross section of interest is obtained by averaging Eq. (28) over a Boltzmann distribution of initial rotational states characterized by a rotational temperature T_{rot} and summing over all final vibrational and rotational states:

inequality[40]. The structural factor is zero unless $j_f = j_i \pm 1$. It also vanishes when $|\Delta\Lambda| > 1$, and so we can have $\Sigma \leftrightarrow \Sigma$, $\Sigma \leftrightarrow \Pi$, and $\Pi \leftrightarrow \Pi$ transitions but not $\Sigma \leftrightarrow \Delta$. Extending the present theory to permit the description of higher order processes would require including additional terms in the multipole expansion of the electron-target interaction. If we assume degenerate rotational states, the structural factor reduces to

$$S^{\alpha_f \alpha_i}_{v_f v_i} = \left(\frac{m_e^2 e^2}{3 g_i \hbar^4}\right) (2 - \delta_{\Lambda_f,0})(2 - \delta_{\Lambda_i,0}) \quad | M^{\alpha_f \alpha_i}_{v_f v_i} |^2 \tag{20}$$

Evaluation of the dynamical factor follows the derivation of Hazi exactly. By assuming that the trajectories for the incident electron are straight lines and energy exchange with the target occurs at the distance of closest approach and requiring conservation of energy and angular momentum, the dynamical factor can be expressed in terms of modified Bessel functions[42] $K_i(\gamma)$ and modified Struve functions[42] $S_i(\gamma)$. The derivation is found in Hazi's paper,[30] and we present only the final result integrated over impact parameter:

$$\begin{aligned} D^{\alpha_f \alpha_i}_{v_f j_f v_i j_i}(E) = \frac{2\pi\hbar^2}{m_e^2 u_i^2} \Big\{ & \gamma_i K_0(\gamma_i) K_1(\gamma_i) + \gamma_f K_0(\gamma_f) K_1(\gamma_f) \\ & - \frac{\pi^2}{4} [\gamma_i S_0(\gamma_i) S_1(\gamma_i) + \gamma_f S_0(\gamma_f) S_1(\gamma_f)] \\ & + \bar{\gamma} \{K_1(\gamma_f) K_0(\gamma_i) + K_0(\gamma_f) K_1(\gamma_i) \\ & + \frac{\pi^2}{4} [S_0(\gamma_i) S_1(\gamma_f) + S_1(\gamma_i) S_0(\gamma_f)]\} \\ & + (u_i^2 - u_f^2)(u_i^2 + u_f^2)^{-1} [\ell n(\gamma_f/\gamma_i) + \frac{\pi}{2} \int_{\gamma_i}^{\gamma_f} d\gamma \, S_0(\gamma)] \Big\} \end{aligned} \tag{21}$$

$$p^{\alpha_f\alpha_i}_{v_f j_f v_i j_i}(t) = \frac{2j_f+1}{27\, g_i}\left(\frac{e^2}{\hbar^2}\right)\left|M^{\alpha_f\alpha_i}_{v_f j_f v_i j_i}\right|^2 \left|\int_{-\infty}^{\infty} dt\, \exp(i\Delta E_{fi}t/h)\,\frac{r'(t)}{r'^3}\right|^2$$

$$\times \sum_{\lambda_f=\pm\Lambda_f} \sum_{\lambda_i=\pm\Lambda_i} |C(j_i j_f 1;\, -\lambda_i\lambda_f)|^2$$

$$\times \sum_{m_f=-j_f}^{j_f} \sum_{m_i=-j_i}^{j_i} |C(j_i j_f 1;\, -m_i m_f)|^2 \qquad (17)$$

We have also used the relation defining the displacement vector in terms of the spherical harmonics[40]

$$\sum_{\mu=-1}^{+1} r'\, Y^*_{1\mu}(\hat{r}')\,\hat{e}_\mu = \left(\frac{3}{4\pi}\right)^{1/2} r' \qquad (18)$$

to simplify the time dependent integral.[30] This form for the probability results from the present restriction to dipole allowed transitions. Thus even with the inclusion of vibrational and rotational degrees of freedom, we still obtain a form analogous to Hazi's, i.e., a factorization of the transition probability into the product of a dynamical factor depending on projectile electron coordinates (classical trajectory) and a unitless structural factor depending only upon properties of the target molecule.[30]

The structural factor is written as

$$S^{\alpha_f\alpha_i}_{v_f j_f v_i j_i} = \left(\frac{m_e^2 e^2}{\hbar^4}\right)\frac{2j_f+1}{27\, g_i}\left|M^{\alpha_f\alpha_i}_{v_f j_f v_i j_i}\right|^2 \sum_{\lambda_f=\pm\Lambda_f} \sum_{\lambda_i=\pm\Lambda_i} |C(j_i j_f 1;\, -\lambda_i\lambda_f)|^2$$

$$\times \sum_{m_f=-j_f}^{+j_f} \sum_{m_i=-j_i}^{+j_i} |C(j_i j_f 1;\, -m_i m_f)|^2 \qquad (19)$$

where m_e is the electron mass. It contains Clebsch-Gordan coefficients that impose optical selection rules due to the requirements of the triangle

where we have used the property[41]

$$D^{j_i *}_{m_i \lambda_i}(\hat{R}) = (-1)^{m_i - \lambda_i} D^{j_i}_{-m_i - \lambda_i}(\hat{R}) \tag{14}$$

Making use of the integral theorem for the product of three rotation matrices[41], we obtain

$$I_R = (-1)^{m_i - \lambda_i} \frac{(2j_f+1)^{\frac{1}{2}}(2j_i+1)^{\frac{1}{2}}}{8\pi^2} \frac{2}{3} \delta_{m_f - m_i, \mu}$$

$$\times C(j_i, j_f, 1; -m_i, m_f)\, C(j_i, j_f, 1; -\lambda_i, \lambda_f) \tag{15}$$

We have now reduced the rotational factor to a simple expression involving the product of two Clebsch-Gordan coefficients. The time-dependent perturbation matrix element now becomes

$$V_{fi}(t) \simeq \frac{2}{3}\left(\frac{4\pi}{3}\right)^{\frac{1}{2}} e \frac{(2j_f+1)^{\frac{1}{2}}(2j_i+1)^{\frac{1}{2}}}{8\pi^2} (-1)^{m_i - \lambda_i} M^{\alpha_f \alpha_i}_{v_f j_f v_i j_i}$$

$$\times C(j_i j_f 1; -m_i m_f)\, C(j_i j_f 1; -\lambda_i \lambda_f)$$

$$\times \frac{1}{r'^2} \sum_{\mu=-1}^{+1} \delta_{m_f - m_i, \mu}\, Y^*_{1\mu}(\hat{r}') \tag{16}$$

Substituting Eq. (16) into Eq. (1), summing over final angular momenta (electronic and rotational), and averaging over initial angular momenta results in the following form for the transition probability

This operator is a spherical tensor of rank 1, so (from the Wigner-Eckart theorem[39]) we have

$$\sum_{m=-1}^{+1} D^{1*}_{\mu m}(\hat{R}) \int d\underset{\sim}{x}\ \psi^{*}_{\alpha_f \lambda_f}(\underset{\sim}{x};R) \sum_{q=1}^{n} er_q\ Y_{1m}(\hat{r}_q)\ \psi_{\alpha_i \lambda_i}(\underset{\sim}{x};R)$$

$$= \left(\frac{3}{4\pi}\right)^{\frac{1}{2}} D^{1*}_{\mu\Delta\lambda}(\hat{R})\ M_{\alpha_f\alpha_i}(R) \tag{9}$$

where the electronic transition dipole moment is

$$M_{\alpha_f\alpha_i}(R) = \left| \int d\underset{\sim}{x}\ \psi^{*}_{\alpha_f \lambda_f}(\underset{\sim}{x};R) \sum_{q=1}^{n} \vec{er}_q\ \psi_{\alpha_i \lambda_i}(\underset{\sim}{x};R) \right| \tag{10}$$

and $\Delta\lambda = \lambda_f - \lambda_i$. The transition matrix element can now be written as

$$V_{fi}(t) \simeq \left(\frac{4\pi}{3}\right)^{\frac{1}{2}} e \left[M^{\alpha_f\alpha_i}_{v_f j_f v_i j_i}\right] \sum_{\mu=-1}^{+1} \frac{1}{r'^2}\ Y^{*}_{1\mu}(\hat{r}')$$

$$\times \int d\hat{R}\ N^{j_f *}_{m_f \lambda_f}(\hat{R})\ D^{1*}_{\mu\Delta\lambda}(\hat{R})\ N^{j_i}_{m_i \lambda_i}(\hat{R}) \tag{11}$$

where the electronic transition dipole moment is averaged over the initial and final vibrational wavefunctions

$$M^{\alpha_f\alpha_i}_{v_f j_f v_i j_i} = \int_0^{\infty} dR\ \chi^{\alpha_f *}_{v_f j_f}(R)\ M_{\alpha_f\alpha_i}(R)\ \chi^{\alpha_i}_{v_i j_i}(R) \tag{12}$$

For the remaining integral over Euler angles, we use the Wigner D-function representation of the symmetric top wavefunctions, Eq. (4),

$$I_R = \left(\frac{2j_f+1}{8\pi^2}\right)^{\frac{1}{2}} \left(\frac{2j_i+1}{8\pi^2}\right)^{\frac{1}{2}} \int d\hat{R}\ D^{j_f}_{m_f \lambda_f}(\hat{R})\ D^{1*}_{\mu\Delta\lambda}(\hat{R})\ D^{j_i *}_{m_i \lambda_i}(\hat{R})$$

$$= (-1)^{m_i - \lambda_i} \left(\frac{2j_f+1}{8\pi^2}\right)^{\frac{1}{2}} \left(\frac{2j_i+1}{8\pi^2}\right)^{\frac{1}{2}} \int d\hat{R}\ D^{1*}_{\mu\Delta\lambda}(\hat{R})\ D^{j_f}_{m_f \lambda_f}(\hat{R})\ D^{j_i}_{-m_i -\lambda_i}(\hat{R}) \tag{13}$$

$$V_{fi}(t) = \int d\underset{\sim}{x} \int R^2 dR \int d\hat{R}\, \psi^*_{\alpha_f \lambda_f}(\underset{\sim}{x};R)\, R^{-1}\, \chi^{\alpha_f *}_{v_f j_f}(R)\, N^{j_f *}_{m_f \lambda_f}(\hat{R})\,,$$

$$\times \sum_{q=1}^{n} \frac{e^2}{|\vec{r}'(t)-\vec{r}'_q|}\, \psi_{\alpha_i \lambda_i}(\underset{\sim}{x};R)\, R^{-1}\, \chi^{\alpha_i}_{v_i j_i}(R)\, N^{j_i}_{m_i \lambda_i}(\hat{R}) \qquad (5)$$

To evaluate this expression, we use the usual multipole expansion[40]

$$|\, r'(t)-r'_q\,|^{-1} = \sum_{\ell=0}^{\infty} \sum_{\mu=\ell}^{+\ell} \left(\frac{4\pi}{2\ell+1}\right) \frac{r_<^{\ell}}{r_>^{\ell+1}}\, Y^*_{\ell\mu}(\hat{r}')\, Y_{\ell\mu}(\hat{r}'_q) \qquad (6)$$

where $r_<(r_>)$ is the lesser (greater) of r' and r_q'. We keep only the asymptotic ($r' > r_q'$) terms of this expansion because the impact parameter treatment is valid only for collisions that do not penetrate the electron cloud of the target.[30] We are presently interested only in optical (dipole-allowed) transitions (for which the dominant contribution is from $\ell = 1$). Therefore, we approximate the electron-target interaction by

$$|\vec{r}'(t)-\vec{r}'_q|^{-1} \simeq \frac{4\pi}{3} \sum_{\mu=-1}^{+1} \frac{r'_q}{r'^2}\, Y^*_{1\mu}(\hat{r}')\, Y_{1\mu}(\hat{r}'_q) \qquad (7)$$

Since the electron coordinates of the electronic wavefunctions employed in the matrix element V_{fi} given by Eq. (5) are expressed in BF coordinates, Eq. (7) must be transformed to BF coordinates before the integration can be carried out. Using the Wigner rotation matrices[41] we obtain

$$|\vec{r}'(t)-\vec{r}'_q|^{-1} \simeq \frac{4\pi}{3} \sum_{\mu=-1}^{+1} \sum_{m=-1}^{+1} \frac{r_q}{r'^2}\, Y^*_{1\mu}(\hat{r}')\, D^{1*}_{\mu m}(\hat{R})\, Y_{1m}(\hat{r}_q) \qquad (8)$$

Substituting this expression into Eq. (5), we note that the part of the resulting expression involving integration over the target electron coordinates is the matrix element of the spherical representation of the dipole operator.

The vibrational wavefunctions for electronic state α are orthonormal eigenfunctions of the equation

$$[-(\hbar^2/2\mu_{AB})\, d^2/dR^2 + V_\alpha(R) + \hbar^2 j(j+1)/2\mu_{AB}R^2]\, \chi^\alpha_{vj}(R) = \epsilon^\alpha_{vj}\, \chi^\alpha_{vj}(R) \qquad (3)$$

where μ_{AB} is the reduced mass of the diatomic molecule, ϵ^α_{vj} is the vibrational energy level, and $V_\alpha(R)$ is the potential energy curve for electronic state α.

The symmetric top functions are represented in terms of Wigner D-functions[39]

$$N^j_{m\lambda}(\hat{R}) = \left(\frac{2j+1}{8\pi^2}\right)^{\frac{1}{2}} D^{j*}_{m\lambda}(\hat{R}) \qquad (4)$$

where the projectile electron is assumed to be initially moving along the spaced-fixed (SF) Z axis, and where $\hat{R}$ represents the two (nontrivial) Euler angles relating the BF frame to SF axes. This normalization assumes integration over all three Euler angles.

In our formulation of the semiclassical impact parameter method, the projectile electron velocity is assumed to be high enough that the collision time is short compared to the periods of molecular vibration or rotation. Then the adiabatic nuclei approximation is expected to be valid, and the time-dependent perturbation matrix element required in Eq. (1) is obtained by taking the matrix element of the projectile-target interaction between initial and final molecular states represented in the form of Eq. (2). If $\vec{r}'(t)$ represents the classical trajectory of the projectile electron, and $\vec{r}'_q$ the coordinates of a target electron (the primes indicate SF coordinates), then this matrix element can be expressed as

II. THEORY

Hazi's implementation of the impact parameter method employs the "fixed nuclei" approximation[4], averaging the semiclassical transition probability[30]

$$P_{fi} = g_i^{-1} \sum_{\lambda_i=\pm\Lambda_i} \sum_{\lambda_f=\pm\Lambda_f} \left| \hbar^{-1} \int_{-\infty}^{\infty} dt\, e^{i\Delta E_{fi} t/\hbar}\, V_{fi}(t) \right|^2 \qquad (1)$$

over all molecular orientations. In this expression g_i is the degeneracy of the initial electronic state, Λ_i and Λ_f are the usual projections of electronic angular momentum on the body-fixed axis, ΔE_{fi} is the transition energy, and $V_{fi}(t)$ is the time-dependent matrix element of the perturbation. We present an extension of the theory to allow treatment of those processes that require consideration of nuclear motion.

We work within the framework of the adiabatic nuclei approximation[37] and employ a Born-Oppenheimer factorization of the wave function for the target molecule

$$\psi^{jm}_{\alpha v\lambda}(\underset{\sim}{x};\, R) = \psi_{\alpha\lambda}(\underset{\sim}{x};\, R)\, \chi^{\alpha}_{vj}(R)\, N^{j}_{m\lambda}(\hat{R}) \qquad (2)$$

The function $\psi_{\alpha\lambda}$ represents an approximate solution (for electronic state α) to the n-electron Schrodinger equation for the electrons in the molecule moving in the field of the "fixed" nuclei. χ^{α}_{vj} is the vibrational wavefunction for the (v,j) rovibrational level of electronic state α, and $N^{j}_{m\lambda}$ is a symmetric-top function for a diatomic molecule with electronic angular momentum component λ.[38] In our notation, $\underset{\sim}{x}$ collectively represents the coordinates of the target electrons, while R and $\hat{R}$ represent the magnitude and angular position of the relative position vector $\vec{R}$. All target electronic coordinates are referred to the body-fixed (BF) frame and the polar z-axis is taken along the line joining the nuclei ($\hat{R}$).

products of Clebsch-Gordon coefficients. By performing suitable averages, the original cross section formula of Hazi is obtained.

The appendixes provides the relevant computational details, while Section IV presents the results of the cross section calculations for several levels of approximation within the IP method. As a test of the method for electronic excitation to bound vibrational states, we apply the IP method to the $X^1\Sigma_g^+$ to $B^1\Sigma_u^+$ and $X^1\Sigma_g^+$ to $B'^1\Sigma_u^+$ transitions in H_2 and compare with previous experimental[32] and theoretical [12,16,23,30] studies. We also apply it to the direct dissociation of $H_2(^1\Sigma_g^+)$ through the $B'^1\Sigma_u^+$ state and compare the results with experimental [33,34] and theoretical[12,26] studies. Section V provides a summary and the conclusions.

wave theories. Thus it is complementary to these approaches and to the high-energy Born-type approximations. In the semiclassical impact-parameter (IP) method the motion of the electrons (including the incident electron) is separated from nuclear motion by the Born-Oppenheimer approximation. This allows the molecular electronic problem to be treated as accurately as necessary, independently of the scattering. Hazi's theory assumes degenerate rotational states and averages the transition probability over molecular orientations. His formulation results in cross-sections that satisfy reciprocity, and this represents a refinement over the original impact-parameter method. However, the Franck-Condon approximation is utilized, and internuclear distances are treated as static. Thus vibrational and rotational motion are neglected. Because of these approximations in Hazi's theory, the resulting cross sections do not distinguish between bound (rovibrational) and unbound (continuum) channels. When the method is extended to include nuclear motion, this differentiation can be made.

In Section II we present extensions of the impact parameter model to include the effects of initial vibrational and rotational excitation upon electron impact induced excitation and dissociation. We are interested in nonresonant optically allowed electronic excitations of diatomic molecules. These involve dipole-allowed spin-conserving transitions. These excitations can be to bound rovibrational levels of the final electronic state or to parts of the potential energy curve above the dissociative limit of the final electronic state. We consider only processes of direct dissociation through excited electronic states rather than the resonance-enhanced dissociative attachment process. When the diatomic molecule is treated as a symmetric top, electronic and rotational angular momentum are coupled; however, the resulting cross section retains a separability of structural and dynamical factors analogous to that of Hazi's original method and involves simple

I. INTRODUCTION

Processes involving electron-molecule collisions are important in gas-laser systems, atmospheric physics and photochemistry. Because of their importance in laser plasmas,[1] collision-induced electronic excitations and dissociation by electron impact have been the subject of recent experimental interest;[2] however, there has been less progress in the theoretical description of these processes. Although electron-molecule scattering theory has been significantly advanced in the areas of elastic scattering and rotational and vibrational excitation,[3-5] the ab initio calculation of electronic excitation of molecules by electron impact is relatively new. Early work in this area includes Born or other "plane-wave" approximation calculations[6-15] that are reliable only at relatively high energies. In addition a two-state close-coupling method[16-18] has been applied to electronic excitation and dissociation of a number of states of H_2 and to the excitation of the $a^1\Pi_g$ state of N_2[19]. In these calculations electron exchange is correctly included, but the treatment of nuclear motion utilizes the Franck-Condon approximation. The theory can treat both singlet-singlet and singlet-triplet transitions. The distorted-wave Born approximation employing the L^2 T-matrix[20-26] or R-matrix[27] methods has also received attention. Most applications of the distorted wave methods have been to processes involving excited electronic states of H_2, although applications to N_2[24] and F_2[25] have also been made. The method is most applicable to spin-forbidden transitions involving short-range interactions.

Hazi has extended the semiclassical impact-parameter method[28-29] to electronic excitation of diatomic molecules[30]. The formulation neglects exchange, and is best suited for the treatment of optically allowed transitions that require many partial waves in conventional close-coupling or distorted

section. The limits of integration in Eq. (38) are rigorously given by the continuum threshold

$$\varepsilon_{min} = V_{\alpha_f} \ (R = \infty) \tag{40}$$

and by energy conservation

$$\varepsilon_{max} = E + \varepsilon^{\alpha_i}_{v_i j_i} \tag{41}$$

The expression for dissociation from selected initial vibrational states in which rotations are treated as degenerate is generalized from Eq. (31)

$$\sigma^{\alpha_i \alpha_f}_{v_i}(E) = \int_{\varepsilon_m}^{\varepsilon_{max}} d\varepsilon \quad D^{\alpha_f \alpha_i}_{\varepsilon v_i}(E) \quad S^{\alpha_f \alpha_i}_{\varepsilon v_i} \tag{42}$$

where the structural factor is given by

$$S^{\alpha_f \alpha_i}_{\varepsilon v_i} = \frac{m^2 e^2}{3\hbar^4} \quad (2 - \delta_{\Lambda_f, 0}) \ |M^{\alpha_f \alpha_i}_{\varepsilon v_i}|^2 \tag{43}$$

and the dynamical factor is given by Eqs. (21) - (26). The cross section defined by Eq. (42) is called the IPVD cross section.

III. COMPUTATIONAL DETAILS

The potential curves for the X $^1\Sigma_g^+$, B $^1\Sigma_u^+$ and B' $^1\Sigma_u^+$ states of H_2 are obtained by fitting accurate ab initio[43,44] and experimental[45] data in a manner similar to that of Blais and Truhlar[46]. Over the region for which the potential data is available the points are fitted to a cubic spline function. For small R values the potential is written as

$$V = A\, R^{-1} \exp(-BR) \tag{44}$$

where the parameters A and B are determined so that the function fits the data points at the two smallest R values. For the region of R values greater than the spline-fit region the potential is fit to the form

$$V = V_o - C_6\, R^{-6} - C_8\, R^{-8} \tag{45}$$

where V_o is the experimental dissociation energy and the parameters C_6 and C_8 are determined so that the function fits the data points at the two largest R values. The cubic spline fit is restricted to match the function values and their derivatives at the end points of the data. Our fits to the three potential curves used in this work are presented in Fig. 1.

The transition dipole matrix elements as a continuous function of R are obtained by 4-point (3rd order) Lagrange interpolation[42] of the accurate ab initio data.[47,48] The fits to the matrix elements are shown in Fig. 2.

The vibrational eigenvalues $\epsilon^{\alpha}_{v_j}$ are obtained by solving Eq. (3) using Cooley's algorithm[49]. Once an eigenvalue is found, the values of the unnormalized wavefunction $\chi^{\alpha}_{v_j}(R)$ are stored on a grid of evenly spaced R values. The normalization factor is determined by extended Simpson's rule

integration,[42] and the stored values are normalized. Unnormalized continuum wavefunctions for a fixed energy ε are obtained by Numerov integration and stored on the same grid of R values used for the vibrational wavefunction. The asymptotic boundary conditions are applied, and the normalization constant of Eq. (35) is obtained using the method described by Chung, Lin, and Lee.[12]

The structural factor $S^{\alpha_f \alpha_i}_{v_f j_f v_i j_i}$ is obtained from Eq. (19), where the summation over the Clebsch-Gordan coefficients is straightforward and the square of the dipole transition matrix element is obtained from Eq. (12). The integration in Eq. (12) is performed using extended Simpson's rule on the grid of R values on which the wavefunctions are saved. In the case of bound-to-continuum transitions, the quantum number v_f is replaced by the energy eigenvalue ε, but the computational procedure is identical.

The dynamical factor is calculated from Eq. (21). Evaluation of all of the modified Bessel and Struve functions, including the finite integral of the Struve function, is accomplished by Lagrange interpolation from the tables of Abramowitz and Stegun.[42] The order of interpolation used is that recommended in the tables.

The impact parameter method requires that a minimum value of the orbital angular momentum of the incident electron be supplied to evaluate Eq. (21). For the comparisons reported here, we have used Hazi's value (b_0=1.7 a_0).[30] In subsequent applications, we define the minimum value of the impact parameter b_0 by requiring the cross section from Eq. (32) to agree with that of the Born approximation at a high energy.[30] The choice of b_0 is discussed further in the following paper.[50]

For dissociative processes, the integral over the final energy is performed using repeated Gauss-Legendre integration. The total range from ε_{min} to ε_{max} need not be considered; only a limited range of ε values contributes significantly to the cross sections for all incident energies.

This range is determined by the behavior of the Franck-Condon factors. Typically 80 to 100 integration points are needed to converge the cross sections to 2 or more significant figures.

IV. RESULTS

In this section we report the results of calculations of various electron-impact processes in H_2 using the theoretical impact-parameter methods of Section II. The calculations permit comparison with experimental and other theoretical results. We have studied excitation and dissociation of ground-state H_2 via the B and B' states and the effect of varying initial molecular vibrational and rotational energy on these processes. The latter studies are the first of their kind for electron impact dissociation to neutral species.

In Table II we present cross sections for electron impact excitation from the ground (X) state to the B state of $H_2(v=0)$. Our IPV results are compared with other theoretical calculations and with experiment. The comparison is also shown in Fig. 3. Because the level of theory in our IPV calculations is meant to be comparable to the treatment of vibration in the majority of other theoretical methods, we use the Franck-Condon approximation for the comparisons in Table II. Our most accurate method employs explicit numerical integration of the dipole transition moment over the vibrational wavefunctions of the target molecule.

The agreement of the Born results with our IPV cross sections in Table II is good at energies above 50 eV but poorer at lower energies, where the Born approximation is known to break down. The fact that the two sets of Born results appear to have a different low energy behavior is somewhat disturbing. The difference is larger between the two Born cross sections than that found in comparing the smaller Born cross section with the Born-Ochkur result (which included exchange). Fliflet and McCoy[23] attribute this difference to the use of different final-state wavefunctions. The IPV results are in reasonable agreement with the distorted wave cross sections,

being somewhat larger at the lower energies. The close-coupling results are also smaller than the IPV cross sections, but the overall agreement of the present impact parameter method with both of these more exact methods is within an acceptible 15 percent above 25 eV. The distorted wave and close-coupling calculations include exchange, which is not treated in the impact-parameter theory. Exchange effects could be included in the IP method by the use of effective exchange potentials.[51] However, one should then worry about higher order terms in the expansion Eq. (6).

The experimental results of Srivastava and Jensen[32] lie about a factor of two below all of the theoretical calculations. Their experiment did not directly measure the integrated cross section to all final vibrational states; it only detected radiation from the $v'=2$ state. The quantity they measured was the differential cross section, which agreed well with the distorted wave calculations of Fliflet and McCoy except in the low angle region, where the experimental cross section was about a factor of two smaller than the calculations. The cross section summed over all final vibrational states was estimated using the Franck-Condon principle. The differences between the theoretical and experimental cross sections in Table II probably stem from the smaller values for low angle scattering obtained in the experiment. The good agreement above threshold among all of the theoretical methods suggests that the predicted values of the excitation cross sections in this energy region for the X-to-B transition in H_2 are reliable.

In Table III we compare the results for this transition of various treatments of molecular vibration within the impact parameter method. The IP method of Hazi,[30] which assumes vibrational degeneracy, underestimates the IPV cross sections obtained with an accurate treatment of vibration (shown in the right-most column) by approximately ten percent. The use of IPV with the Franck-Condon approximation shows the improvement over IP that can be

achieved by including vibrational motion. The IP method implicitly assumes a sum over bound and continuum vibrational levels, while the IPV method only includes bound levels. For this comparison, however, the major differences arise from errors in treating these bound states since the dissociation cross section is small. This comment applies only for this case (v=0). As will be seen below, there is a considerable enhancement of the dissociation cross section with increasing target vibrational excitation.

Table IV presents results from excitation to the B' state of H_2. For this transition there are fewer calculations for comparison and (to our knowledge) no experimental results. The most accurate theoretical calculations available for comparison are the distorted wave results of Mu-Tao, Lucchese, and McCoy[26]. These results include bound vibrational states through a Franck-Condon factor in the differential cross section so that the most meaningful comparison is with our IPV(FC) calculations in the fourth column. The agreement with the present IPV cross sections is typically to within thirty to forty percent of the distorted-wave result. The agreement between the present results and the Born calculations of Arrighini et. al.[15] is poor, the difference being a factor of four at low energies. The simple IP method overstimates the IPV and DW cross sections by approximately a factor of two. This is due to the implicit sum over continuum states discussed above for the IP method. The sum over all bound vibrational levels of the B' state of the Franck-Condon factors involving ground-state H_2 is 0.48, so that approximately fifty percent of the IP cross section comes from the continuum. This comparison of the IP and IPV cross sections indicates that a realistic treatment of molecular vibration is important for this transition due to the importance of dissociative processes.

In Table V we present cross sections for the production of H(1s) + H(2s) via excitation to continuum levels of the B' state. The agreement between

the various theoretical results is good; the largest difference is less than twenty percent at energies above the maximum in the cross section. The theoretical results all lie approximately fifty percent below the experimental results of Vroom and de Heer. The latter have been scaled by 0.8 as suggested by Mumma and Zipf[34] to correct for molecular radiation observed in the experiment. Because the experimental cross sections contain contributions from other states that produce H(1s) + H(2s), they are expected to be larger than the theoretical calculations. Figure 4 illustrates these results and shows the good agreement of the various theoretical treatments.

In Fig. 5 the effect of increasing the energy in molecular vibration (up to v=3) for the bound-bound X-B transition is shown. For this range of vibrational quanta the cross section doubles. In Fig. 6 the corresponding vibrational dependence for dissociative excitation is seen to be even greater, although the cross sections are smaller than for nondissociative excitation. The enhancement in both cases results form the larger Franck-Condon factors for the excited vibrational levels of the X state.

In Fig. 7 the vibrational dependence of the cross section for nondissociative X-B' excitation is shown. Instead of increasing monotonically with v, the v=1 and v=2 cross sections reverse order. The cross sections for dissociation to H(1s) + H(2s) in Fig. 8 are monotonically decreasing with v, in contrast to all of the other processes discussed here. Again, this behavior is primarily determined by the magnitude of the structural factor.

The impact parameter method as formulated in this work is capable of providing information on final-state vibrational distributions. In Fig. 9 we show vibrational distributions for both the B and B' states resulting from electron-impact excitation from the ground vibrational level of the X state. The two distributions reflect the difference in the number of

vibrational levels supported by the two excited electronic states. Both the B and B' distributions have maxima for v>0, indicating a preference for vibrationally inelastic processes.

Table VI presents the rotational temperature dependence of the X-B excitation of H_2 initially in the ground vibrational state. The cross section increases by approximately forty-five percent over the temperature range from zero to 20,000 K. The corresponding dissociative cross section (not shown) to form H(1s) + H(2p) increases by thirty percent over the same range of temperatures. For v=0 the dissociation cross section has a maximum for 300 K of 2.9×10^{-19} cm^2 at 50 eV compared to 5.6×10^{-17} cm^2 for the bound-bound excitation. For the X-B transition bound-bound transitions dominate over bound-continuum processes regardless of rotational temperature or initial vibrational temperature. The effect of initial vibrational energy is much more significant than the effect of rotational temperature.

In Table VII the nondissociative excitation ccross section for the X-B' transition decreases monotonically with temperature. This is the opposite of the behavior seen in Table VI for the X-B transition. The explanation lies in the far fewer bound rotational states that can be supported by the B' electronic state. At higher temperatures, therefore, the tail of the Boltzmann distribution becomes severly truncated. The cross sections for dissociation through the B state, shown in Table VIII, increase monotonically with temperature. We also found this increase with temperature for the X-B dissociation cross sections. We are not reporting the latter since they are small in magnitude for v=0 (the only case studied when rotational motion was included) and the trends follow those for the B' state.

V. CONCLUSIONS

The purpose of this work was to extend the impact parameter method for diatomic molecules to permit a realistic treatment of vibrational and rotational motion and to allow the study of dissociative processes. To test the theory, applications were made to nondissociative excitation of the B state of H_2 and to dissociation to H(1s) + H(2s) via the B' state. Agreement with previous theoretical results is generally good. Comparison with experiment was hampered by the lack of direct experimental information for the processes we studied. However, the magnitudes of the theoretical cross sections are very consistent with our understanding of the processes probed by the experiments. New results from this work include the dependence on initial vibrational state and rotational temperature of nondissociative and dissociative processes involving the X, B, and B' states of H_2. While the dependence of the cross sections on initial rotational temperature is modest, we find that increasing initial vibrational energy can have a dramatic effect on the cross sections. There is to our knowledge no experimental data providing information on the effect of internal energy on the processes reported here. However, the trends we find concerning the effect of internal energy on dissociation are similar to those seen in dissociative attachment processes in H_2.[52,53]

In summary, the impact parameter theory presented here should be useful in studying the effect of internal energy in excitation and dissociation processes in diatomic molecules. It is a first order theory, and thus is most valid at high energies, i.e. at some distance above threshold. It is also best applied to qualitative studies of integral cross sections. Applications of the methods developed here to heavier diatomic molecules are given in the following paper[50] and in forthcoming publications.[54,55]

ACKNOWLEDGEMENT

This research was supported by the Air Force Wright Aeronautical Laboratories, Aero Propulsion Laboratory, Air Force Systems Command, United States Air Force, Wright-Patterson AFB, Ohio 43433 under Contract No. F33615-82-C-2241.

REFERENCES

. G. J. Schultz in Principles of Laser Plasmas, edited by B. Bekefi (Wiley, New York, 1976), p. 33.

. See for example, Abstracts of Contributed Papers, XIIth ICPEAC (Berlin, West Germany, 1983); S. Trajmar and D. C. Cartwright in Electron-Molecule Interactions and their Applications, Volume 1, edited by L. G. Christophorou (Academic Press, Inc., New York, 1984), P. 155.

. Electron-Molecule and Photon-Molecule Collisions, edited by T. Rescigno, V. McKoy, and B. Schneider (Plenum, New York, 1979).

. N. F. Lane, Rev. Mod. Phys. 52, 29 (1980).

. Electron-Atom and Electron-Molecule Collisions, edited by J. Hinze (Plenum, New York, 1983).

. S. P. Khare and B. L. Moiseiwitsch, Proc. Phys. Soc. London 88, 605 (1966).

. S. P. Khare, Phys. Rev. 157, 107 (1967).

. K. J. Miller and M. Krauss, J. Chem. Phys. 47, 3754 (1967).

. M. Inokuti, Rev. Mod. Phys. 43, 297 (1971).

. D. C. Cartwright, Phys. Rev. A. 2, 1331 (1970); 5, 1974 (1972).

. S. Chung and C. C. Lin, Phys. Rev. A 6, 988 (1972); 9, 1954 (1974).

. S. Chung, C. C. Lin, and E. T. P. Lee, Phys. Rev. A. 12, 1340 (1975).

. C. W. McCurdy and V. McKoy, J. Chem. Phys. 61, 2820 (1974).

. T. N. Rescigno, C. F. Bender, and V. McKoy, J. Phys. B. 8, L433 (1975).

. G. P. Arrighini, F. Biondi, C. Guidotti, A. Biagi, and F. Marinelli, Chem. Phys. 52, 133 (1980).

. S. Chung and C. C. Lin, Phys. Rev. A 17, 1874 (1978).

. C. A. Weatherford, Phys. Rev. A 22, 2519 (1980).

. T. K. Holly, S. Chung, C. C. Lin, and E. T. P. Lee, Phys. Rev. A 26, 1852 (1982).

19. T. K. Holly, S. Chung, C. C. Lin, and E. T. P. Lee, Phys. Rev. A. 24, 2946 (1981).

20. T. N. Rescigno, C. W. McCurdy, V. McKoy, and C. F. Bender, J. Phys. B. 8, 216 (1976).

21. T. N. Rescigno, C. W. McCurdy, V. McKoy, and C. F. Bender, Phys. Rev. A 13, 216 (1976).

22. A. W. Fliflet, Ref. 1, p. 87.

23. A. W. Fliflet and V. McKoy, Phys. Rev. A 21, 1863 (1980).

24. A. W. Fliflet, V. McKoy, and T. N. Rescigno, J. Phys. B. 12, 3281 (1979).

25. A. W. Fliflet, V. McKoy, and T. N. Rescigno, Phys. Rev. A 21, 788 (1980).

26. L. Mu-Tao, R. R. Lucchese, and V. McKoy, Phys. Rev. A 26, 3240(1982).

27. B. D. Buckley and P. G. Burke, Ref. 1, p. 133.

28. M. J. Seaton, Proc. Phys. Soc. London 79, 1105 (1962).

29. A. D. Stauffer and M. R. C. McDowell, Proc. Phys. Soc. London 85, 61, (1965); 89, 289 (1966).

30. A. W. Hazi, Phys. Rev. A 23, 2232 (1981).

31. A. W. Hazi, T. N. Rescigno, and A. E. Orel, Appl. Phys. Lett. 35, 477 (1979).

32. S. K. Srivastava and S. Jensen, J. Phys. B. 10, 3341 (1978).

33. D. A. Vroom and F. J. de Heer, J. Chem. Phys. 50 580 (1969).

34. M. J. Mumma and E. C. Zipf, J. Phys. Chem. 55, 1661 (1971).

35. M. J. Seaton, Proc. Phys. Soc. London, 79, 1105 (1962).

36. A. D. Stauffer and M. R. C. McDowell, Proc. Phys. Soc. London, 85, 61 (1965); 89, 289 (1966).

37. M. Shugard and A. Hazi, Phys. Rev. A 12, 1895 (1975).

38. G. Herzberg, Molecular Spectra and Molecular Structure, (Van Nostrand, New York, 1950).

D. M. Brink and G. R. Satchler, Angular Momentum, (Clarendon Press, Oxford, 1968).

G. Arfken, Mathematical Methods for Physicists, (Academic Press, New York, 1968) p. 453.

M. E. Rose, Elementary Theory of Angular Momentum, (Wiley, New York, 1957).

Handbook of Mathematical Functions, edited by M. Abramowitz and I. A. Stegun, (U. S. Department of Commerce, Washington, DC, 1972).

W. Kolos and L. Wolniewicz, J. Chem. Phys. 43, 2429 (1965).

W. Kolos and L. Wolniewicz, J. Chem. Phys. 45, 509 (1966).

R. J. Spindler, Jr., J. Quant. Spectrosc. Radiat. Transfer 9, 1041 (1969).

N. C. Blais and D. G. Truhlar, J. Chem. Phys. 65, 5335 (1977).

L. Wolniewicz, J. Chem. Phys. 51, 5002 (1969).

A. L. Ford, J. C. Browne, E. J. Shipsey, and P. DeVries, J. Chem. Phys. 63, 362 (1975).

J. W. Cooley, Math. Comput. 15, 363 (1961).

B. C. Garrett, L. T. Redmon, C. W. McCurdy, and M. J. Redmon, Phys. Rev. A 00, 0000 (1985).

D. W. Schwenke, G. Staszewska, and D. G. Truhlar, J. Chem. Phys. 78, 275 (1983).

M. Allan and S. F. Wong, Phys. Rev. Lett. 41, 1791 (1978).

J. M. Wadehra and J. N. Bardsley, Phys. Rev. Lett. 41, 1795 (1978).

B. C. Garrett, L. T. Redmon, and M. J. Redmon, submitted to Phys. Rev. A.

M. J. Redmon, B. C. Garrett, and L. T. Redmon, submitted to Appl. Phys. Lett.

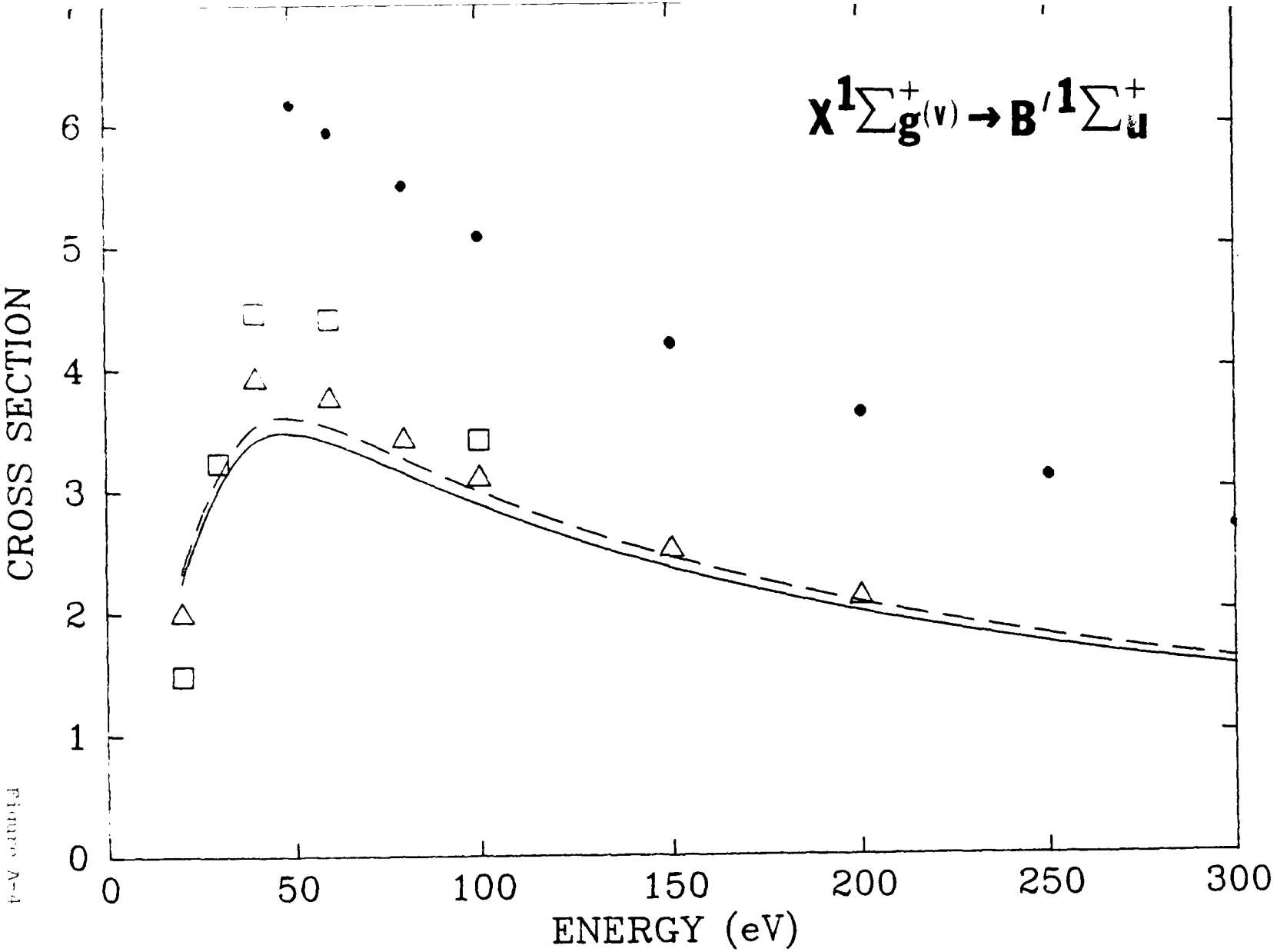
$X^1\Sigma_{g(v)}^+ \rightarrow B'^1\Sigma_u^+$
CROSS SECTION
ENERGY (eV)
0
1
2
3
4
5
6
0
50
100
150
200
250
300

Figure A-4

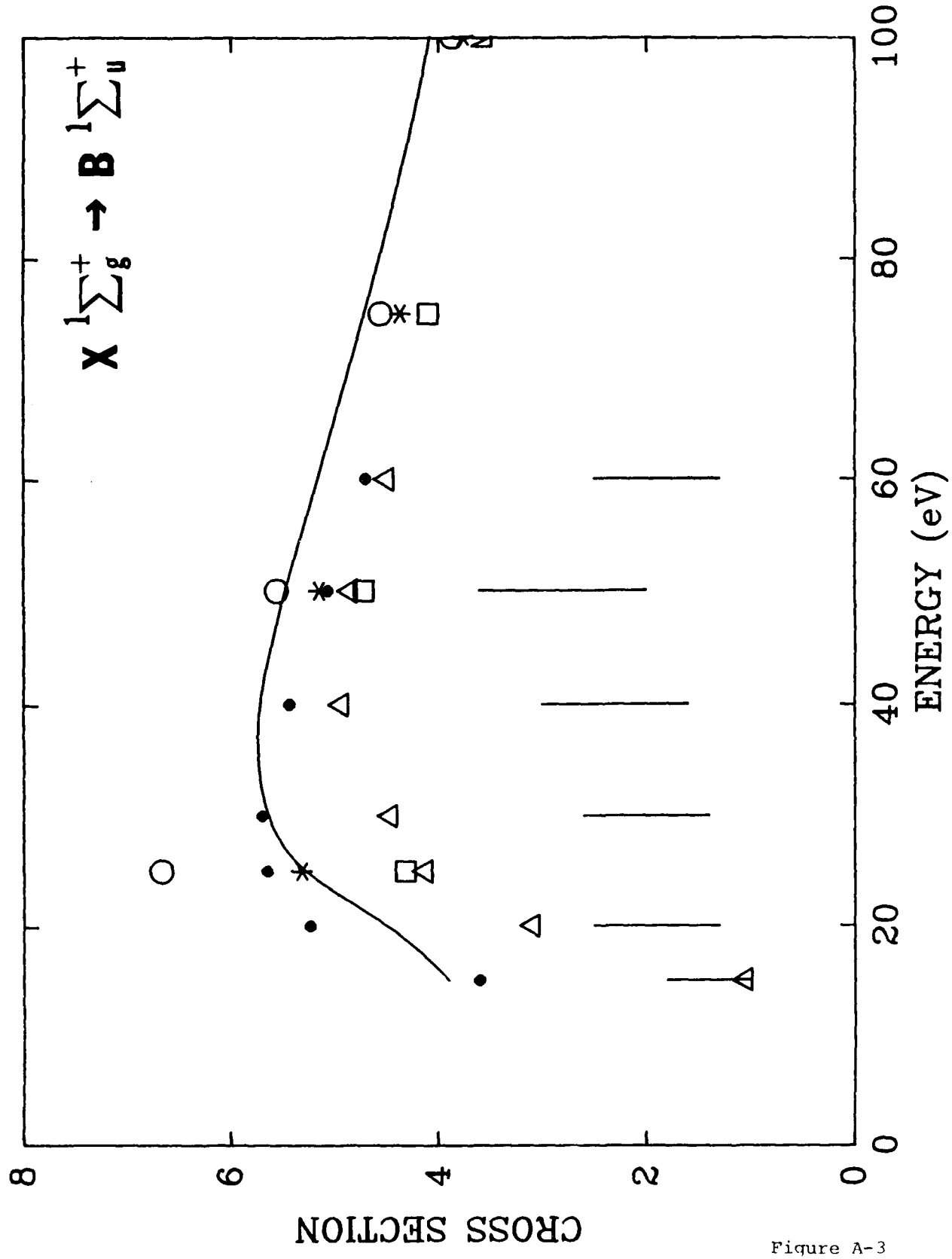
X $^1\Sigma_g^+$ → B $^1\Sigma_u^+$
CROSS SECTION
ENERGY (eV)
0
2
4
6
8
0
20
40
60
80
100

Figure A-3

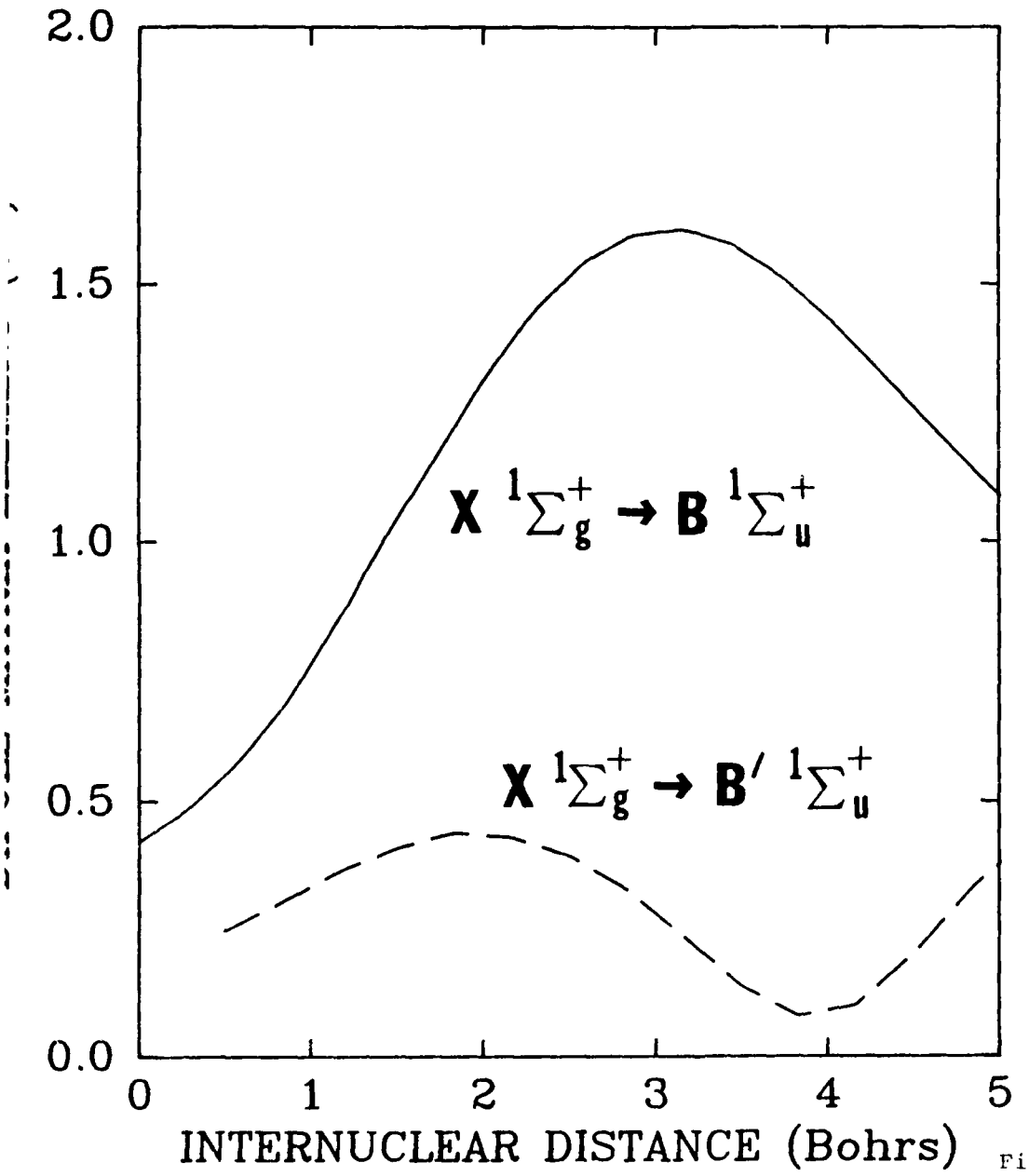
2.0
1.5
1.0
0.5
0.0
0
1
2
3
4
5
INTERNUCLEAR DISTANCE (Bohrs)
X $^1\Sigma_g^+ \rightarrow$ B $^1\Sigma_u^+$
X $^1\Sigma_g^+ \rightarrow$ B′ $^1\Sigma_u^+$

Figure A-2

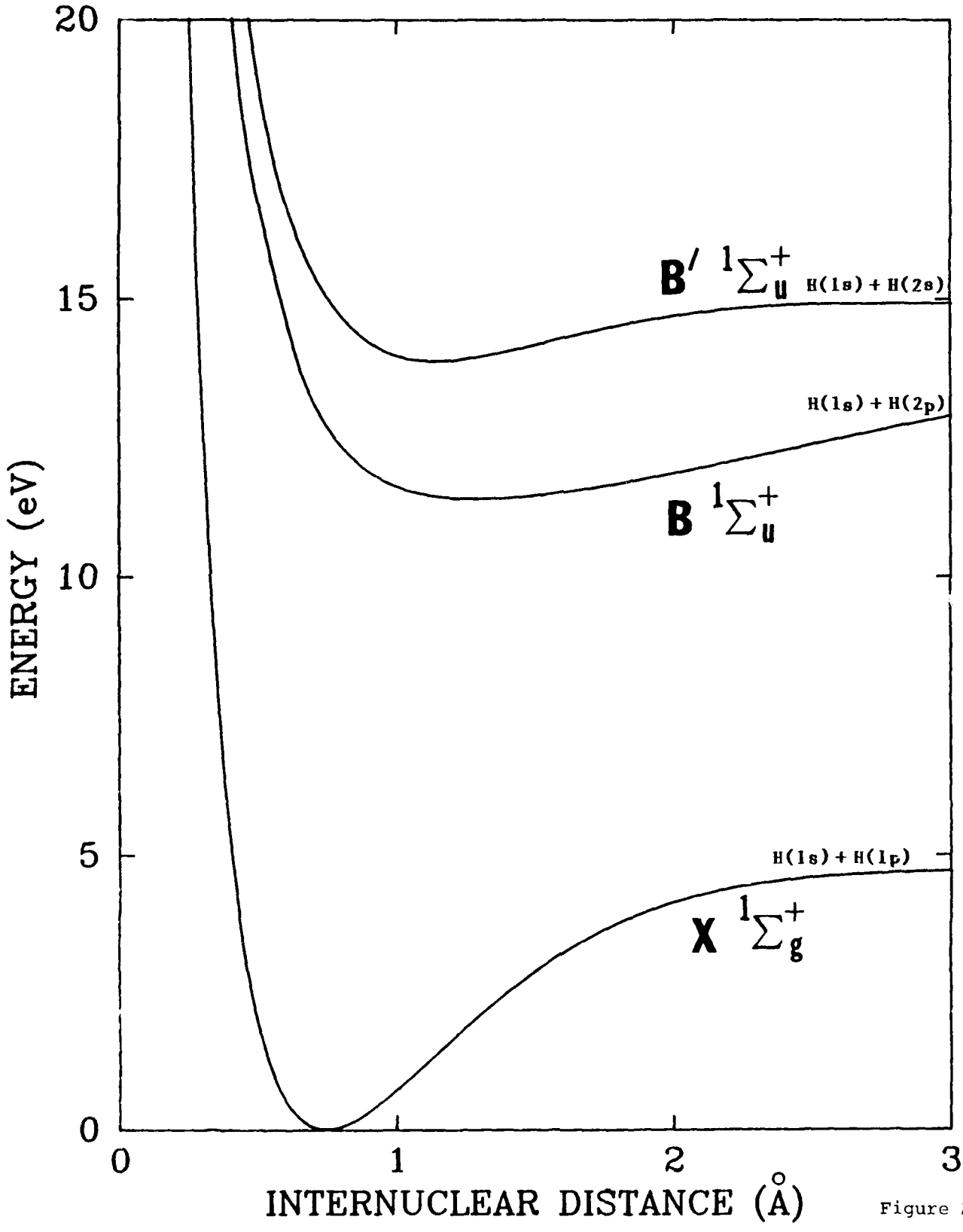
20
15
10
5
0
ENERGY (eV)
0
1
2
3
INTERNUCLEAR DISTANCE (Å)
B′ $^1\Sigma_u^+$
H(1s) + H(2s)
H(1s) + H(2p)
B $^1\Sigma_u^+$
H(1s) + H(1p)
X $^1\Sigma_g^+$

Figure A-1

represent the Born-Rudge results of Ref. 12 and the triangles represent the L^2 distorted-wave results of Ref. 23. The experimental results of Ref. 30 (multiplied by 0.8 according to the recommendation of Ref. 31) are shown as bullets. The experimental results include contributions from states other than B' $^1\Sigma_u^+$.

5. Dependence of the cross section (summed over final vibrational states) for excitation of the B $^1\Sigma_u^+$ state on initial vibrational quantum number (in units of 10^{-17} cm^2). The solid curve represents v=0, the dashed curve v=1, the long dash-short dash curve v=2, and the long dash curve v=3.

6. Dependence on initial vibrational quantum number of the electron impact dissociation cross section to produce H(1s) + H(2p) via the B $^1\Sigma_u^+$ state of H_2 (in units of 10^{-18} cm^2). The solid curve represents v=0, the dashed curve v=1, the long dash-short dash curve v=2, the long dash curve v=5, and the long dash-double short dash curve v=10.

7. Dependence of the cross section (summed over final vibrational states) for excitation of the B' $^1\Sigma_u^+$ state on initial vibrational quantum number. (in units of 10^{-18} cm^2). The solid line represents v=0, the dashed line v=1, the long dash-short dash curve v=2, and the long dash curve v=3.

8. Dependence on initial vibrational quantum number of the electron impact dissociation cross section to produce H(1s) + H(2s) via the B' $^1\Sigma_u^+$ state of H_2 (in units of 10^{-18} cm^2). The solid curve represents v=0, the long dash-short dash v=1, the long dash curve v=2, and the short dash curve v=3.

9. Final vibrational distributions (in units of cm^2) of the B $^1\Sigma_u^+$ and B' $^1\Sigma_u^+$ states of H_2 resulting from electron impact excitation of the X $^1\Sigma_u^+$ (v=0) state.

FIGURE CAPTIONS

1. Potential energy curves for the three states of H_2 studied in this work. The X $^1\Sigma_g^+$ and B $^1\Sigma_u^+$ potentials are fits to the calculations of Kolos and Wolniewicz (Ref. 40 and Ref. 41, respectively), while the B' $^1\Sigma_u^+$ potential is a fit to the data of Spindler (Ref. 42).

2. Dipole matrix elements used in the calculations. The matrix element for the X $^1\Sigma_g^+$ to B $^1\Sigma_u^+$ transition is a fit to the calculation of Wolniewicz (Ref. 44) while that for the X $^1\Sigma_g^+$ to B' $^1\Sigma_u^+$ transition is a fit to the calculation of Ford (Ref. 45).

3. Electron-impact excitation cross sections (units of 10^{-17} cm^2) for the X $^1\Sigma_g^+$ (v=0) to B $^1\Sigma_u^+$ transition in H_2. The solid curve represents the results (summed over final vibrational states) of the present impact-parameter IPV cross section [Eq. (31)] with the Franck-Condon approximation used to evaluate the vibrational integrals. The circles and bullets are the results of Born approximation calculations (Ref. 16 and Ref. 20, respectively). The triangles are from the L^2 distorted wave calculations of Ref. 20. The asterisks are the Born-Ochkur calculations of Ref. 16, and the squares are the results of two-state close-coupling calculations. The vertical lines represent error bars for the experimental results of Ref. 29.

4. Electron-impact dissociation cross sections (in units of 10^{-18} cm^2) for production of H(1s) + H(2s) via excitation of the B' $^1\Sigma_u^+$ (v=0) state of H_2. The solid curve is the result of applying the IPVD method of Section II.B with accurate numerical evaluation of the integrals over vibrational wavefunctions. The dashed curve represents the IPVD result when the Franck-Condon approximation is used to evaluate the integrals. The squares

TABLE A-VIII. Rotational temperature dependence of the cross section for dissociation of H_2 through the B′ state.[a]

	Temperature (Kelvin)					
E(eV)	0	4.2	300	1000	5000	20000
20	2.28	2.28	2.31	2.40	2.77	2.96
30	3.06	3.06	3.11	3.24	3.77	4.04
40	3.46	3.46	3.51	3.65	4.21	4.49
50	3.52	3.52	3.57	3.70	4.25	4.53
60	3.45	3.45	3.49	3.62	4.14	4.41
80	3.19	3.19	3.23	3.34	3.81	4.05
100	2.92	2.92	2.96	3.06	3.48	3.69
150	2.38	2.38	2.42	2.50	2.84	3.00
200	2.02	2.02	2.04	2.12	2.40	2.54
250	1.76	1.76	1.78	1.84	2.08	2.20
300	1.56	1.56	1.58	1.63	1.85	1.95

[a] Cross sections are in units of 10^{-18} cm^2.

TABLE A-VII. Rotational temperature dependence of the cross section for electronic excitation to the B′ state of H_2.[a]

	Temperature (Kelvin)					
E(eV)	0	4.2	300	1000	5000	20000
20	2.10	2.10	2.10	2.14	1.87	1.65
30	2.90	2.90	2.89	2.94	2.57	2.27
40	3.15	3.15	3.14	3.19	2.78	2.44
50	3.13	3.13	3.12	3.17	2.75	2.42
60	3.03	3.03	3.01	3.06	2.65	2.32
80	2.82	2.82	2.74	2.78	2.41	2.12
100	2.50	2.50	2.49	2.52	2.18	1.92

[a] Cross sections from Eq. (29) are in units of 10^{-18} cm^2.

TABLE A-VI. Rotational temperature dependence of the cross section for electronic excitation to the B state of H_2.[a]

	Temperature (Kelvin)					
E(eV)	0	4.2	300	1000	5000	20000
15	3.87	3.87	3.89	3.94	4.31	5.53
20	4.47	4.46	4.49	4.57	5.15	6.83
25	5.25	5.24	5.27	5.37	5.97	7.63
30	5.61	5.60	5.63	5.72	6.31	7.93
35	5.72	5.70	5.74	5.82	6.39	7.91
40	5.68	5.67	5.71	5.79	6.32	7.75
45	5.58	5.57	5.60	5.68	6.19	7.54
50	5.45	5.44	5.47	5.54	6.02	7.29
60	5.14	5.14	5.15	5.23	5.66	6.81
80	4.55	4.55	4.57	4.63	5.00	5.95
100	4.07	4.06	4.08	4.14	4.45	5.27

[a] Cross sections from Eq. (29) are in units of 10^{-17} cm^2.

TABLE A-V. Electron impact dissociation cross sections for production of H(1s) + H(2s) via excitation to the B′ state of H_2.[a]

E(eV)	BR[b]	DW[c]	IPVD(FC)[d]	IPVD[e]	EXP.[f]
20	1.98	1.48	2.32	2.24	
30		3.23	3.12	3.02	
40	3.91	4.46	3.54	3.41	
50			3.60	3.47	6.17
60	3.75	4.41	3.52	3.40	5.94
70			3.40	3.28	
80	3.41		3.26	3.14	5.50
90			3.12	3.00	
100	3.09	3.41	2.99	2.88	5.08
150	2.50		2.44	2.35	4.19
200	2.10		2.07	1.99	3.62
250			1.80	1.73	3.10
300			1.60	1.54	2.69

[a] Cross sections are in units of 10^{-18} cm^2. Results are for 0 K.

[b] Born-Rudge results of Ref. 12.

[c] L^2 distorted-wave results of Ref. 26.

[d] Impact parameter results with IPVD cross section from Eq. (42) evaluated using the Franck-Condon approximation for vibrational integrals.

[e] Impact parameter results with IPVD cross section from Eq. (42) with the vibrational integrals evaluated numerically.

[f] Experimental results of Ref. 33 scaled by 0.8 according to the recommendation of Ref. 34. The experimental cross section contains contributions from states other than B′.

TABLE A-IV. Cross sections for electron impact excitation from the X to the B′ state of H_2.[a]

E(eV)	Born[b]	DW[c]	IP[d]	IPV(FC)[e]	IPV[f]
20	8.88	1.7	4.03	1.93	2.14
30		3.9	5.49	2.66	2.95
40		4.8	6.19	2.89	3.21
50	9.41	4.9	6.28	2.88	3.19
60		4.7	6.14	2.78	3.08
70		4.4	5.91	2.66	2.94
80		4.1	5.79	2.53	2.80
90		3.8	5.42	2.41	2.67
100	6.75	3.4	5.18	2.30	2.54

[a] Cross sections are in units of 10^{-18} cm^2. Results are for 0 K.

[b] Born Results of Ref. 15.

[c] L^2 distorted-wave results interpolated from Fig. 4 of Ref. 26.

[d] Impact parameter IP results from Eq. (32) corresponding to the original method of Hazi [Ref. 30] which assumes vibrational degeneracy. Continuum contributions, implicit in this method, are large for this case.

[e] Impact parameter results with the IPV cross section of Eq. (31). The vibrational integrals are evaluated using the Franck-Condon approximation.

[f] Impact parameter results with the IPV cross section of Eq. (31). The vibrational integrals are evaluated using numerical integration.

TABLE A-III. A comparison of various impact-parameter approximations for the X to B excitation of H_2.[a]

E(eV)	IP[b]	IPV(FC)[c]	IPV[d]
15	3.47	3.61	3.87
20	3.83	4.10	4.47
25	4.58	4.84	5.25
30	4.95	5.19	5.61
35	5.09	5.29	5.72
40	5.08	5.27	5.68
45	5.01	5.18	5.58
50	4.90	5.06	5.45
55	4.78	4.93	5.30
60	4.64	4.79	5.14
70	4.39	4.51	4.84
75	4.26	4.37	4.69
80	4.14	4.25	4.57
85	4.02	4.12	4.42
90	3.91	4.01	4.30
95	3.81	3.90	4.18
100	3.71	3.80	4.07

[a] Cross sections are in units of 10^{-17} cm^2. Results are for 0 K.

[b] IP results of Eq. (32) corresponding to Hazi's method of Ref. 30. Continuum contributions (small in this case) are implicitly included.

[c] IPV results of Eq. (31) with the Franck-Condon approximation used to evaluate integrals over the vibrational wavefunctions.

[d] IPV results of Eq. (31) with the integrals over vibrational wavefunctions evaluated explicitly.

TABLE A-II. A comparison of the present impact-parameter results for the electron-impact excitation of the B-state of H_2 with other results.[a]

E(eV)	CC[b]	Born I[c]	BO[d]	DW[e]	Born II[f]	IPV[g]	Exp.[h]
15				1.05	3.60	3.61	1.4 ± 0.4
20				3.09	5.23	4.10	1.9 ± 0.6
25	4.31	6.66	5.31	4.12	5.64	4.84	
30				4.46	5.69	5.19	2.0 ± 0.6
40				4.93	5.43	5.27	2.3 ± 0.7
50	4.71	5.55	5.14	4.84	5.06	5.06	2.8 ± 0.8
60				4.49	4.70	4.79	1.9 ± 0.6
75	4.09	4.55	4.36			4.37	
100	3.58	3.87	3.76			3.80	

[a] Cross sections are in units of 10^{-17} cm^2. Results are for 0 K.

[b] Two-state close-coupling reslts of Ref. 16.

[c] Born results of Ref. 16.

[d] Born-Ochkur results of Ref. 16.

[e] L^2 distorted-wave results of Ref. 23.

[f] Born results of Ref. 23.

[g] IPV results of the present work from Eq. (31) with Franck-Condon evaluation of vibrational integrals.

[h] Experimental data from Ref. 32.

TABLE A-I. Nuclear spin degeneracy factors required for homonuclear diatomic molecules in sigma states.

	d_j	
	g^+ or u^- and 2I+1 even or g^- or u^+ and 2I+1 odd	g^- or u^+ and 2I+1 even or g^+ or u^- and 2I+1 odd
even j	(I+1)(2I+1)	I(2I+1)
odd j	I(2I+1)	(I+1)(2I+1)

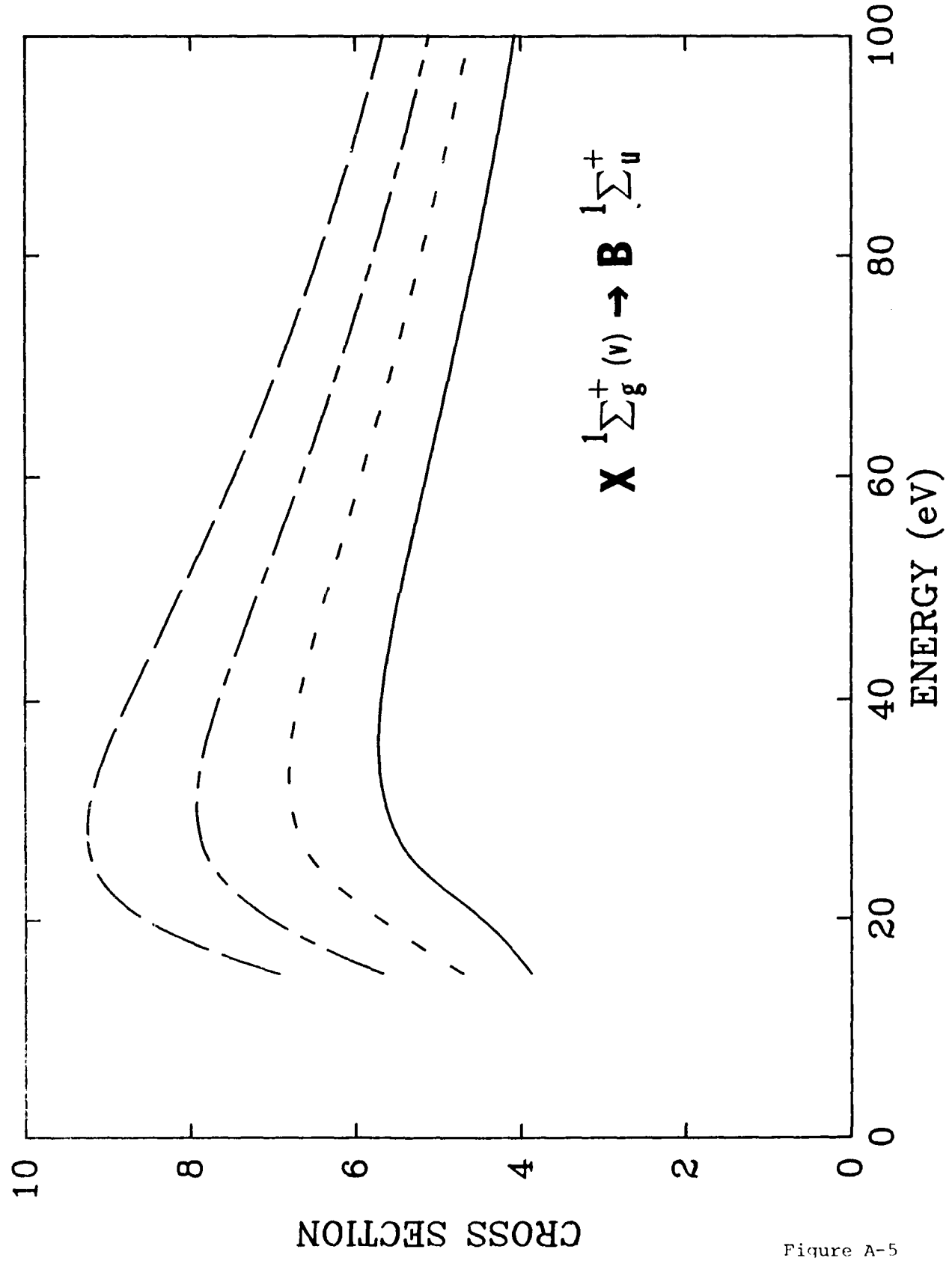
CROSS SECTION
10
8
6
4
2
0
0
20
40
60
80
100
ENERGY (eV)
X $^1\Sigma_g^+$ (v) → B $^1\Sigma_u^+$

Figure A-5

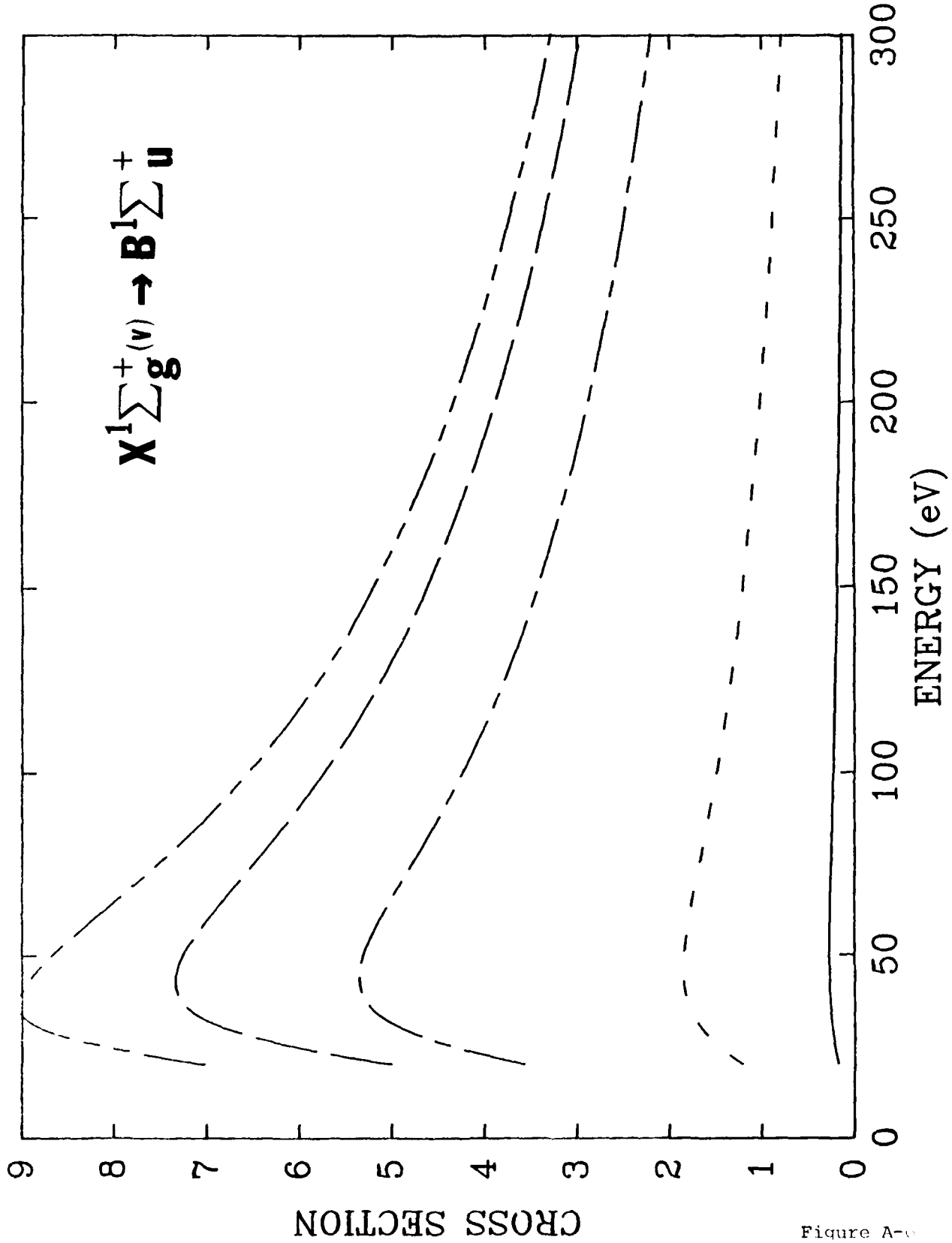
$X^1\Sigma_g^{+(v)} \rightarrow B^1\Sigma_u^+$
CROSS SECTION
ENERGY (eV)
0
1
2
3
4
5
6
7
8
9
0
50
100
150
200
250
300

Figure A-

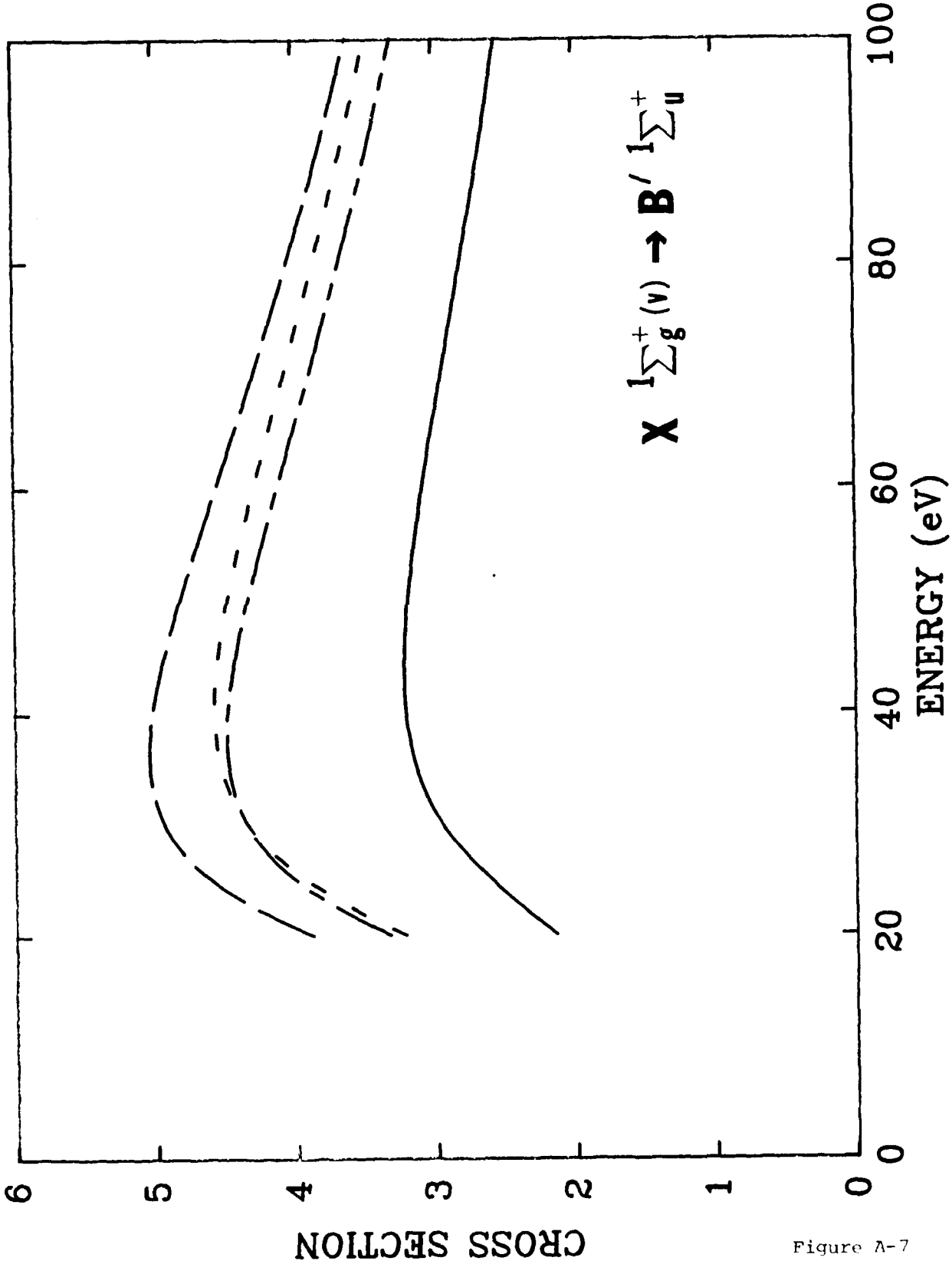
CROSS SECTION
0
1
2
3
4
5
6
0
20
40
60
80
100
ENERGY (eV)
X $^1\Sigma_g^+(v) \rightarrow B'\,^1\Sigma_u^+$

Figure A-7

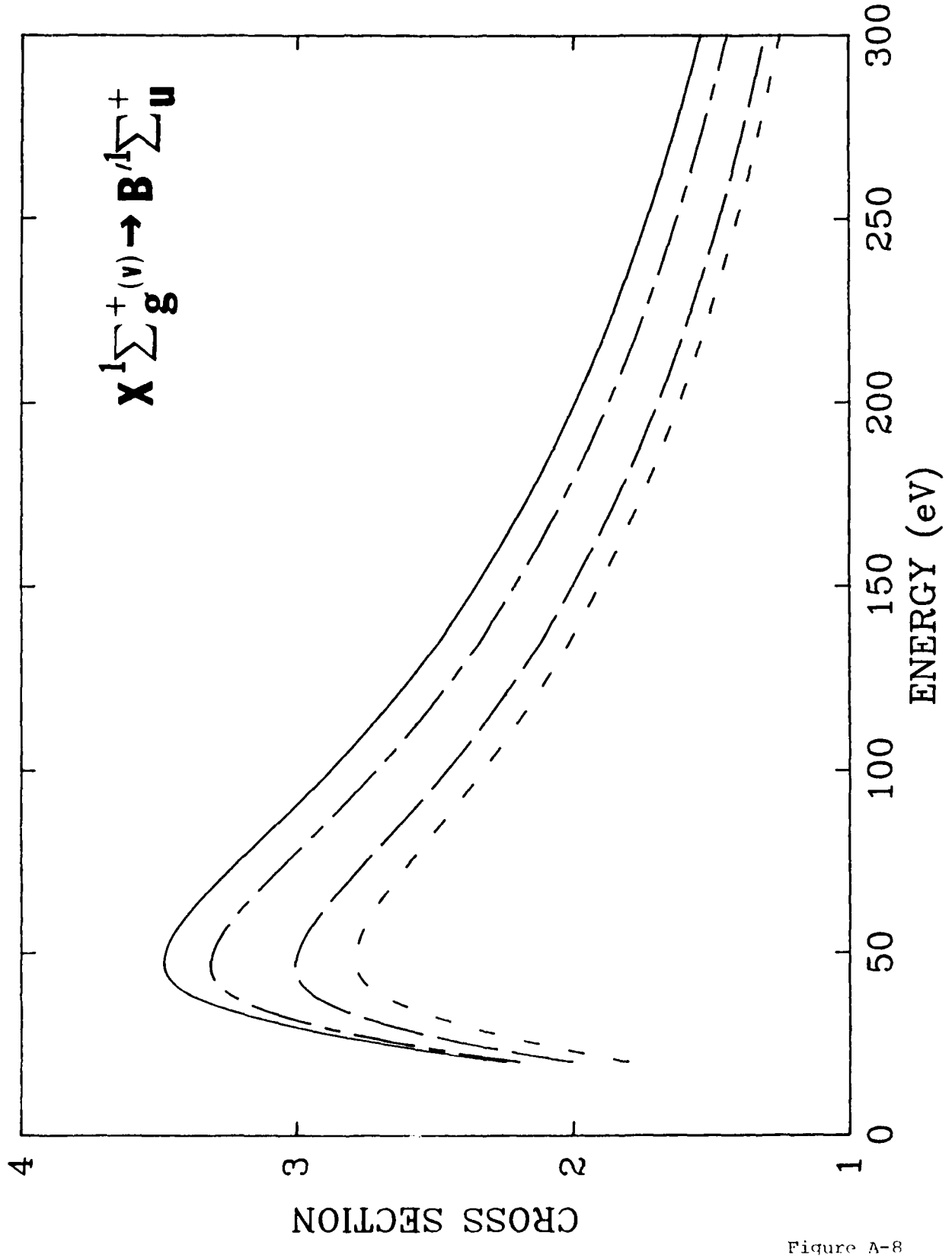
$X^1\Sigma_g^+(v) \rightarrow B'^1\Sigma_u^+$
CROSS SECTION
ENERGY (eV)
1
2
3
4
0
50
100
150
200
250
300

Figure A-8

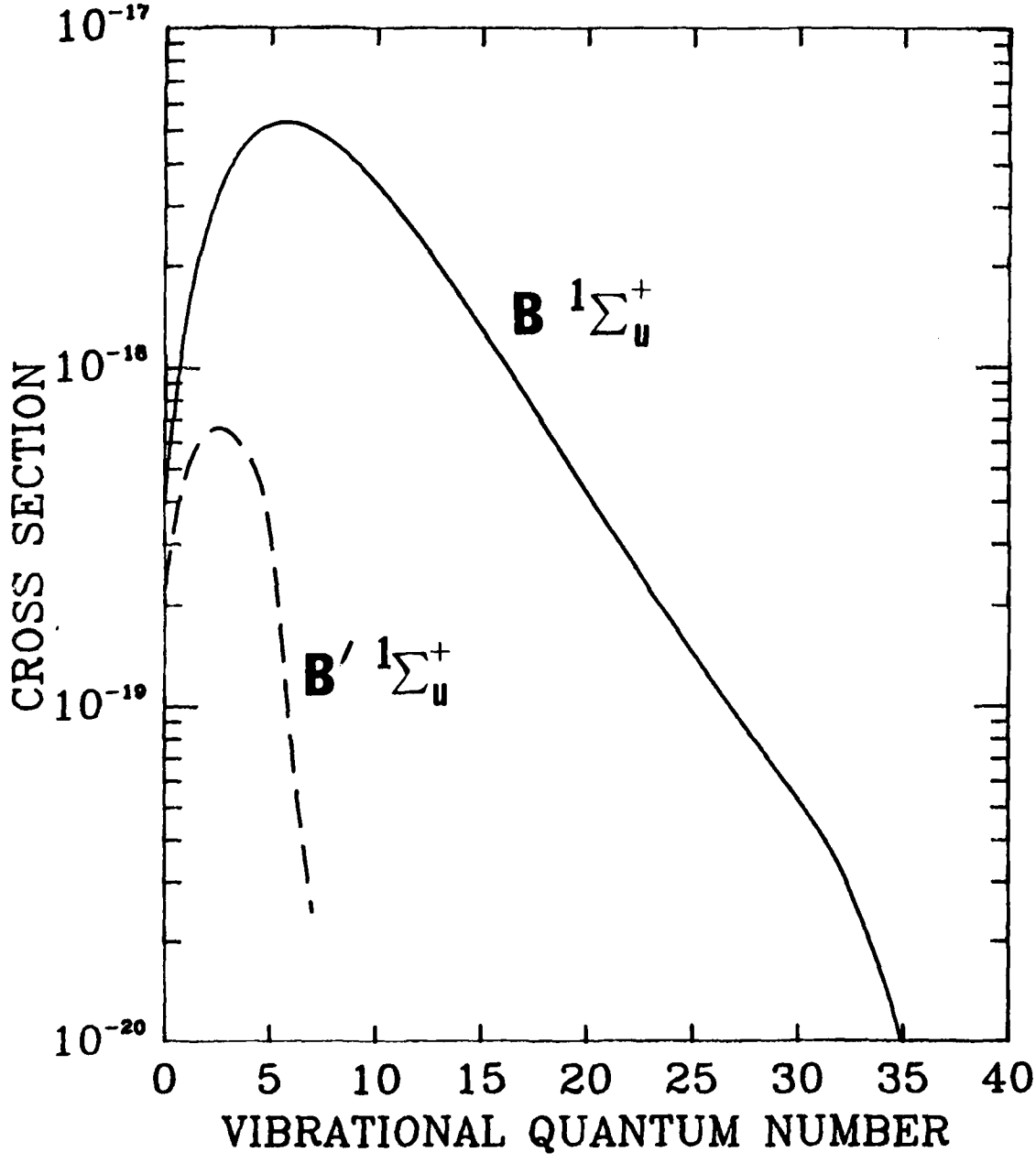
10^{-17}
10^{-18}
10^{-19}
10^{-20}
CROSS SECTION
B $^1\Sigma_u^+$
B′ $^1\Sigma_u^+$
0
5
10
15
20
25
30
35
40
VIBRATIONAL QUANTUM NUMBER

Figure A-9

APPENDIX B

MCSCF Calculations of the Potential Curves and Dipole Transition Moments for Low-Lying States of O_2 and S_2

by

L. T. Redmon and R. N. Diffenderfer

Chemical Dynamics Corporation
1550 West Henderson Road
Columbus, Ohio 43220

This paper describes multiconfiguration self-consistent field (MCSCF) calculations of potential energy curves for low-lying states of O_2 and S_2. The states of interest are those to which transitions from the ground state are dipole-allowed. The dipole transition moments are also presented here. The results of dynamical calculations of electron impact cross sections employing the present data are given elsewhere[1-2].

O_2

The potential curves for O_2 were obtained using a basis set of 44 atomic orbitals. This contracted set was designed by starting from Dunning's 4s 3p basis set[3], adding d orbitals with exponents of 1.21 and 0.2, and adding a set of diffuse p orbitals (with orbital exponents of 0.03) to describe the Rydberg character of these states. The first $^3\Pi_u$ and $^3\Sigma_u^-$ states have been shown[4-6] to become Rydberg-like at short internuclear distances as a result of avoided crossings of Rydberg and valence type diabatic states. In the case of the $^3\Pi_u$ states a multiconfiguration (MC) space consisting of the 48 terms resulting from the full excitation of the $2\sigma_g^2 2\sigma_u^2 3\sigma_g^2 1\pi_u^4 1\pi_g^1 3\sigma_u^1$ valence reference configuration into the $1\pi_g$ and $3\sigma_u$ orbitals is sufficient to describe the purely repulsive potential. The MCSCF method is even able to describe this state in its Rydberg region because of its ability to change the orbitals from valence to Rydberg type in order to satisfy its optimal variational requirements. However, the method would not be expected to describe both the upper and lower states in the avoided crossing region unless the MC space is expanded.

Since we have not obtained exact (full CI) results for the X and $^3\Pi_u$ states, the orbitals in terms of which they are described are not perfectly

orthogonal to each other. Our transition dipole moment codes require orthogonality. Therefore, there are two ways of obtaining matrix elements between these states. We can use the (optimal) ground state orbitals to obtain a nonoptimal (though variational) wavefunction for the pi state and then evaluate the moment, or we can use the pi-state orbitals to obtain a ground state wavefunction. In practical cases, two different values of the dipole transition moment are obtained. As the MC space is enlarged, increasing the flexibility of the wavefunction, the discrepancy should decrease since, in the limit that the MC space becomes the full CI, all orbital choices give the same result. The transition dipole moments we report have been evaluated using the orbitals optimized for the upper state. Because the X-to-pi dipole transition moments were very small, no improved calculations were done.

On the other hand, the transition dipole moment between the X state and the $B^3\Sigma_u^-$ state has been shown[4,7] to be on the order of unity. The B state is known experimentally to be bound by 1.01 eV. However, MCSCF calculations for the B state (in the basis set described above) using a configuration space analogous to that used for the pi state calculations show no binding. The wavefunctions of ref. 7 for the B state are slightly better, but still rather poor in both the valence region and particularly in the Rydberg region, where their basis set is inadequate.

Our calculations on the B state were modelled after the selection of (19) configurations of ref. 7. We exclude their last two terms (by requiring that $2\sigma_u$ remain doubly occupied), but include a total of 158 configurations resulting from expanding the valence orbital space to include a set of 2π orbitals. Rather than using the CAS-MC (i.e., the full CI within this orbital space), configurations were allowed subject to (a) not more than one electron in the 2π orbitals and (b) a total of at least two electrons in $3\sigma_g$ and $3\sigma_u$.

With this MC space, the description of binding (relative to the $^3P + {}^1D$ asymptote) was improved considerably. Our value (relative to the total energy at a separation of 8 a_o) was 0.74 eV.

It is well known that avoided curve crossings can cause difficulties in the convergence of MCSCF wavefunctions because the solution at a preceding point on the potential curve is likely to be a relatively poor starting point when the character of the wavefunction has changed significantly. Moreover, we were able to obtain multiple solutions for certain values of the internuclear separation R. In particular, in preceding from large values of R to smaller ones, we obtained wavefunctions in to R = 2.1 a_o. Inside of this, convergence problems were encountered. After much difficulty, solutions were obtained for the Rydberg-like portion of the curve (as far in as R = 1.8 a_o). Following the solutions from small to large R-values, we obtained a solution higher in energy than the previous one at R = 2.281, and at R = 2.4 the solution returned to the one previously found. I.e., between R = 2.1 and 2.4 we have two solutions. The transition moment with the X state (using the B-state orbitals) is large for the "valence-diabatic" wavefunction and smaller for the Rydberg-like one. The ground state curve is less well described by the latter orbitals because of its valence character. If we choose to use the B-state orbitals from the solution with the lower total energy, we obtain a discontinuous curve for the transition moment (and for the ground state energy). We also know that using X-state-optimized orbitals to evaluate the transition moment will not be accurate either; it yields values similar to those of the valence-diabatic B-state orbitals. Thus, treatments which do not account for valence-Rydberg mixing cannot obtain correct values for the transition moment.

To improve the accuracy of the moments and the agreement between the values obtained with the two orbital sets, we expanded the MC space (using

:he same basis set) to 310 configurations. This expansion mainly involved ıdding single excitations to an additional set of pi orbitals; we also allowed :he $3\sigma_g 3\sigma_u$ pair to be only singly occupied. We redid the calculations for ℜ-values of 1.8-2.4 a_o. At R = 2.4 we were able to obtain an MC310 ıavefunction starting from the MC158 orbital solution. However, this new ;olution could not be used for smaller R. We redid the calculations for ℜ = 1.8 starting from the MC158 orbitals, and we were able to move to larger ℜ and obtain an energy which differed (from the point at R = 2.4 a_o) by only).0065 eV. The energy difference between the lowest values obtained from 1C310 and MC158 at R = 2.4 a_o is only 0.12 eV, so the dipole transition moments for larger R were calculated from the smaller MC.

The MC310 configuration space used for the B state also facilitates study of the $2^3\Sigma_u^-$ (or E state) potential, at least for R > 2.1 a_o. This curve comes in from the same asymptotic limit as the B state, but the potential is purely repulsive in the valence region. Near R = 2.75 a_o it undergoes an avoided crossing with the same Rydberg state that affects the B state near R = 2.25 a_o. In this case, a relative maximum occurs in the potential near R = 2.75 a_o. The curve then follows the Rydberg diabat until it must assume valence character near R = 2.25 a_o. At this point the magnitude of the transition moment rises dramatically to values approaching unity. Thus as has been previously observed,[4] the dipole transition moments to the B and E states undergo a crossing where their potentials have an avoided crossing. Unfortunately, difficulties in the MCSCF calculations occur for R < 2.05, probably indicating an avoided crossing with a second Rydberg state.

The results of the calculations are summarized graphically in Figure 1. The solid line marked by "X" and the dashed curve marked by dots are

MC48 calculations for the ground and pi states, respectively. The absolute values of the X to pi dipole transition moments (M) are marked by dots in the upper portion of the figure. The two sets of MC158 results for the B state are indicated by the open circles, and the dipole transition moment is marked accordingly. The MC310 calculations for the B and E states are marked by asterisks and squares, respectively. The long-dashed curve (marked with squares) is the ground state MC310 curve obtained using the E-state-optimized orbitals. The unmarked lines show the available RKR data for the X and B states, with the ground state minimum arbitrarily plotted at -149.8 au. A portion of the data for Fig. 1 are given in Table I.

S_2

A basis set of 54 atomic orbitals was used for S_2. It consisted of the 6s 4p contracted set of McLean and Chandler[8] augmented by a set of diffuse p functions[9] (exponent = 0.02) and a set of d orbitals with exponent 0.12.

Although S_2 and O_2 have analogous excited state spectra, the potential energy curves differ considerably in shape. The asymptotic limits are closer together in S_2, but the ground state is less bound than O_2. The diabatic Rydberg state is also shallower. As a result, no avoided crossing occurs in the first $^3\Pi_u$ state or the $B^3\Sigma_u^-$ state outside of R = 3.0 a_o. (Calculations without diffuse functions have been reported for these two states.[10] Calculations of Rydberg character in states of other symmetries have also appeared.[11]) As in O_2, the $2^3\Sigma_u^-$ state has a local minimum.

The total energy curves and dipole transition moments (from the ground state) for these three states are shown in fig. 2. Because the pi state

of greater importance in S_2 (for dynamical reasons[1]) calculations were e using the MC48 analogous to that for O_2 and using a 183 term MC. The ter orbital space was similar to that for the B state (analogous to the B state calculations), except that $6\sigma_g$ and $6\sigma_u$ orbitals were included itead of a 2π set and single excitations from $4\sigma_u$ were allowed. The dashed ve with data points marked by dots is from the smaller treatment, and one with pluses is from the MC183. The larger MC calculations are required order to obtain a very slight binding in this state.

The B state calculations employed a 162 term MC. This configuration ace was the same as the analogy to the MC158 for O_2, except that $5\sigma_g$ and $_u$ could be unoccupied. The B state data is marked by open circles, and e long-dashed curve is the ground state resulting from the B-state-optimized bitals.

When comparable MC's are used for the B and pi states, their energy rves nearly coincide over a significant range of R. This is in agreement th the experimental observation[12,13] of their interaction.

The calculations for the $2^3\Sigma_u^-$ state used 162 terms in the valence region d 310 terms in the Rydberg region. The data are marked by triangles and uares, respectively. The local minimum occurs at a shorter distance elative to the ground state equilibrium distance) than in O_2 because the state includes the minimum of the Rydberg diabatic state (whereas the B ate did in O_2). The location of this potential and the root-flipping fficulties encountered in the MCSCF calculations for smaller R indicate at interaction of the Rydberg diabat with the B state near R = 3.0 au is obable. We note that the magnitude of the dipole transition moment between is state and the ground state is significant for values of R near their nima. We expect that for values of $R < 3.0\ a_o$ the dipole transition moment the $2\ \Sigma_u^-$ state will probably be larger than that to the B state.

RKR data for the X and B states are indicated by solid unmarked lines dots. The X state minimum has been arbitrarily shifted to -795.15 au. Selected data from Fig. 2 are given in Table 2.

REFERENCES

B. C. Garrett, L. T. Redmon and M. J. Redmon, Phys. Rev. A, submitted (1984)

B. C. Garrett and L. T. Redmon, J. Chem. Phys., submitted (1984).

T. H. Dunning, Jr., J. Chem. Phys. 53, 2823 (1970)

R. J. Buenker and S. D. Peyerimhoff, Chem. Phys. 8, 324 (1975), Chem. Phys. Letter, 34, 225 (1975), ibid. 42, 383 (1976)

R. P. Saxon and B. Liu, J. Chem. Phys. 73, 876 (1980)

H. Tatewaki, K. Tanaka, S. Obara, F. Sasaki, K. Ohno, and M. Yoshimine, Prog. Rept. No. 9, Rsch. Group on At. and Mol. (Japan), P. 13 (1976)

P. S. Julienne, D. Neumann, and M. Krauss, J. Chem. Phys. 64, 2990 (1976)

A. D. McLean and G. S. Chandler, J. Chem. Phys. 72, 5639 (1980)

T. H. Dunning, Jr. and P. J. Hay, from Methods of Electronic Structure Theory, ed. by H. F. Schaefer, III, Plenum (1977)

W. C. Swope, Y.-P. Lee, and H. F. Schaefer, III, J. Chem. Phys. 70, 947 (1979)

R. P. Saxon and B. Liu, J. Chem. Phys. 73, 5174 (1980)

V. E. Bondybey and J. H. English, J. Chem. Phys. 69, 1865 (1978)

Y. Matsumi, T. Munakata, and T. Kasuya, J. Chem. Phys. 81, 1108 (1984)

AD-A154 827 VIBRATIONALLY ENHANCED DISSOCIATION OF DIATOMIC MOLECULES(U) CHEMICAL DYNAMICS CORP COLUMBUS OH B C GARRETT ET AL. MAY 85 CDTR-85-1 AFWAL-TR-85-2020 2/3

UNCLASSIFIED F33615-82-C-2241 F/G 7/4 NL

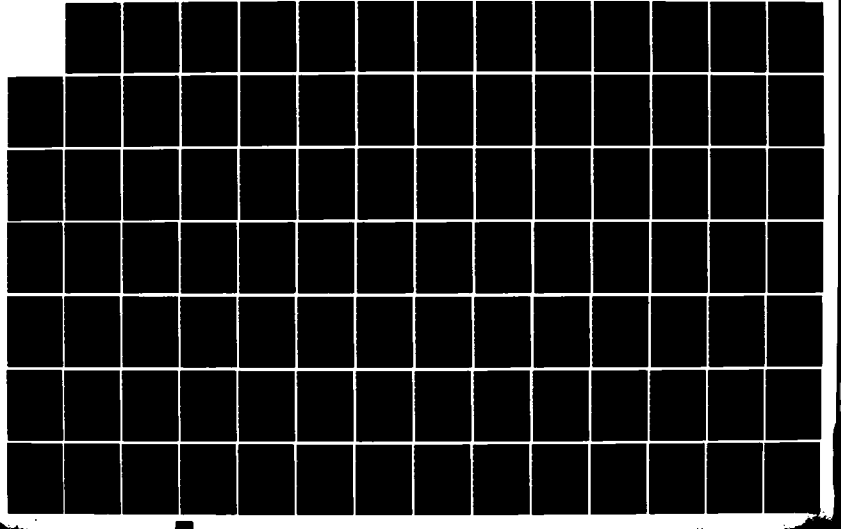

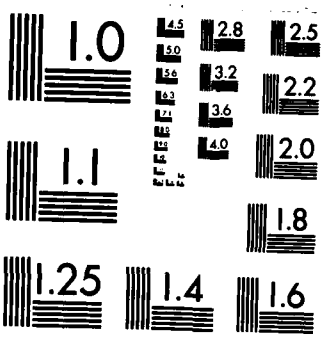

MICROCOPY RESOLUTION TEST CHART
NATIONAL BUREAU OF STANDARDS-1963-A

RKR data for the X and B states are indicated by solid unmarked lines dots. The X state minimum has been arbitrarily shifted to -795.15 au. Selected data from Fig. 2 are given in Table 2.

REFERENCES

1. B. C. Garrett, L. T. Redmon and M. J. Redmon, Phys. Rev. A, submitted (1984)
2. B. C. Garrett and L. T. Redmon, J. Chem. Phys., submitted (1984).
3. T. H. Dunning, Jr., J. Chem. Phys. 53, 2823 (1970)
4. R. J. Buenker and S. D. Peyerimhoff, Chem. Phys. 8, 324 (1975), Chem. Phys. Letter, 34, 225 (1975), ibid. 42, 383 (1976)
5. R. P. Saxon and B. Liu, J. Chem. Phys. 73, 876 (1980)
6. H. Tatewaki, K. Tanaka, S. Obara, F. Sasaki, K. Ohno, and M. Yoshimine, Prog. Rept. No. 9, Rsch. Group on At. and Mol. (Japan), P. 13 (1976)
7. P. S. Julienne, D. Neumann, and M. Krauss, J. Chem. Phys. 64, 2990 (1976)
8. A. D. McLean and G. S. Chandler, J. Chem. Phys. 72, 5639 (1980)
9. T. H. Dunning, Jr. and P. J. Hay, from Methods of Electronic Structure Theory, ed. by H. F. Schaefer, III, Plenum (1977)
10. W. C. Swope, Y.-P. Lee, and H. F. Schaefer, III, J. Chem. Phys. 70, 947 (1979)
11. R. P. Saxon and B. Liu, J. Chem. Phys. 73, 5174 (1980)
12. V. E. Bondybey and J. H. English, J. Chem. Phys. 69, 1865 (1978)
13. Y. Matsumi, T. Munakata, and T. Kasuya, J. Chem. Phys. 81, 1108 (1984)

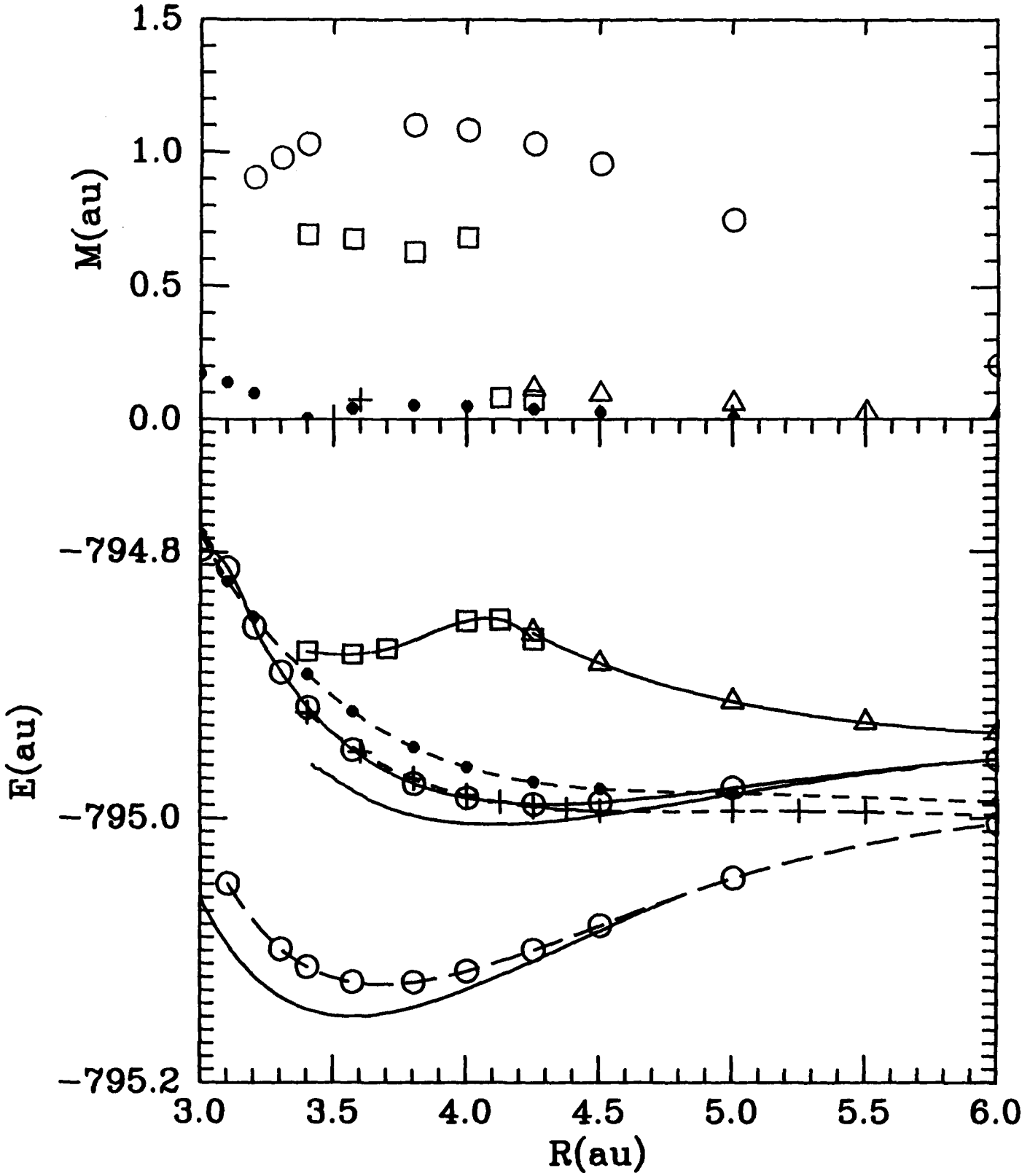

Figure B-1

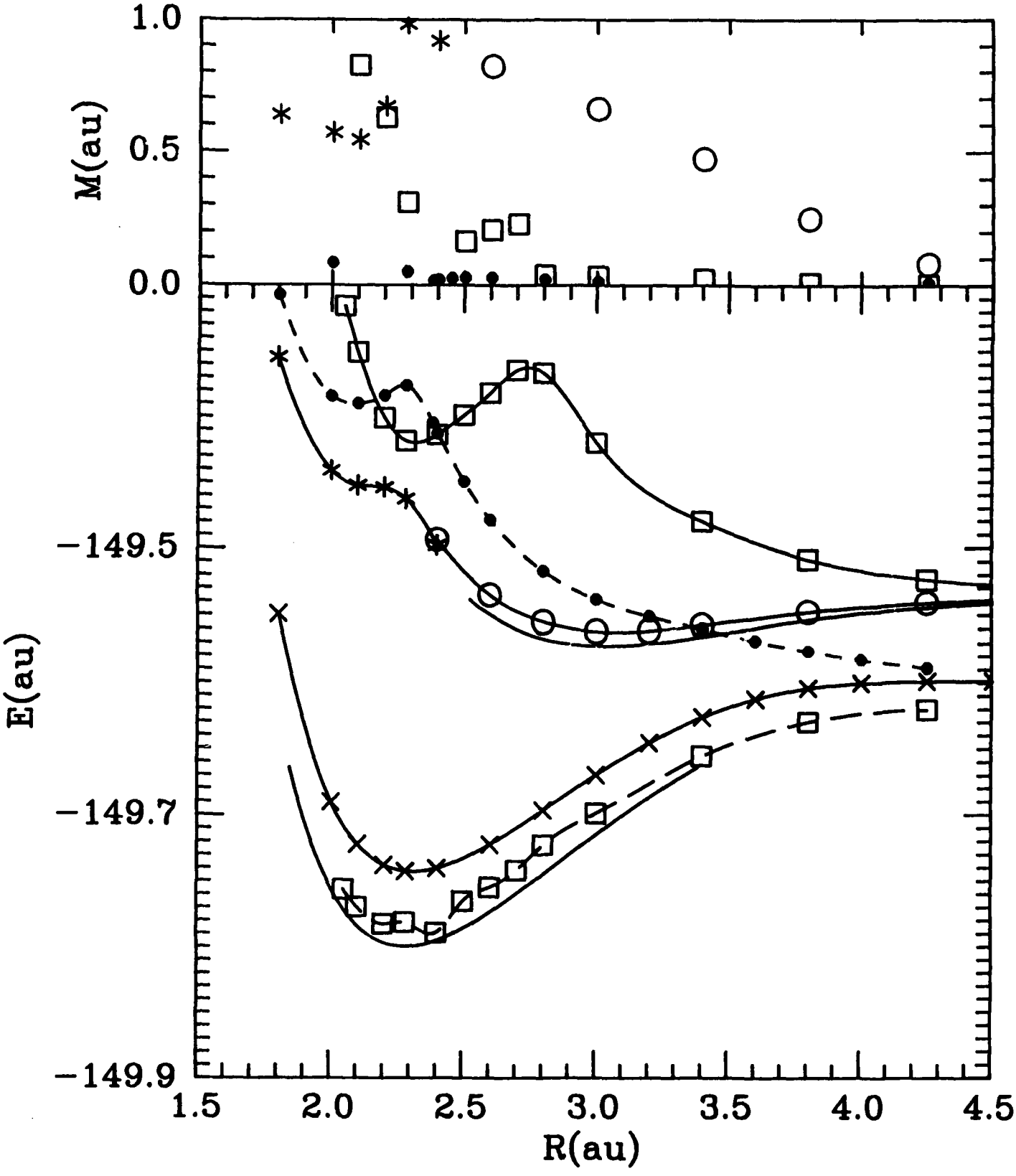

Figure B-2

APPENDIX C

The Effect of an Avoided Crossing on the O_2 Schumann-Runge Photodissociation Continuum

Bruce C. Garrett

Lynn T. Redmon, and Michael J. Redmon

Chemical Dynamics Corporation
1550 West Henderson Road
Columbus, Ohio 43220

Experimental observation of the O_2 Schumann-Runge photodissociation continuum dates back to the early work of Landenburg, Voorhis, and Boyce[1]. Since then, many photometric techniques have been applied to quantitative measurement of the absorption spectrum[2] and, more recently, an electron energy-loss spectrum has been measured for this system.[3] The absorption spectrum is asymmetric. It peaks near the transition energy of 8.61 eV and falls off rapidly for higher energies. The more recent experiments[3-5] show fine structure in the spectrum.

The first theoretical calculations of the O_2 $X^3\Sigma_g^-$ - $B^3\Sigma_u^-$ photodissociation continuum that were based on full potential energy curves were those by Jarmain and Nicholls[6] and Bixon, Rez, and Jortner[5]. These studies used realistic potentials for the bound part of the B state, but the repulsive parts of these potentials were extrapolations. Their computed continuum absorption spectra were much more symmetric than the observed spectrum. In an attempt to reproduce the rapid falloff at high transition energies, Allison[7] proposed that a part of the B-state potential was less repulsive than those previously used and that the dipole transition moment $M_{XB}(R)$ should decrease rapidly as the internuclear distance R decreased.

Bixon, Rez, and Jortner[5] attributed the fine structure in the absorption spectrum to continuum resonances resulting from the bound nature of the B-state potential. Jarmain and Nicholls[6] also used a bound potential for the B-state and observed no structure in their calculated Franck-Condon factors. Huebner et. al.[3] interpreted the small peaks at low energies as contributions from transitions to a $^3\Pi_g$ Rydberg state.

Since the last theoretical calculations on this system, <u>ab initio</u> potential energy curves for the B state V_B and the X-to-B dipole transition moment M_{XB} have been calculated as a function of R.[8,9] An avoided crossing

between the B and E states occurs near the X-state equilibrium geometry. This causes $V_B(R)$ to have a shoulder in its repulsive wall and $M_{XB}(R)$ to change rapidly in this region. We find that this shoulder in $V_B(R)$ is responsible for the rapid decrease and fine structure in the absorption spectrum at high energies.

In this paper we present continuum oscillator strengths df/dE as a function of transition energy ΔE calculated using the most accurate potential curves and dipole transition moments[10] available and compare them with the "apparent" df/dE obtained from the experiments of Huebner et. al.[3] The potential curves for the X and B states of O_2 are shown in Fig. 1 and described in reference 10. The bound parts of the potentials are from RKR data (see reference 2). The repulsive part of the B-state potential is from ab initio data[9] in to R = 1.8 a_o and is an extrapolation for smaller R. At R = 1.8 a_o the B-state potential energy is 11.6 eV above the ground-state vibrational energy in the X-state potential. The continuum oscillator strength goes to zero for energies above 10 eV; therefore, the potential is known over a sufficiently wide range of R for the present calculations.

The ab initio dipole transition moment[9] for the X-to-B transition $M_{XB}(R)$ is shown as the long-dashed curve in Fig. 1 and described in Ref. 10. As a test of the accuracy of the computed $M_{XB}(R)$ we calculated absolute oscillator strengths $f_{\nu'\nu''}$ for bound X-to-B transitions for ν'' = 0, 1, and 2 and ν' = 0 to 20. These are compared with experimental results[11,12] in Table I. The accurate calculations evaluate $f_{\nu'\nu''}$ by numerical integration (over R) of the product of the initial and final vibrational wavefunctions and $M_{XB}(R)$, and the Franck-Condon approximation assumes $M_{XB}(R)$ is constant and equal to its value at the equilibrium geometry of the X state. In general, the calculations employing the Franck-Condon approximation (FC) give oscillator

strengths which are smaller than the numerically accurate ones. For $v'' = 0$ and 1 the errors are systematic, both calculations underestimate experiment at low v' and overestimate at high v'. Therefore, the accurate results are better at low v' and the FC ones are better at high v'. The worst errors are for $v' = 17$; for $v'' = 0$ the accurate and FC results are too high by 43% and 23%, respectively, and for $v'' = 1$ the errors are 29% and 14%. For $v'<16$ the accurate results are within 17.5% for $v'' = 0$ and 8.5% for $v'' = 1$, and the errors are even smaller for $v'<10$. For $v'' = 2$ the errors are not as systematic but the accurate results agree within 24% and the FC results agree within 27%. For higher v', the vibrational wavefunction is determined by parts of the potential that are less accurately known, the vibrational wavefunction is more diffuse, and a greater range of $M_{XB}(R)$ is sampled. The overall agreement with experiment is acceptable, especially at low v', so $M_{XB}(R)$ should be sufficiently accurate for calculating nearly quantitative values of continuum oscillator strengths.

To elucidate the effect of the avoided crossing in the B-state potential on df/dE, calculations were also performed using a B-state potential curve in which the avoided crossing was removed. This curve was obtained by extrapolating the RKR data using the functional form $V_B(R) = \alpha R^{-1} \exp(-\beta R)$, where the parameters are determined by matching the points at the two smallest R values available. This model potential curve is shown as a dashed line in Fig. 1.

The computed df/dE are shown in Fig. 2; the solid and short-dashed curves are those obtained using the accurate and model potentials, respectively. These calculations are for transitions (of energy ΔE) from the ground vibrational level ($v'' = 0$) of the X-state to the B state; rotational motion is neglected. The results using the accurate B-state potential show a much

more rapid falloff at higher energies and also exhibit an interesting second peak past 9.0 eV. The results using the model B-state potential lack both these features and exhibit only the usual nearly symmetric single maximum.

The lack or presence of these features can be better understood by considering the overlap of the ground vibrational and continuum wavefunctions, $\chi_o(R)$ and $\chi_\varepsilon(R)$, respectively. For the model B-state potential, the major peak in $\chi_\varepsilon(R)$ shifts gradually to the left as the transition energy is increased. At energies near 7.1 eV, only the exponential tail of $\chi_\varepsilon(R)$ overlaps with $\chi_o(R)$ so df/dE is small. As the energy is increased the overlap increases as the major peak becomes centered over $\chi_o(R)$. The overlap then decreases because of negative contributions from the next peak in $\chi_\varepsilon(R)$. Near 9.4 eV df/dE goes to zero when the contributions perfectly cancel; above 9.4 eV df/dE remains small because of this cancellation.

The maximum in df/dE for the accurate potential occurs at a higher energy (than for the model potential) because the accurate potential is more repulsive for energies below 8.9 eV. The rapid drop in df/dE and its second maximum are better understood by examining Fig. 3 which shows $\chi_\varepsilon(R)$ for the transition energies 8.9, 9.04 and 9.14 eV, corresponding to the extrema in df/dE. As the energy is increased from the B-state energy at the avoided crossing (8.9 eV), $\chi_E(R)$ shifts rapidly to the left and its major peak moves from a position of favorable overlap to one of less favorable overlap with the ground-state vibrational wavefunction $\chi_o(R)$, accounting for the first maximum and zero of df/dE. The second peak in df/dE is caused by the overlap of the un-usually large second peak in $\chi_E(R)$ with $\chi_o(R)$.

In the previously described calculations of df/dE, we numerically integrated $M_{XB}(R)$, $\chi_o(R)$ and $\chi_E(R)$ over R. In Fig. 2 we also show the results of calculations employing the Franck-Condon approximation as the long-dashed

curves. Although there are quantitative changes in df/dE at low energies, the qualitative features discussed above are still present in these calculations. This indicates that these features are the result of the shape of $V_B(R)$ and do not depend strongly upon the shape of $M_{XB}(R)$.

To compare with the experimental results for df/dE, we average our computed df/dE over a 300 K and 1000 K distribution of initial vibrational and rotational states and sum over final orbital angular momentum,

$$\langle df/dE \rangle_T = Q_{vr}^{-1} \sum_{v_i j_i} e^{-\epsilon_{v_i j_i}/k_B T} \sum_{\ell_f} df_{v_i j_i \ell_f}/dE \qquad (1)$$

where the rovibrational partition function is given by

$$Q_{vr} = \sum_{v_i j_i} e^{-\epsilon_{v_i j_i}/k_B T} \qquad (2)$$

$\epsilon_{v_i j_i}$ is the rovibrational energy level of the X state for vibrational state v_i and rotational state j_i, k_B is Boltzmann's constant, and $df_{v_i j_i \ell_f}/dE$ is the continuum oscillator strength per unit energy for transition from state $v_i j_i$ of the X state to the B state with orbital angular momentum ℓ_f. (Note that only odd j states are allowed for the X state and $\Delta j = \pm 1$ transitions are optically allowed.) The computed $\langle df/dE \rangle_T$ for the accurate potential is compared with experiment[3] in Fig. 4. Although the calculated peak is a little too high and too narrow, the falloff at high energies is in qualitative agreement with experiment.

In conclusion, the rapid decrease of df/dE and the presence of structure at higher energies are due to an avoided crossing in the B-state potential curve. A rapid variation in $M_{XB}(R)$ is not necessary, as evidenced by the validity of the Franck-Condon approximation for this transition.

ACKNOWLEDGEMENT

This research was supported by the Air Force Wright Aeronautical Laboratories, Aero Propulsion Laboratory, Air Force Systems Command, United States Air Force, under contract no. F33615-82-C-2241.

$\nu''=$	0			1			2		
ν'	acc.[a]	FC[b]	exp.[c]	acc.[a]	FC[b]	exp.[c]	acc.[a]	FC[b]	exp.[c]
0	3.17E-10	3.15E-10	3.45E-10	8.77E-09	8.99E-09		1.16E-07	1.23E-07	
1	3.80E-09	3.73E-09	3.90E-09	9.53E-08	9.63E-08		1.13E-06	1.18E-06	
2	2.34E-08	2.26E-08	2.38E-08	5.31E-07	5.30E-07	5.35E-07	5.67E-06	5.83E-06	
3	9.84E-08	9.41E-08	9.90E-08	2.03E-06	2.00E-06	2.08E-06	1.95E-05	1.98E-05	
4	3.20E-07	3.03E-07	3.21E-07	6.02E-06	5.87E-06	6.15E-06	5.19E-05	5.21E-05	
5	8.60E-07	8.04E-07	8.52E-07	1.47E-05	1.42E-05	1.53E-05	1.14E-04	1.13E-04	
6	1.98E-06	1.83E-06	1.91E-06	3.10E-05	2.96E-05	3.15E-05	2.17E-04	2.13E-04	2.13E-04
7	4.00E-06	3.66E-06	3.81E-06	5.75E-05	5.42E-05	5.78E-05	3.63E-04	3.52E-04	3.39E-04
8	7.22E-06	6.56E-06	6.68E-06	9.55E-05	8.93E-05	9.40E-05	5.47E-04	5.26E-04	5.46E-04
9	1.18E-05	1.06E-05	1.06E-05	1.44E-04	1.34E-04	1.38E-04	7.50E-04	7.16E-04	9.87E-04
10	1.75E-05	1.56E-05	1.57E-05	1.99E-04	1.83E-04	1.91E-04	9.44E-04	8.94E-04	1.03E-03
11	2.38E-05	2.11E-05	2.09E-05	2.52E-04	2.30E-04	2.38E-04	1.10E-03	1.03E-03	1.04E-03
12	2.96E-05	2.60E-05	2.53E-05	2.94E-04	2.67E-04	2.73E-04	1.19E-03	1.11E-03	1.22E-03
13	3.38E-05	2.96E-05	2.88E-05	3.18E-04	2.87E-04	2.93E-04	1.20E-03	1.11E-03	1.04E-03
14	3.53E-05	3.08E-05	3.03E-05	3.17E-04	2.85E-04	2.95E-04	1.13E-03	1.04E-03	
15	3.38E-05	2.93E-05	2.92E-05	2.92E-04	2.61E-04	2.77E-04	9.84E-04	9.07E-04	
16	3.46E-05	2.99E-05	2.59E-05	2.89E-04	2.57E-04	2.42E-04	9.34E-04	8.58E-04	
17	3.19E-05	2.75E-05	2.23E-05	2.59E-04	2.30E-04	2.01E-04	8.07E-04	7.38E-04	
18	2.44E-05	2.10E-05	1.83E-05	1.94E-04	1.72E-04		5.87E-04	5.37E-04	
19	1.84E-05	1.58E-05	1.44E-05	1.44E-04	1.28E-04		4.28E-04	3.90E-04	
20	8.38E-05	7.19E-06		6.50E-05	5.75E-05		1.90E-04	1.74E-04	
$\sum_{19}$	3.09E-04	2.70E-04	2.55E-04	$\sum_{17}$ 2.57E-03	2.33E-03	2.36E-03			
$\nu'=0$				$\nu'=2$					

[a] numerically accurate calculations

[b] calculations using Franck-Condon approximation

[c] experiment: for $\nu''=0$ and 1, M. Ackerman, F. Biaume, and G. Kockarts, Planet. Space Sci. 18, 1639 (1970); for $\nu''=2$, R. D. Hudson and V. L. Carter, J. Opt. Soc. Amer. 58, 1621 (1968).

ipole transition moments vanish asymptotically. $M_{\alpha_i\alpha_f}(R)$ is extended to arge R values by fitting the functional form

$$M_{\alpha_i\alpha_f}(R) = C \exp(-DR) \tag{3}$$

o reproduce $M_{\alpha_i\alpha_f}(R)$ at the two largest R values in the interpolated region. ubroutines for generating the transition dipole moments and potentials sed in this work are available from the authors.

1. O_2

Transitions were considered from the ground electronic state of O_2 ($X^3\Sigma_g^-$) :o three electronic states: the two lowest states of $^3\Sigma_u^-$ symmetry (labeled 3 and E) and the lowest state of $^3\Pi_u$ symmetry. The potential curves for :hese states are illustrated in Fig. 1.

For the X state, the RKR data compiled by Krupenie[1] was used in the region from 0.9761 Å to 1.7915 Å and the results of Saxon and Liu[25] were used from 1.852 Å to 5.292 Å. The Saxon-Liu results were shifted to have the experimental asymptotic value at 10.584 Å.

The RKR data for the B state[1] were used for values of the internuclear separation between 1.33515 Å and 2.57557 Å. The results of Saxon and Liu[25] were used from 2.646 to 5.292 Å. The ab initio points were shifted to have :he experimental asympotic value at 10.584 Å. From 0.953 to 1.270 Å, the results of Redmon[26] were used. The points were adjusted to match the inter-polated RKR data at 1.376 Å.

No RKR data are available for the $^3\Pi_u$ and E states so the fits were to ab initio data. For the $^3\Pi_u$ state, the data points at 0.953 Å and for

II. INPUT DATA

A. Potential energy curves and dipole transition matrix elements

All potential energy curves and transition dipole moments are fitted as described in paper I: the potential is fitted to the available experimental and/or ab initio data points by a cubic spline function and represented at smaller R values by the functional form

$$V(R) = A\, R^{-1} \exp(-BR) \tag{1}$$

where the parameters are determined by requiring that Eq. (1) reproduce the two innermost data points. For R values larger than the spline-fit region, the potential has the functional form

$$V(R) = V_0 - C_6\, R^{-6} - C_8\, R^{-8} \tag{2}$$

where V_0 is the experimental dissociation energy and the parameters are determined by requiring Eq. (2) to reproduce the outermost potential data points. The cubic spline function is fitted so that the first derivatives at the left and right ends of the spline-fit range match the derivatives of the functional forms of Eqs. (1) and (2), respectively.

Over the range of internuclear distances for which dipole transition moments are available, $M_{\alpha_i\alpha_f}(R)$ is fitted by fourth-order Lagrange interpolation. For smaller values of R, the dipole transition moment is assumed to be constant and equal to the value at the smallest R value for which data is available. For all of the transitions considered here, the

In this paper, electron-impact cross sections for optically-allowed transitions of ground state O_2 and S_2 to bound and dissociative states are presented. The cross sections are for conditions relevant to laser plasmas: initial relative translational energies are taken from threshold to 25 eV, initial vibrational states are selected from the lowest few states, and rotational distributions are characterized by temperatures from 0 to 1000 K.

The impact parameter (IP) method for diatomic molecules as presented by Hazi[11,12] is designed to treat optically allowed transitions. In the preceding paper[13] (paper I) the present authors extended the IP method to treat excitation of vibrationally and rotationally excited initial electronic states to either dissociative or bound energy levels of the final electronic states. The IP method has been shown to give reliable estimates of integral cross sections for high-energy collisions which are comparable to those obtained from the Born approximation and other "plane-wave" methods[8,14-23], and it agrees well with theoretical methods which are not based upon plane-wave approximations[11,13]. Although the assumptions of the IP model may often not be valid at low energies, it can still provide qualitative information about the effects of vibrational and rotational energy on the cross sections in this region.

The impact parameter method is described in detail in paper I. Section II describes the data input into the IP calculations. Both RKR (Rydberg-Klein-Rees[24]) and ab initio electronic structure data are combined and fitted to obtain the best possible potential curves. The dipole transition matrix elements are obtained from ab initio calculations. The Born calculations used to calibrate the IP calculations are also presented in Sec. II. In Sec. III the results of the dynamical calculations are presented. Section IV discusses the results and Sec. V summarizes the study.

I. INTRODUCTION

The electronic excitation and dissociation of O_2 in collisions with low-energy electrons is an important process in the photochemistry of the upper atmosphere and in some gas-discharge lasers. For example, in gas lasers dissociative excitation can significantly affect the efficiency of the laser. Although the spectroscopy of the oxygen molecule has been studied extensively,[1] there have been only a few experimental measurements of cross sections for electronic excitation by electron impact. Lawrence[2] and Mumma and Zipf[3] have measured electron-impact cross sections for dissociation through excited electronic states which are higher than 15 eV above the ground state. Linder and Schmidt[4] have measured integral cross sections for spin-forbidden transitions to bound vibrational states and Trajmar et. al.[5,6] have measured differential and integral cross sections for spin-forbidden transitions to bound vibrational states. More recently, Wakiya[7] has measured differential and integral cross sections for the X-to-B and some spin-forbidden transitions and there has been one calculation by Chung and Lin[8] of the cross section for dissociation through the B state of O_2. In the present paper we are interested in optically allowed transitions to bound vibrational states and to dissociative states of low-lying electronic states which are accessible in collisions with low-energy electrons that are present in gas-discharge lasers.

The sulfur molecule is a possible candidate for a gas laser[9] and has been extensively studied spectroscopically,[10] but little is known about its cross sections for electron-impact excitation and dissociation. Because the O_2 and S_2 molecules are isoelectronic, it is interesting to compare the analogous electron-impact cross sections of these systems.

The impact parameter method is used to calculate integral cross sections for electronic excitation and dissociation of O_2 and S_2 by electron impact. For both molecules, excitations to bound and dissociative states are considered for transitions from the ground electronic state ($X^3\Sigma_g^-$) to the two lowest states of $^3\Sigma_u^-$ symmetry (labeled B and E for O_2 and B and 2 for S_2) and the lowest state of $^3\Pi_u$ symmetry. The dependence of the cross sections upon initial vibrational and rotational state is studied for low collision energies (threshold to 25 eV). For some transitions a change in initial vibrational state can have a significant effect upon the cross sections, but, in general, the effect of changing the initial rotational state is small.

APPENDIX D

Electronic excitation and dissociation of O_2 and S_2 by electron impact

Bruce C. Garrett, Lynn T. Redmon,

C. W. McCurdy* and Michael J. Redmon

Chemical Dynamics Corporation
1550 West Henderson Road
Columbus, Ohio 43220

Permanent address: Department of Chemistry, Ohio State University
Columbus, Ohio 43210

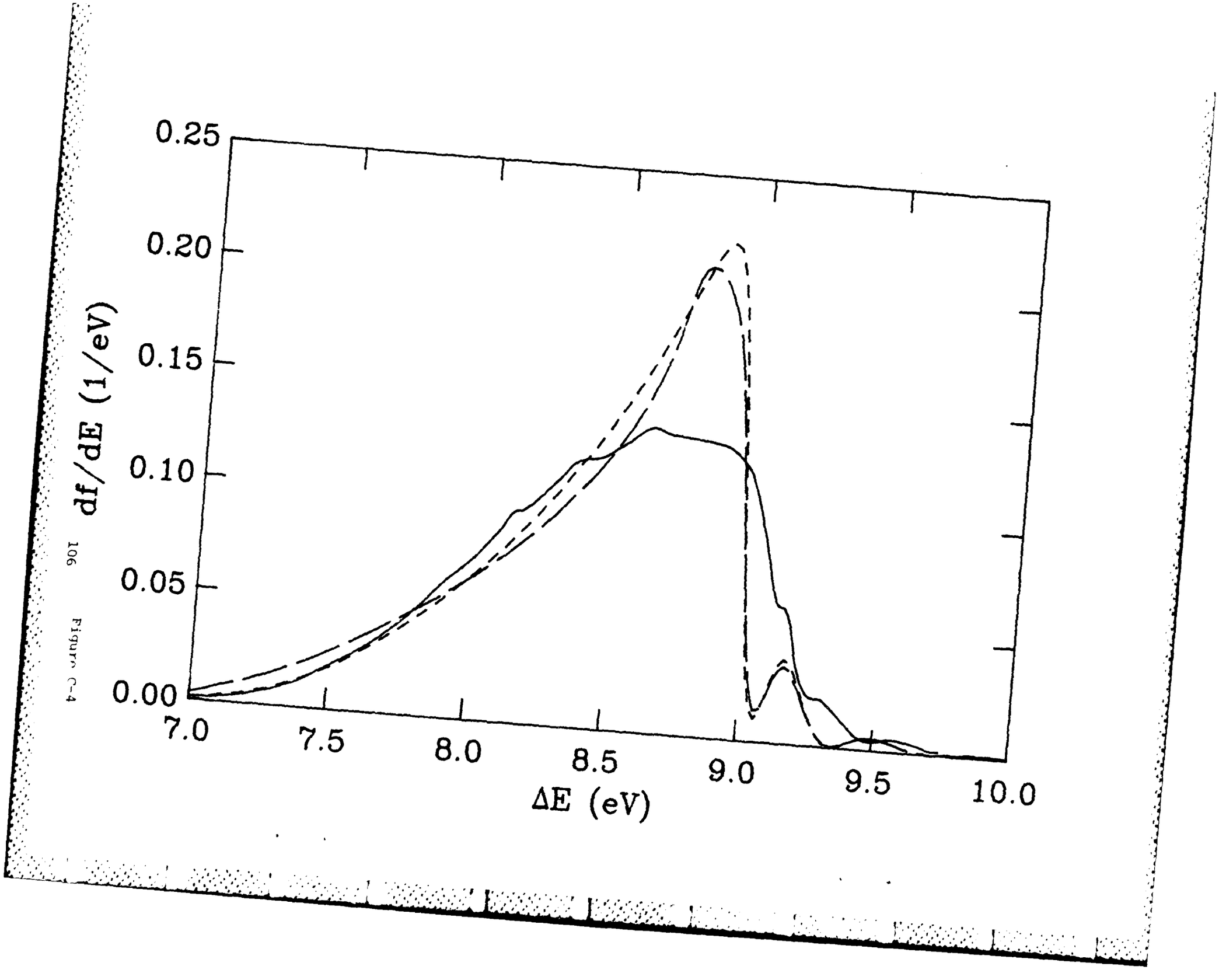

Figure C-4

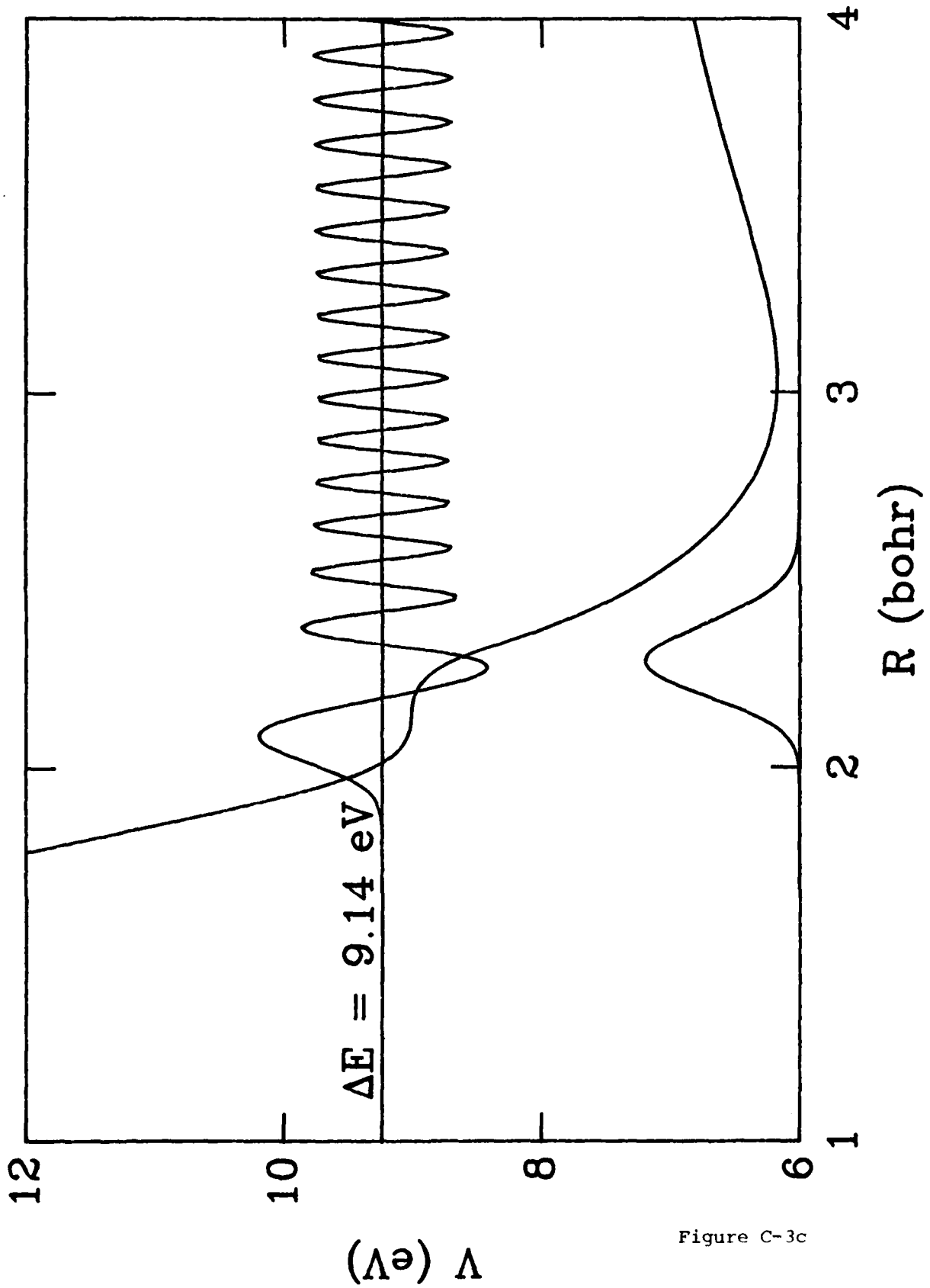

Figure C-3c

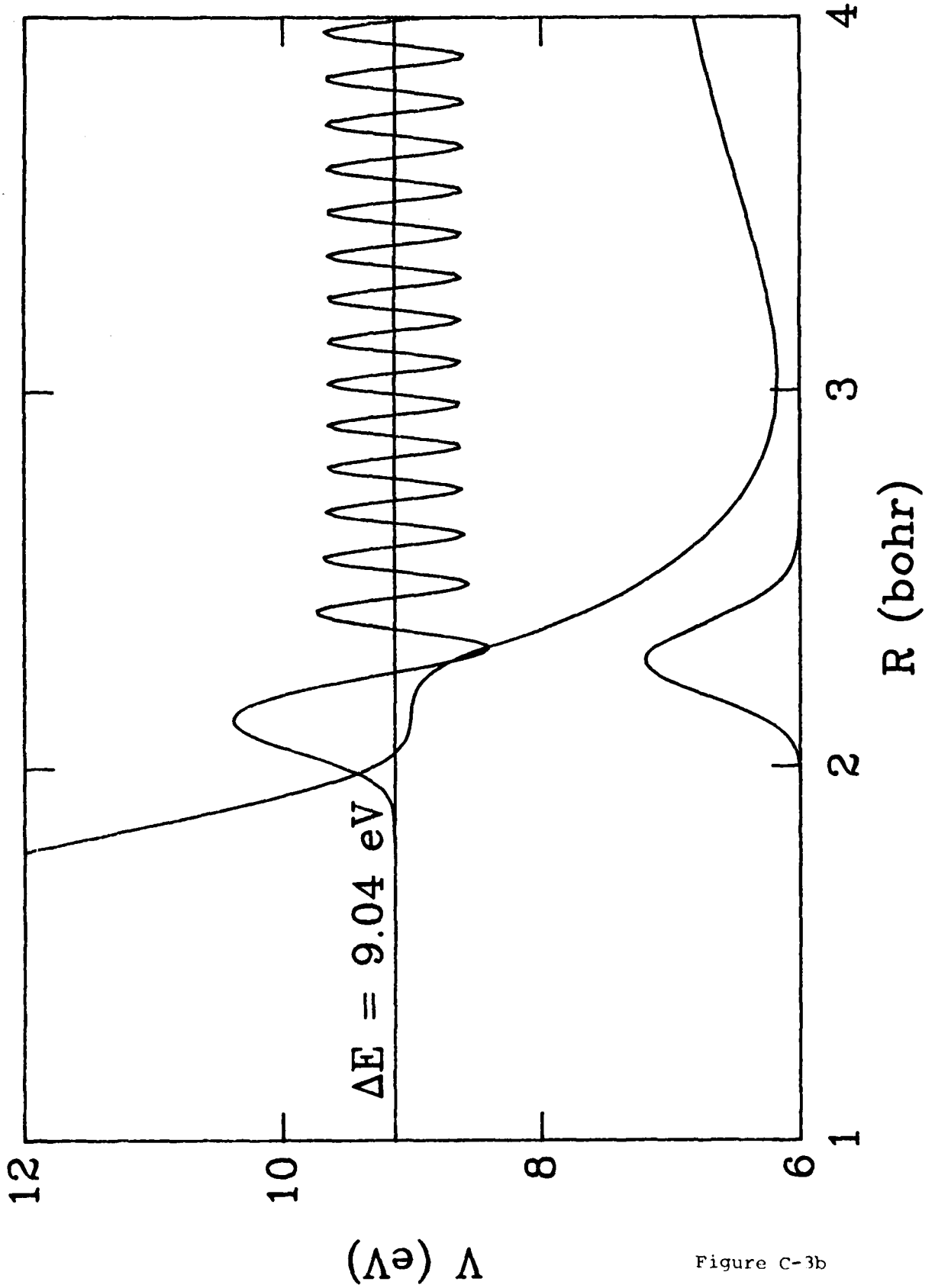

Figure C-3b

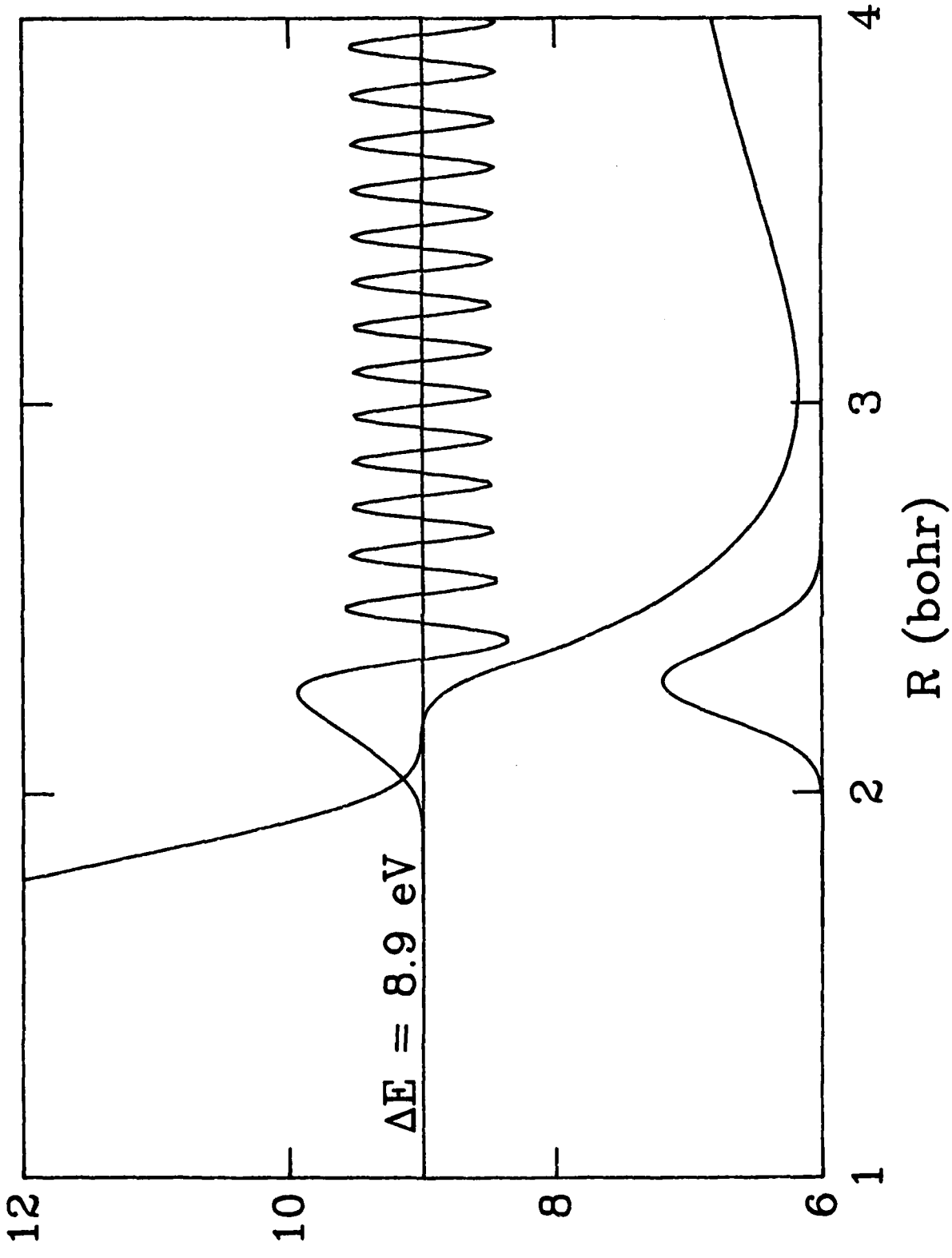

Figure C-3a

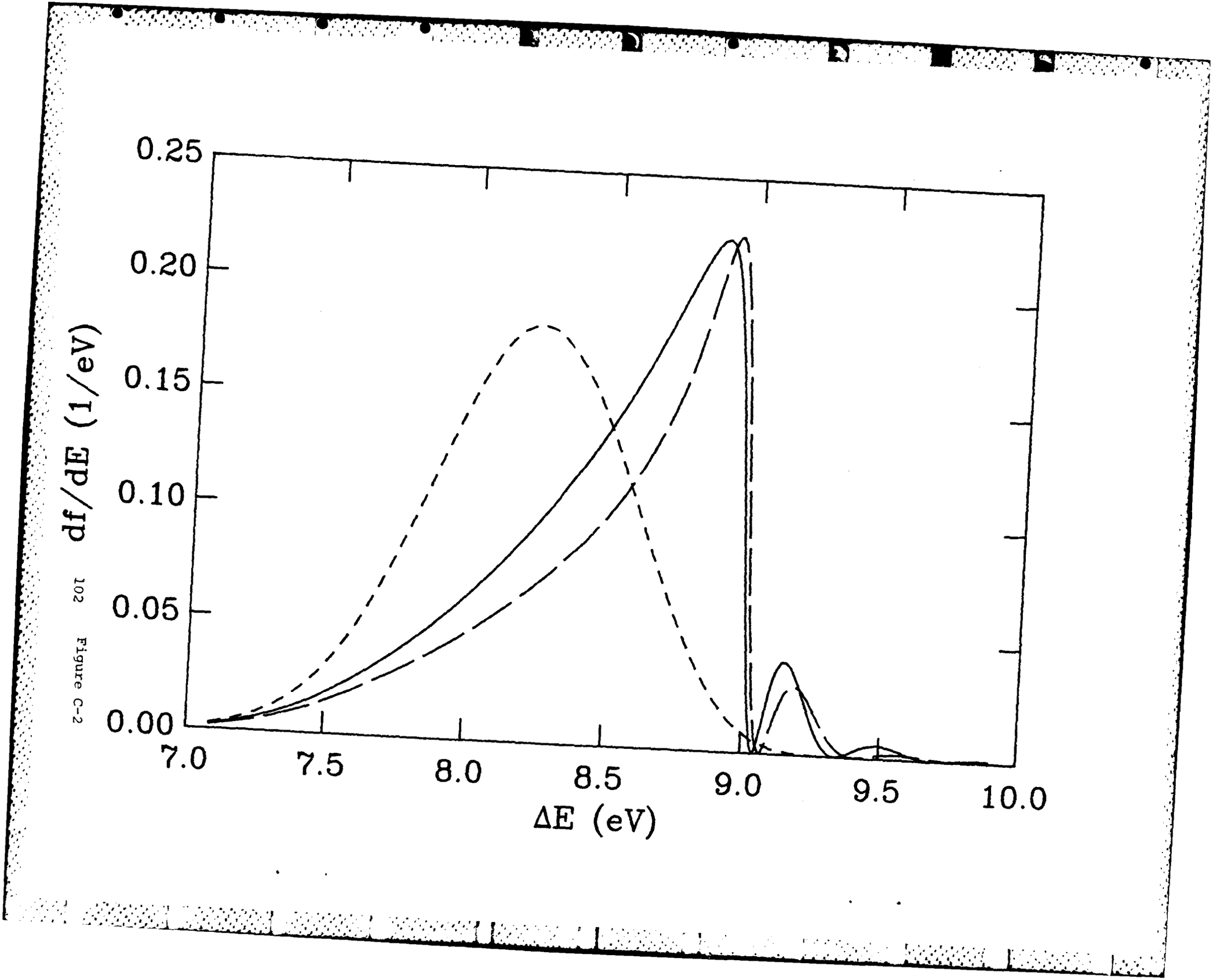

Figure C-2

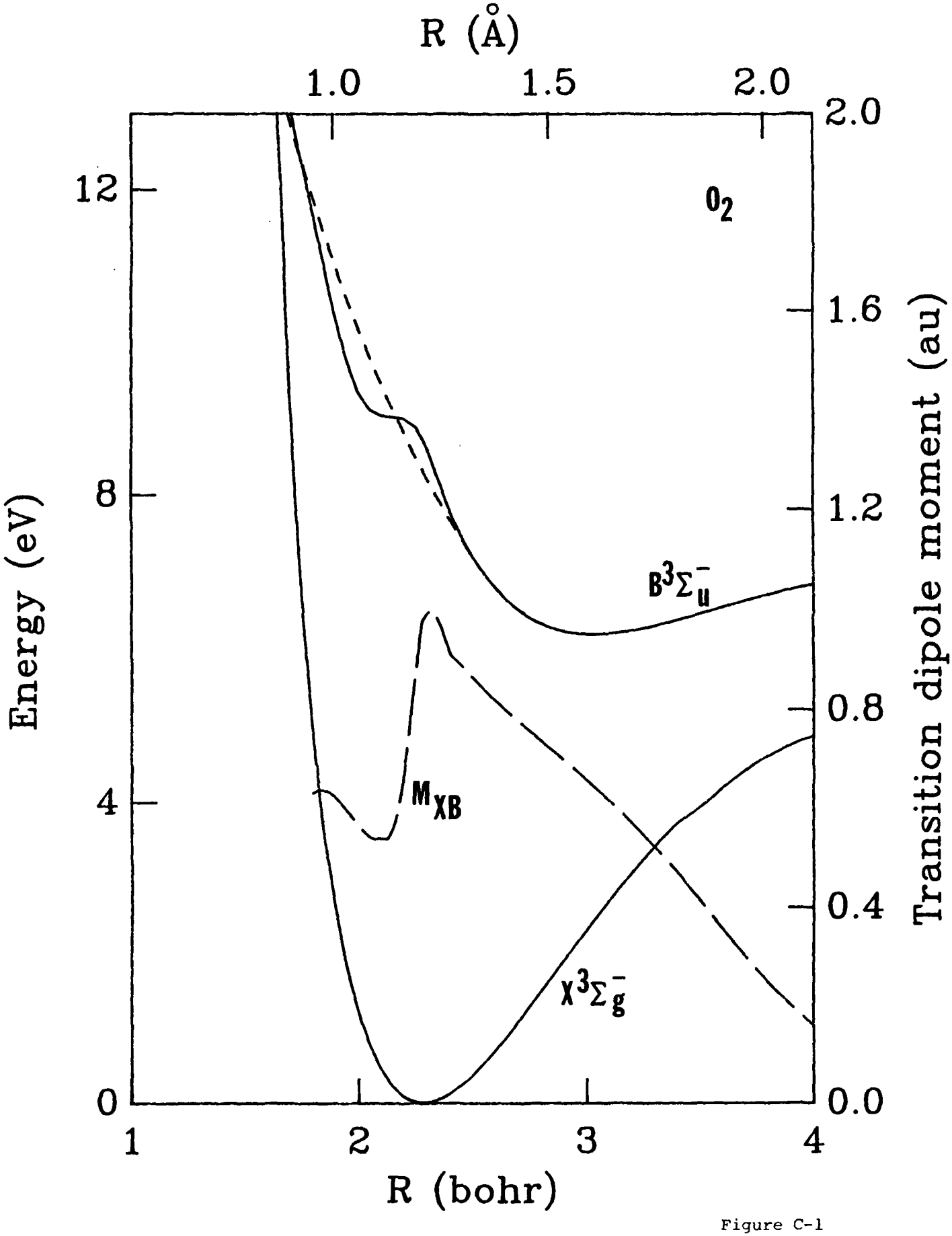
R (Å)
1.0
1.5
2.0
12
8
4
0
Energy (eV)
O_2
$B^3\Sigma_u^-$
M_{XB}
$X^3\Sigma_g^-$
2.0
1.6
1.2
0.8
0.4
0.0
Transition dipole moment (au)
1
2
3
4
R (bohr)

Figure C-1

Figure Captions

1. Potential energy curves for the X and B states of O_2 and the transition dipole moment for the X-to-B transition. The two solid curves are the accurate fits to the X- and B-state potentials from Ref. 10. The short dashed curve is a model potential for the B state which has no avoided crossing. The long-dashed curve is the fit to the ab initio transition dipole moment of Ref. 9. (An atomic unit of dipole moment is equal to 2.54177 Debye.)
2. Continuum oscillator strength per unit energy as a function of transition energy for the X-to-B transition in O_2. The solid and long-dashed curves are obtained using the accurate B-state potential and the short-dashed curve uses the model B-state potential. The solid and long-dashed curves are evaluated by accurate numerical integration over R of the initial and final wavefunctions and transition dipole moment, whereas the long-dashed curves employs the Franck-Condon approximation using the transition dipole moment at the X-state equilibrium geometry.
3. Continuum wavefunctions for the B state of O_2 at three transition energies: a) 8.9 eV, b) 9.04 eV, and c) 9.14 eV. Also shown in each part is the B-state potential curve and the ground-state vibrational wavefunction for the X state. The amplitudes of the wavefunctions are arbitrary and the amplitude of the continuum wavefunctions have been sealed by a factor of 0.08 relative to the vibrational wavefunction.
4. Continuum oscillator strength per unit energy as a function of transitin energy for the X-to-B transition in O_2. The solid curve is the experimental data of Huebner et. al. (Ref. 3) and the two dashed curves are computed for rotational temperature of 300 and 1000 K.

REFERENCES

1. R. Landenburg, C. C. Van Voorhis, J. C. Boyce, Phys. Rev. 40, 1010 (1932); R. Landenburg, C. C. Van Voorhis, Phys. Rev. 43, 315 (1933)
2. D. H. Krupenie, J. Phys. Chem. Ref. Data 1, 423 (1972)
3. R. H. Huebner, R. J. Celotta, S. R. Mielezarek, C. E. Kuyatt, J. Chem. Phys. 63 241 (1975)
4. R. Goldstein and F. N. Mastup, J. Opt. Soc. Am. 56, 765 (1966)
5. M. Bixon, B. Rey, and J. Jortner, Mol. Phys. 17, 593 (1969).
6. W. R. Jarmain and R. W. Nicholls, Proc. Phys. Soc. 84, 417 (1964)
7. A. C. Allison - Abstract of paper of the VIIth International Conference on the Physics of Electronic and Atomic Collisions, 192 (1971)
8. R. J. Buenker and S. D. Peyerimhoff, Chem. Phys. 8, 324 (1975); Chem. Phys. Lett. 34, 225 (1975); 36, 415 (1975); R. J. Buenker, S. D. Peyerimhoff, and M. Peric, Chem. Phys. Lett. 42, 383 (1976)
9. L. T. Redmon and R. N. Diffenderfer, in preparation
10. B. C. Garrett, L. T. Redmon, and M. J. Redmon, in preparation
11. M. Ackerman, F. Biaume, and G. Kockants, Planet. Space Sci. 18, 1639 (1970)
12. R. D. Hudson and V. C. Carter, J. Opt. Soc. Amer. 53, 1621 (1968)

1.376-2.646 Å were taken from Ref. 26 and the points in the range 0.995-1.312 Å were taken from Buenker and Peyerimhoff.[27,28] The ab initio points were shifted to match the experimental asymptote and to fit smoothly from 1.312 to 1.376 Å.

For the E state, the data points of Ref. 26 were used in the range from 0.953 Å to 3.175 Å and the results of Saxon and Liu[25] were used from 3.440 to 5.292 Å. The ab initio points were shifted to match the experimental asymptote at 10.584 Å and to match each other at 3.175 Å.

All three excited state curves exhibit either a shoulder or a local well in the potential energy curves between 1.111 and 1.164 Å. These features are the result of avoided crossings, where the electronic wavefunction changes character. For example, the B state wavefunction changes from a state of Rydberg character to the left of the shoulder to one of valence character to the right of the shoulder.

The transition dipole moments used in the cross section calculations are plotted in Fig. 2. These are all fits to the ab initio results of Ref. 26, which are similar to those of Ref. 28. For the X to B and X to $^3\Pi_u$ transitions, the ab initio data was available from 0.953 to 2.646 Å; for the X to E transition the ab initio data was available from 1.111 to 2.249 Å. The dipole transition moment changes rapidly with increasing internuclear distance in the region of the avoided crossing. This type of behavior is not unexpected since the electronic wavefunction changes character rapidly in this region.

2. S_2

The S_2 molecule is isoelectronic to O_2, so the same transitions were considered: from the ground electronic state $X^3\Sigma_g^-$ to the two lowest states of $^3\Sigma_u^-$ symmetry (B and 2) and the lowest state of $^3\Pi_u$ symmetry (B''). The potential curves for these states are illustrated in Fig. 3.

For the X state, the RKR data of Brabson and Volkmar[29] was used in the range 1.5870 to 2.5456 Å. The RKR data[29] for the B state was used in the range 1.8093 to 3.0554 Å, and the ab initio results of Ref. 26 were used in the range 1.640 to 1.799 Å. The ab initio points were shifted to match an extrapolation of the RKR data at 1.799 Å. The $2^3\Sigma_u^-$ and $B''^3\Pi_u$ states used the results of Ref. 26 in the range 1.588 to 3.969 Å. The results for the $2^3\Sigma_u^-$ were shifted to reproduce the experimental dissociation energy asympotically and the B" state results were shifted to reproduce the experimental dissociation energy at 3.969 Å.

No evidence of avoided crossings in the B and B" states was found in the region of the potential below 10 eV, but the $2^3\Sigma_u^-$ state exhibits a local well above the dissociation limit much like the E state of O_2. The equilibrium geometries of the B and X states of S_2 are more nearly equal than those of O_2, so the energy of the S_2 B-state at the X-state equilibrium geometry lies below the *B state dissociation limit.*

The transition dipole moments used in the cross section calculations are plotted in Fig. 4. All were fits to the ab initio results of Ref. 26. For the X to B transitio.., ab initio data was available from 1.693 to 3.969 Å; for the X to B" transition, the data extended from 1.588 to 3.969 Å; and, for the *X to* $2^3\Sigma_u^-$, *transition* the data extended from 1.588 to 2.910 Å.

B. Minimum impact parameter

In the impact parameter method, a non-zero b_0 is used as the lower limit in the integration of the transition probability over initial impact parameter to prevent divergence of the *cross section.*[11,13] The minimum impact parameter is determined by requiring that the results of the impact parameter method agree with those of the Born approximation (BA) at high energies (800 eV in the present application). For comparison of the BA and IP results

at very high energies the following approximations are made: rotational and vibrational states are treated as being degenerate and the Franck-Condon approximation is assumed to be valid. Within these approximations, the cross sections calculated are for purely electronic transitions summed over all final vibrational and dissociative states, and the IP method reduces to the method as originally formulated by Hazi[11]. At sufficiently high energy the IP cross sections become

$$\sigma^{\alpha_i\alpha_f}(E) \simeq -\frac{2\pi f_{\alpha_i\alpha_f}}{E|\Delta E_{\alpha_i\alpha_f}|} \ln\left[\frac{b_0 |\Delta E_{\alpha_i\alpha_f}|}{(2E)^{\frac{1}{2}}}\right] \tag{4}$$

where $\Delta E_{\alpha_i\alpha_f}$ is the transition energy between electronic states, E is the electron translational energy, and $f_{\alpha_i\alpha_f}$ is the electronic oscillator strength, which is related to the dipole transition moment by

$$f_{\alpha_i\alpha_f} = \frac{2m}{3\hbar^2e^2} |\Delta E_{\alpha_i\alpha_f}| \sum_{\Lambda_i\Lambda_f} \frac{|M_{\alpha_i\alpha_f}(Re)|^2}{g_i} \tag{5}$$

The sum is over projections of the initial and final electronic angular momentum along the body fixed axis, m and e are the mass and charge of the electron, h is Planck's constant, and g_i is the degeneracy of the initial electronic state. In the Franck-Condon approximation $M_{\alpha_i\alpha_f}(R)$ is assumed to be a slowly varying function of R and is evaluated at a fixed R value, the equilibrium geometry R_e of the ground electronic state in this case. For a given transition at a fixed translational energy E, $f_{\alpha_i\alpha_f}$ and $\Delta E_{\alpha_i\alpha_f}$ are known and the rhs of Eq. (4) is equated to the calculated BA cross section and solved to obtain b_0.

The input required for the Born-approximation calculations consists of the transition energy $\Delta E_{\alpha_i\alpha_f}$, the atomic basis functions, the transformation matrix for constructing the molecular orbitals, and the transition density

matrix. The details of the Born calculations are as described by McCurdy and McKoy.[21] The transition energy is obtained from the fits to the potential curves and is the vertical transition energy at R_e, and the electronic structure information is obtained from MCSCF calculations.[26] The minimum impact parameters obtained from these calculations are presented in Table I along with the transition energies $\Delta E_{\alpha_i \alpha_f}$. All b_0's were evaluated at E = 800 eV. For O_2, all were evaluated at R_e = 1.207 Å and for S_2, values of b_0 were evaluated at R_e = 1.889 Å.

III. RESULTS

First, the vibrational dependence of the electron impact cross sections was examined. In these calculations the rotational levels were assumed to be degenerate and the cross sections for excitation to bound and dissociative states were calculated from Eqs. (31) and (40) of paper I, respectively. These equations represent the IPV (bound → bound) and IPVD (bound → dissociative) extensions to the original IP method.[11] The effect of rotational excitation is discussed in section III.C.

A. O_2

Excitation to the $B^3\Sigma_g^-$ state of O_2 is predominately dissociative. Figures 5 and 6 present the cross sections for excitation to bound states and the dissociative continuum, respectively. Dissociation is favored for this state because its potential in the region of the ground state equilibrium geometry is repulsive and the overlap of the resultant continuum wavefunction

with the ground-state vibrational wavefunction is better than its overlap with the bound vibrational energy levels of the excited electronic state. As the initial vibrational energy is increased, the vibrational wavefunction becomes more diffuse and its overlap with the bound-state wavefunctions of the excited electronic state improves, causing a large enhancement in this cross section. Near threshold, the dissociative cross sections also increase with increasing initial vibrational energy, mainly because the energetic threshold is decreased as v_i is increased. However, they gradually decrease with increasing initial vibrational energy for higher energies. The IP results for v_i=0 agree well with those computed by Chung and Lin[8] using the Born-Ochkur approximation and with the experiment results of Wakiya.[7]

The cross sections for dissociation through the lowest $^3\Pi_u$ state are shown in Fig. 7. These cross sections are typically twenty to thirty times smaller than those for dissociation through the B state, largely because of the smaller transition dipole matrix elements (see Fig. 2.)

The interpretation of the cross sections for excitation to the second excited $^3\Sigma_u^+$ state (the E state) is complicated by the local well in the potential energy curve above the dissociation limit (see Fig. 1). The potential barrier is 1.5 eV above the local minimum, and the well supports six quasibound states, which will appear as resonances in the elastic cross section for collision of two O atoms. We have performed stabilization[30] calculations to determine the locations of the quasibound states of this potential. Because this local well in the E state lies almost directly above the equilibrium geometry of the X state, there is a large overlap between the vibrational wavefunctions of the ground state and the quasibound states. Therefore, most of the transitions from the X state go to these quasibound states of the E electronic curve, and there will be very little direct dissociation. However, dissociation from these quasibound states

can occur by tunneling. The contribution of these quasibound states to the dissociation cross section is determined by the competition between radiative relaxation to the X state and tunneling predissociation.

The radiative lifetimes of these states have been obtained from the Einstein A factors and are calculated to be on the order of 10^{-10} seconds. The predissociation tunneling lifetimes can be obtained from the resonance linewidths, which are, in turn, estimated from the Gamow formula.[31] The predissociation tunneling lifetimes are calculated to range from 0.04 seconds for the lowest quasibound state to 10^{-7} seconds for the third quasibound state. Thus the radiative deexcitation will be the predominant process for the three lowest quasibound states, and they will not contribute to the dissociation cross section.

The cross sections for excitation to these quasibound vibrational states of the E state are presented in Fig. 8. The resonances that occur because of the three upper quasibound states are much broader (i.e., the linewidths are larger and the predissociation lifetimes are of the magnitude or shorter than the radiative lifetime) so they should contribute to the dissociation cross sections. Therefore contributions for final energies above the first three quasibound states were included in the calculations of the dissociation cross sections shown in Fig. 9. The experimental cross section of Wakiya[7] for excitation to bound electronic states in the energy range 9.7 to 12.1 eV from $v_i=0$ is also shown. The state or states responsible for the transition in this energy range is not definitely known, but it has been suggested that the E state contributes a significant amount to this cross section. The experimental cross section is about 2.5 times lower than the IP results. The descrepancies may be the result of a breakdown in the IP method.

The cross sections for bound-state excitation decrease with increasing initial vibrational state while the dissociative cross sections are greatly

enhanced. The dissociative cross sections from the ground vibrational level are ten to twenty times smaller for the E state than those for the B state, but for the v_i=2 state they are only smaller by a factor two.

B. S_2

In S_2 the B-state potential curve in the region of the equilibrium geometry for the X state lies below the dissociation limit of the B state; therefore, excitation to bound states predominates. The B-state excitation cross sections are shown in Figs. 10 and 11. The cross sections for transitions to bound states are two to three orders of magnitude larger than the dissociation cross sections. Unlike the O_2 X-to-B case, the vibrational dependence of the bound-state cross sections is very weak and the dissociation cross sections are greatly enhanced as v_i is increased. Again, the smaller cross sections are caused by poor overlap between the initial vibrational wavefunction and the final wavefunction for nuclear motion and larger cross sections result from the wavefunctions for higher initial vibrational quantum numbers being more diffuse and overlapping better with the final wavefunction.

The cross sections for dissociation through the B'' state are shown in Fig. 12. These cross sections display only a weak dependence upon initial vibrational state. Compared to the cross sections for the O_2 X-to-$1^3\Pi_u$ transition, the S_2 cross sections have a much earlier threshold, rise to an earlier peak (only 2 eV above threshold), then decrease more rapidly for higher energies.

Excitation to the $2^3\Sigma_u^-$ state of S_2 is very similar to the excitation to the E state of O_2. The $2^3\Sigma_u^-$ state has a local well with its minimum almost directly above the X state minimum; therefore, most of the electron-impact excitation to this state is to the nine quasibound levels of the local well. As for the O_2 E state, the contribution of these quasibound states to the dissociation cross section is determined by the competition between the predissociation tunneling and radiative deexcitation. The lifetimes for predissociation tunneling range from 10^{17} s for v_f=0

to 6×10^{-7} s for $v_f=5$. The radiative lifetimes for these states are all approximately 5×10^{-9} seconds; therefore, excitation to the six lowest quasibound states is considered nondissociative. The cross sections for excitation to the lowest six quasibound states are presented in Fig. 13 and those for dissociation through the $2^3\Sigma_u^-$ state are shown in Fig. 14. The dissociative cross sections are more than four orders of magnitude smaller than the cross sections for excitation to the quasibound states, but they show relatively greater enhancement with increasing v_i.

C. Rotational effects.

The effect upon the excitation cross sections of increasing the initial rotational state was investigated for excitations from vibrational levels of the X states of O_2 and S_2. The cross sections for bound-to-bound and bound-to-continuum transitions were computed from Eqs. (29) and (38) of paper I, respectively. The method treats the diatomic molecule as a symmetric top, with spin conserved. Thus there are no transitions allowed between multiplet levels. The effect of changing initial rotational states is expected to be much smaller than the effect of increasing the vibrational state. Within the IP method, only transitions in which the rotational quantum number j changes by ±1 are allowed. Therefore increasing j_i does not change the transition energy appreciably and the threshold energy for excitation changes only slightly. The main effect of increasing j_i is to increase the effective potential by the centrifugal term $j(j+1)/2\mu R^2$. The increase in the potential is larger for smaller R, so the potential well and the vibrational wavefunction for a given level v_i are shifted to larger internuclear distances and changed in shape slightly. However, changing j_i is a small perturbation on the wavefunction compared to changing v_i.

Cross sections have been calculated for initial vibrational state v_i=0 as a function of translation energy E and rotational temperature T_{rot} for all of the dissociative transitions considered. These are shown in Tables II and III. The cross sections reported in Secs. III.A and III.B, which assume degeneracy of the rotational states, agree with those computed at T_{rot}=0 K using Eqs. (29) and (38) of paper I. Further calculations were performed to test the rotational dependence of v_i=1 and 2 and the same quantitative trends were observed.

For O_2 the dissociation cross sections for the X-B and X-Π transitions show very little dependence upon the rotational temperature. However, for the X-E transitions the cross sections increase by almost a factor of 2 as the rotational temperature is increased from 0 K to 300 K. This is caused by the centrifugal potential decreasing the bound nature of the E-state potential as j_f is increased and making the effective potential more repulsive, thereby creating better overlap between the initial and continuum wavefunctions. Since the X-to-E transition contributes very little to the total v_i=0 dissociative cross section no rotational enhancement will be seen, but for v_i=2 the X-to-E transition contributes 30% to 40% to the total dissociation cross section and a slight enhancement will be seen.

The rotational effects are very similar for S_2, the cross sections for both the X-B and X-Π dissociative transitions show very little dependence upon rotational temperature but the cross section for the X-to-E dissociative transition shows a large enhancement. For S_2 the X-to-2 dissociative cross sections are much smaller than those for the X-to-Π transitions for v_i=0-4; however, a large rotational enhancement will be seen for the total dissociation cross sections for these v_i (ranging from a factor of 2 to a factor of 8 for v_i=0 and v_i=4) as the rotational temperature is increased from 0 K to 1000 K.

D. Discussion

In the IP method it is assumed that the contributions from large impact parameters dominate the cross section. The minimum impact parameter excludes small b where the transition probabilities have unphysical divergent behavior. The extremely small value of b_0 for the X-to-B" transition in S_2, therefore, reduces the confidence in the reliability of the IP method for this transition at low to intermediate energies.

To estimate the possible contributions to the cross section from small impact parameters, an alternative treatment of the small b region was tested. Instead of assuming the contribution from this region is negligible, the contribution is assumed to be a constant for this range of impact parameters and the cross section is approximated by

$$\tilde{\sigma}^{IP}(E) = \tilde{\sigma}^{IP}_{b_0} + 2\pi \int_{\tilde{b}_0}^{\infty} db\ b\ P^{IP}(b,E) \tag{6}$$

where

$$\tilde{\sigma}^{IP}_{b_0} = \pi \tilde{b}_0^2\ P(\tilde{b}_0,E) \tag{7}$$

We adjusted $\tilde{b}_0$ to make $\tilde{\sigma}^{IP}(E)$ agree with the BA cross section at 800 eV. A measure of the importance of the region between b=0 and $\tilde{b}_0$ is then given by the ratio of $\tilde{\sigma}^{IP}_{b_0}$ to $\tilde{\sigma}^{IP}$. The ratio of $\tilde{\sigma}^{IP}_{b_0}$ to σ^{IP} gives an estimate of the error in $\sigma^{IP}(E)$ due to the treatment of small impact parameter contributions to the cross section. The value obtained for $\tilde{b}_0$ was generally less than a factor of two larger than b_0, and the errors were usually less than 50%.

A source of quantitative errors in the present description of the X-to-B" transition in S_2 is the potential energy curve used for the B" state. The B" curve of Fig. 3 does have a slight shoulder near 2.5 Å that is not an artifact of the fitting procedure, but previous experimental[32,33] and theoretical[34] evidence indicates that the B state should be slightly bound. Previous (although not definitive) ab initio calculations[34] have obtained a minimum in this curve near 2.2 Å at an energy only 0.5 eV below the dissociation limit. In any event, it is very likely that the accessible portion of the B" potential (near the equilibrium geometry of the X state) does lie above the dissociation limit (of the B" state) so that electron-impact dissociation will still dominate over excitation to bound states of the well. The shape of the potential will change, thereby changing the quantitative values of the dissociation cross section; most notably the threshold energy should be shifted to lower energies. However, the qualitative prediction that the B" state will be the major route for electron-impact dissociation will remain the same.

One further complication that arises in both the O_2 and S_2 systems is predissociation by nonadiabatic mechanisms. In O_2 the B state is known to be perturbed by the $1^3\Pi_u$ state,[35,36] and, similarly, the S_2 B state is perturbed by the B" state. In both cases the coupling arises from spin-orbit interactions[10,33,37,38]. The IP method does not account for predissociation by nonadiabatic mechanisms. For the O_2 system, the cross sections for excitation to bound states of the B state are small and predissociation will not contribute significantly to the dissociation cross sections. For S_2 the cross sections for excitation to the bound states are larger than the dissociation cross sections, and predissociation could make a non-negligible contribution to the observed dissociation cross section. Nonadiabatic predissociation could also be important in the $E^3\Sigma_u^-$ state of

O_2 and the $2^3\Sigma_u^-$ state of S_2 since the $1^3\Pi_u$ state also crosses these Σ states. However, much less is known about these states (compared to the B states) so it is difficult to estimate the importance of nonadiabatic predissociation for them.

V. SUMMARY

Electron-impact cross sections have been calculated for excitation to bound energy levels of excited electronic states and for dissociation through excited electronic states of O_2 and S_2 using the impact parameter method. The cross sections were the most strongly influenced by the magnitude of the transition dipole moment and the overlap of the initial vibrational wavefunction with the final wavefunction for nuclear motion. The overall dissociation cross sections were often sensitive to the initial vibrational state, but they were nearly independent of the temperature characterizing the thermal distribution of initial rotation states. The major route for electron-impact dissociation of the O_2 ground state at intermediate translational energies (i.e., 5 to 20 eV above threshold) via dipole-allowed transitions is through the $B^3\Sigma_u^-$ state. The X-to-B dissociation cross sections are only weakly dependent upon the initial vibrational state. Although the cross section for the X-to-$^3\Pi_u$ transition does show significant enhancement with increasing v_i, its contribution to dissociation is small; therefore, the total dissociation cross sections show little dependence upon initial vibrational state.

The major dipole-allowed contribution to the cross section for electron-impact dissociation of the S_2 ground vibrational level of the X state comes from transitions to the $B''^3\Pi_u$ state. The B''-state cross sections

e only slightly enhanced with increasing v_i, but the cross sections for ssociation through the $B^3\Sigma_u^-$ state increase significantly and for $v_i=2$ e similar in magnitude to the X-to-B'' dissociation cross sections. erefore, for S_2, the IP methods predict considerable vibrational enhancement the overall dissociation cross section.

ACKNOWLEDGEMENT

This research was supported by the Air Force Wright Aeronautical iboratories, Aero Propulsion Laboratory, Air Force Systems Command, United :ates Air Force, Wright-Patterson AFB, Ohio 43433 under Contract No.)3615-82-C-2241.

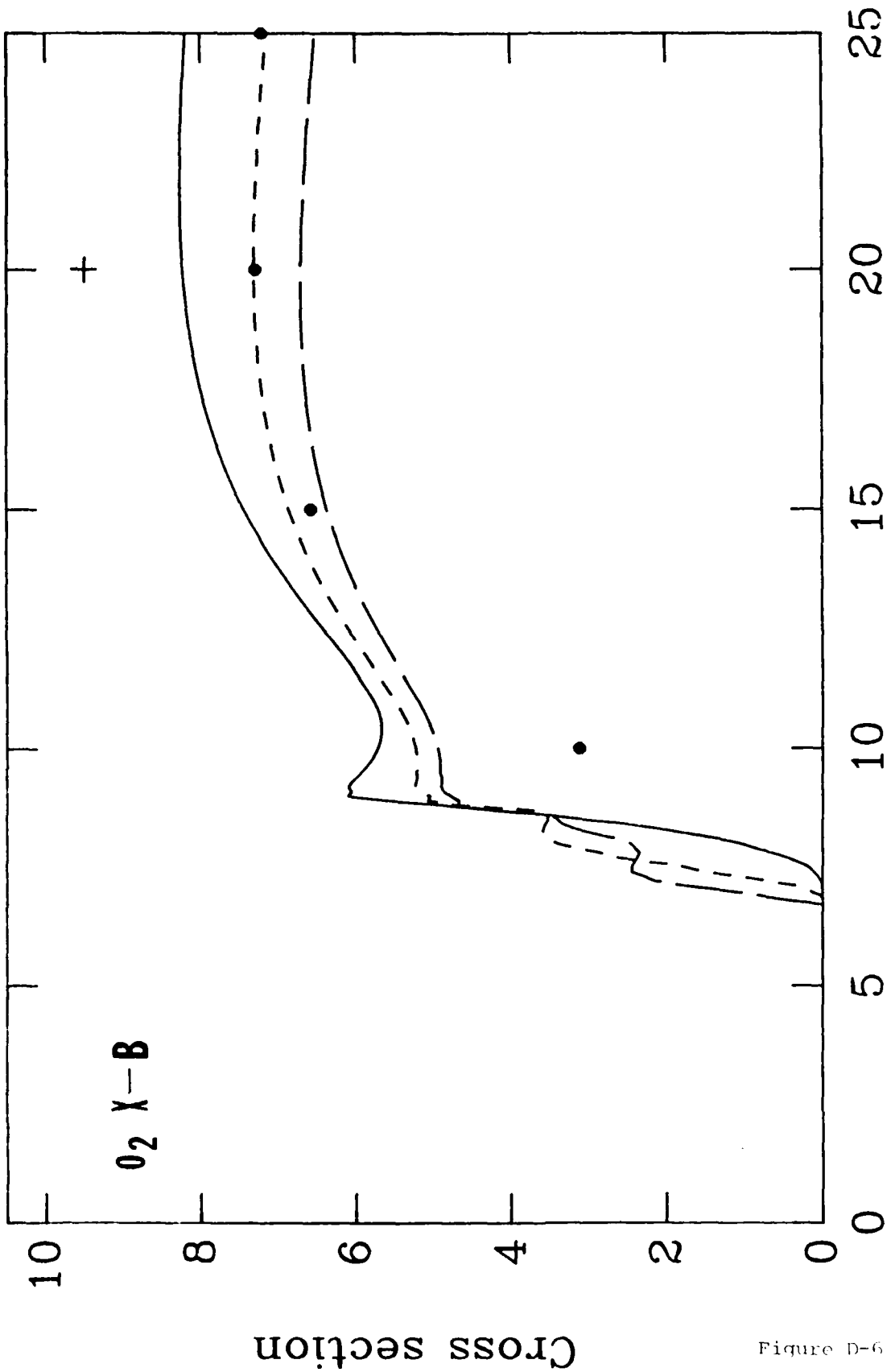

Figure D-6

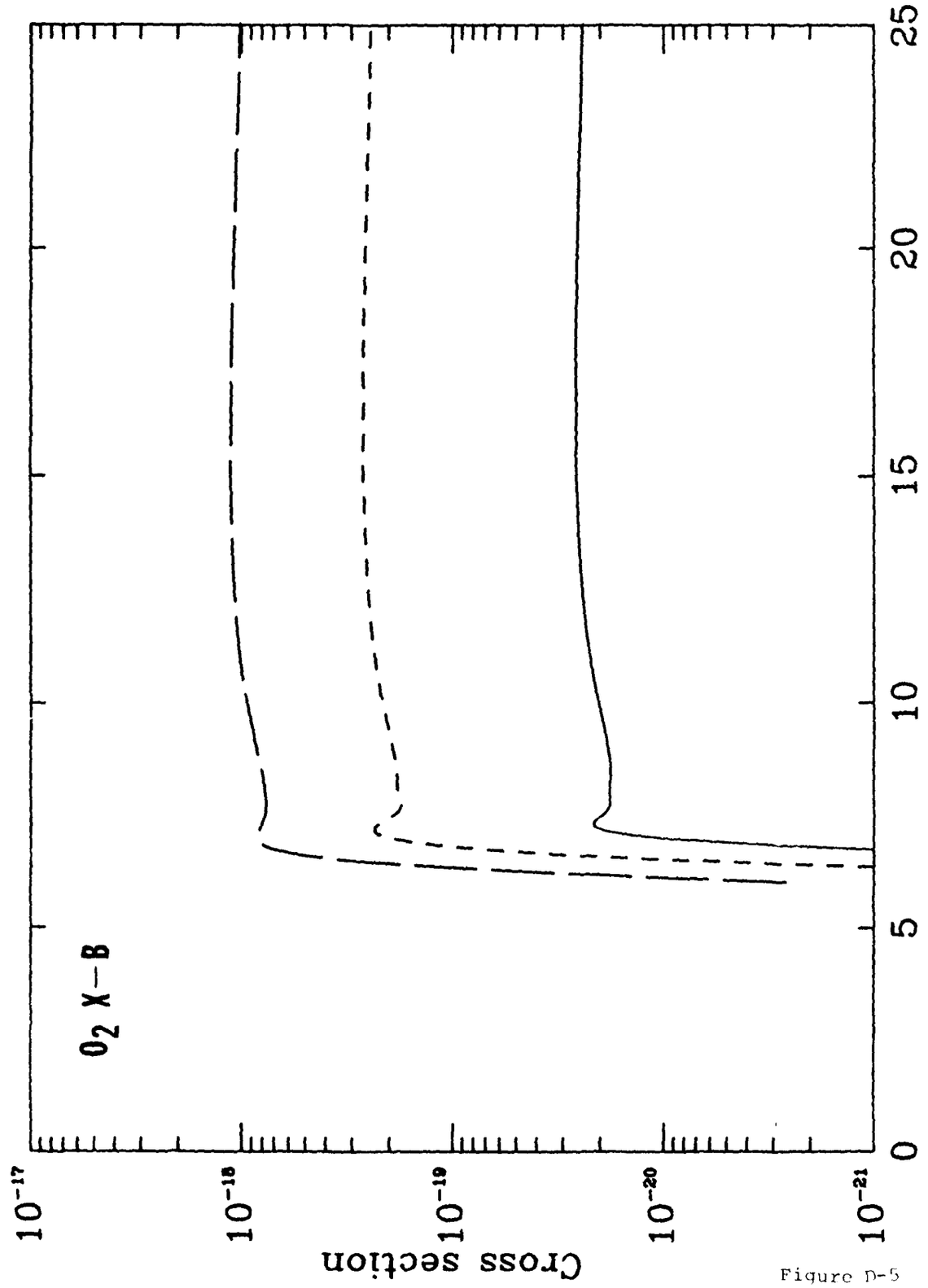

Figure D-5

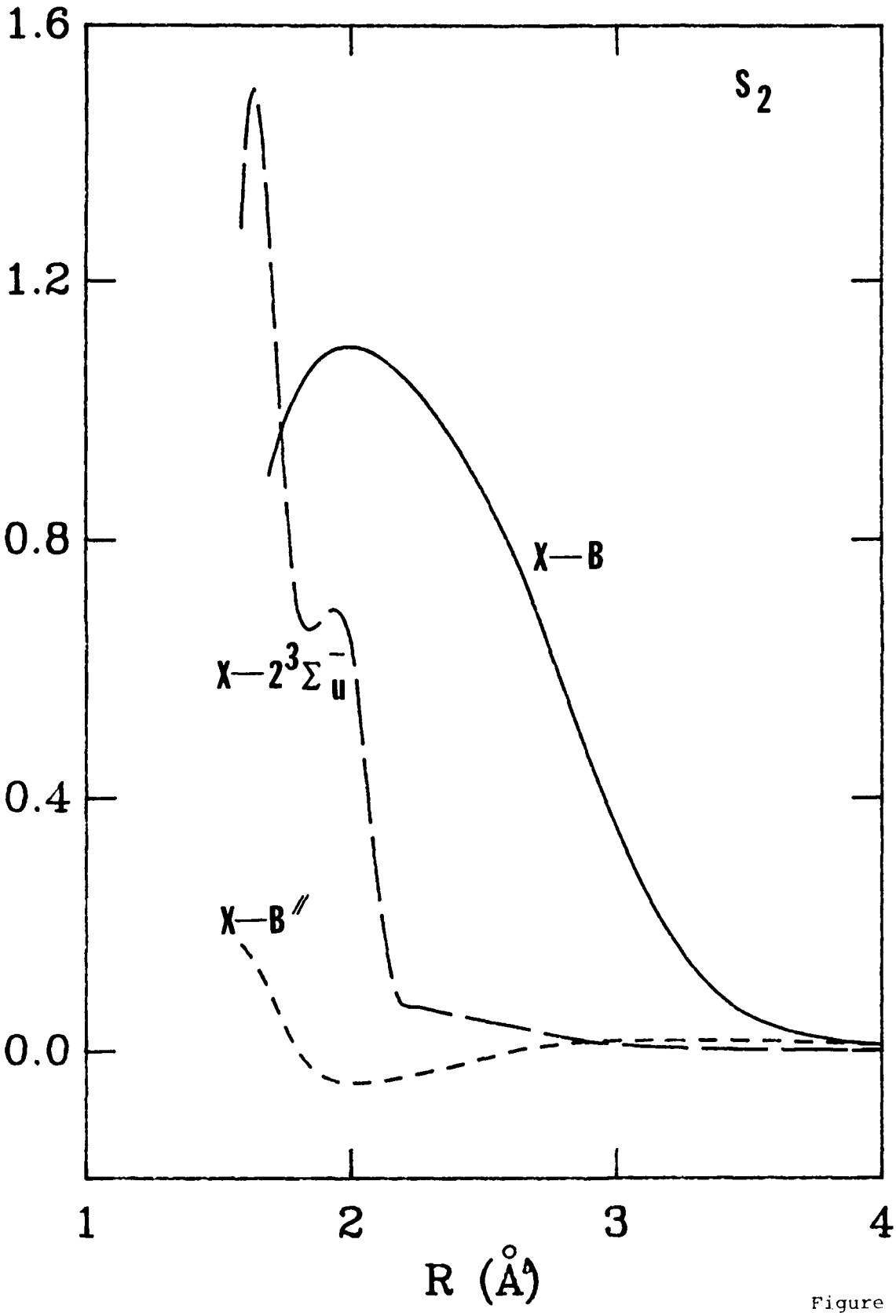

Figure D-4

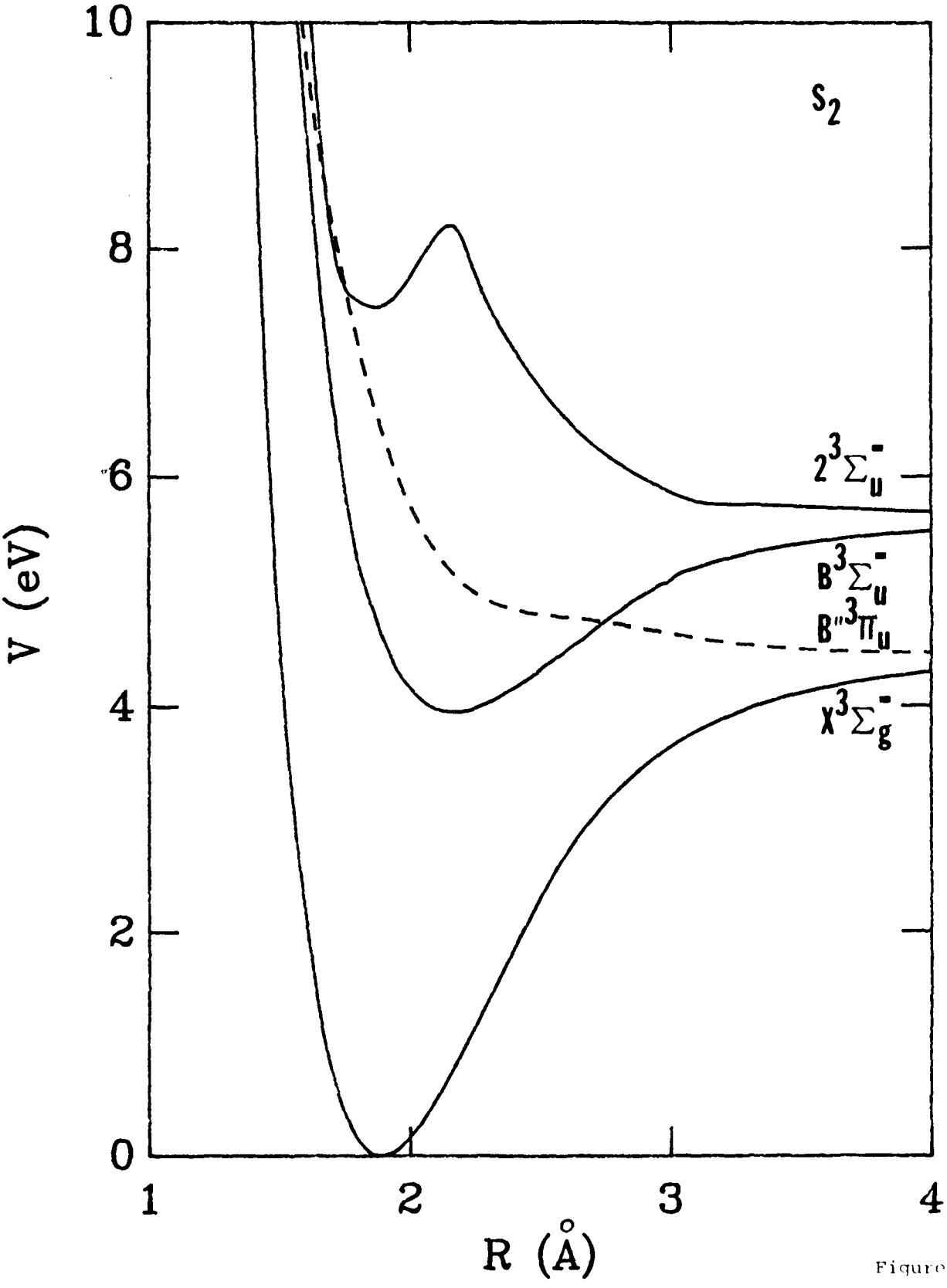

Figure D-3

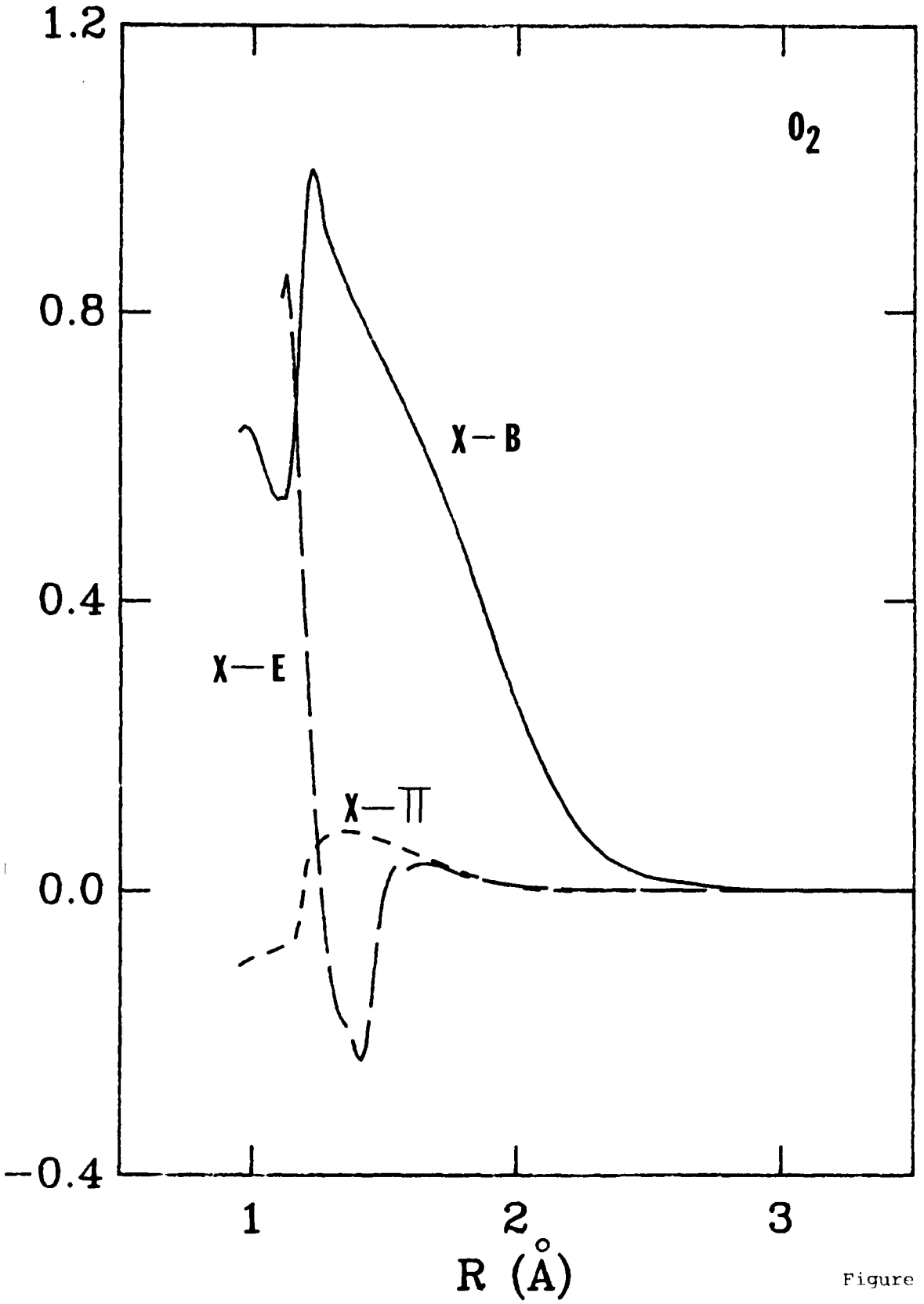

Figure D-2

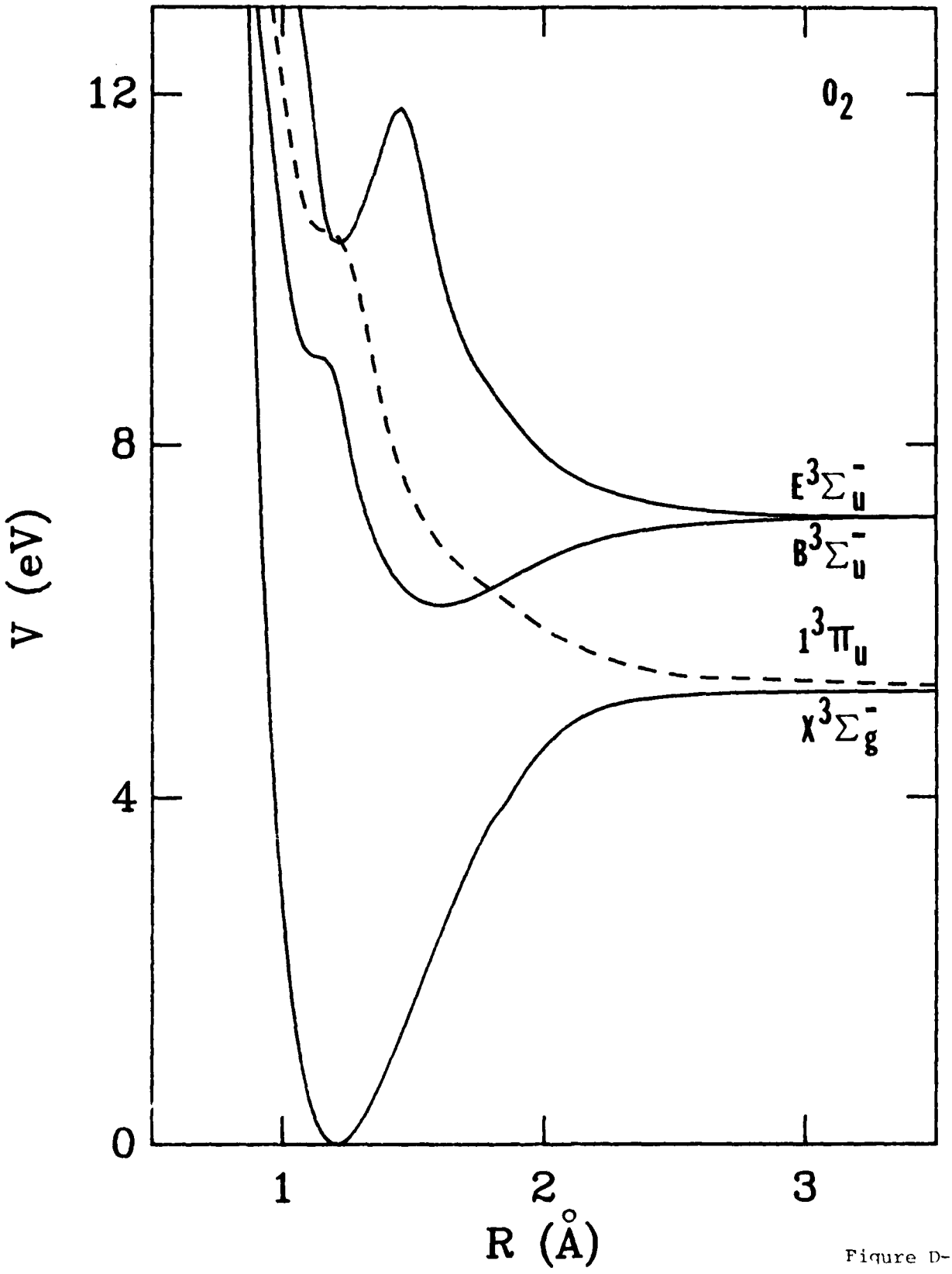

Figure D-1

are larger at high energy are for v_i = 0 and 1, respectively. The long-dashed curve is for v_i = 2 and the other solid and short-dashed curves are for v_i = 3 and 4, respectively.

11. Cross sections $\sigma_{v_i}^{\alpha_i \alpha_f}(E)$ in units of cm^2 versus electron translational energy E for electron-impact dissociation from the ground electronic state of S_2 through the B state from initial vibrational states v_i = 0-4. The cross sections are monotonically increasing functions of v_i at all energies.

12. Cross sections $\sigma_{v_i}^{\alpha_i \alpha_f}(E)$ multiplied by a factor of 10^{17} in units of cm^2 versus electron translational energy E for electron-impact dissociation from the ground electronic state of S_2 through the B" state from initial vibrational states v_i = 0-4 The solid and short-dashed curves which have the highest threshold energy and one smaller at high energy are for v_i = 0 and 1, respectively. The long-dashed curve is for v_i = 2 and the other solid and short-dashed curves are for v_i = 3 and 4, respectively.

13. Cross sections $\sigma_{v_i}^{\alpha_i \alpha_f}(E)$ multiplied by a factor of 10^{17} in units of cm^2 versus electron translational energy E for electron-impact excitation from the ground electronic state of S_2 to quasibound vibrational states of the $2^3\Sigma_u^-$ state from initial vibrational states v_i = 0-4.

14. Cross sections $\sigma_{v_i}^{\alpha_i \alpha_f}(E)$ in units of cm^2 versus electron translational energy E for electron-impact dissociation from the ground electronic state of S_2 through $2^3\Sigma_u^-$ state from initial vibrational states v_i = 0-4. The cross sections are monotonically increasing functions of v_i at all energies. The solid curve which is smaller at high energy is for v_i = 0. The short-dashed curve which is larger at high energy is for v_i = 1. The long-dashed curve is for v_i = 2 and the other solid and short-dashed curves are for v_i = 3 and 4, respectively.

vibrational states v_i = 0, 1, and 2, respectively. The dots are the Born-Ochkur results of Chung and Lin (Ref. 8) and correspond to v_i=0. The plus sign is Wakiya's experimental cross section for dissociation from the v_i=0 state (Ref. 7).

7. Cross sections $\sigma_{v_i}^{\alpha_i\alpha_f}(E)$ multiplied by a factor of 10^{17} in units of cm^2 versus electron translational energy E for electron-impact dissociation from the ground electronic state of O_2 through the $1^3\Pi_u$ state. The solid, short-dashed, and long-dashed curves are for initial vibrational states v_i = 0, 1, and 2, respectively.

8. Cross sections $\sigma_{v_i}^{\alpha_i\alpha_f}(E)$ multiplied by a factor of 10^{17} in units of cm^2 versus electron translational energy E for electron-impact excitation from the ground electronic state of O_2 to quasibound vibrational states of the E state. The solid, short-dashed, and long-dashed curves are for initial vibrational states v_i = 0, 1, and 2, respectively. The plus sign is Wakiya's experimental cross section for excitation to bound electronic states in the energy region 9.7 to 12.1 eV (Ref. 7). It is believed to be dominated by optically allowed transitions, especially to the E $^3\Sigma_u^-$ state (see Ref. 7).

9. Cross sections $\sigma_{v_i}^{\alpha_i\alpha_f}(E)$ in units of cm^2 versus electron translational energy E for electron-impact dissociation from the ground electronic state of O_2 through the E state. The solid, short-dashed, and long-dashed curves are for initial vibrational states v_i = 0, 1, and 2, respectively.

10. Cross sections $\sigma_{v_i}^{\alpha_i\alpha_f}(E)$ multiplied by a factor of 10^{17} in units of cm^2 versus electron translational energy E for electron-impact excitation from the ground electronic state of S_2 to bound vibrational states of the B state from initial vibrational states v_i = 0-4. The solid and short-dashed curves which have the highest threshold energy and

FIGURE CAPTIONS

1. Potential energy curves for selected electronic states of O_2. The fits of the curves are described in section II.A.1.
2. Dipole transition moments in atomic units as a function of internuclear distance R for transitions from the $X^3\Sigma_g^-$ state of O_2 to the $B^3\Sigma_u^-$ state (solid line), to the $E^3\Sigma_u^-$ state (long-dashed line), and to the $1^3\Pi_u$ state (short-dashed line). The curves are interpolations of ab initio data as described in section II.A.1. (An atomic unit of dipole moment is equal to 2.54177 Debye.)
3. Potential energy curves for selected electronic states of S_2. The fits of the curves are described in section II.A.2. The zero of energy is the minimum of the ground electronic state.
4. Dipole transition moments in atomic units as a function of internuclear distance R for transitions from the $X^3\Sigma_g^-$ state of S_2 to the $B^3\Sigma_u^-$ state (solid line), to the $2^3\Sigma_u^-$ state (long-dashed line), and to the $B''^3\Pi_u$ state (short-dashed line). The curves are interpolations of ab initio data as described in section II.A.2. (An atomic unit of dipole moment is equal to 2.54177 Debye.)
5. Cross sections $\sigma_{v_i}^{\alpha_i\alpha_f}(E)$ in units of cm^2 versus electron translational energy E for electron-impact excitation from the ground electronic state of O_2 to bound vibrational states of the B state. The solid, short-dashed, and long-dashed curves are for initial vibrational states $v_i = 0$, 1, and 2, respectively.
6. Cross sections $\sigma_{v_i}^{\alpha_i\alpha_f}(E)$ multiplied by a factor of 10^{17} in units of cm^2 versus electron translational energy E for electron-impact dissociation from the ground electronic state of O_2 through the B state. The solid, short-dashed, and long-dashed curves are for initial

TABLE D-III. Cross sections for dissociation of S_2 by electron impact for v_i=0

E(eV)	T_{rot}= 0	300	600	1000
		X→B		
6	2.11(-20)	2.07(-20)	2.07(-20)	2.07(-20)
10	2.82(-20)	2.83(-20)	2.83(-20)	2.85(-20)
15	3.02(-20)	3.03(-20)	3.03(-20)	3.05(-20)
20	2.82(-20)	2.82(-20)	2.82(-20)	2.84(-20)
		X→Π		
6	2.33(-18)	3.26(-18)	3.38(-18)	3.42(-18)
10	1.69(-17)	1.69(-17)	1.70(-17)	1.70(-17)
15	1.14(-17)	1.14(-17)	1.14(-17)	1.14(-17)
20	8.58(-18)	8.63(-18)	8.63(-18)	8.64(-18)

TABLE D-II. Cross sections for dissociation of O_2 by electron impact for v_i=0.

E(eV)	T_{rot} = 0	300	600	1000
		X-B		
10	5.7(-17)[a]	5.7(-17)	5.7(-17)	5.8(-17)
15	7.4(-17)	7.5(-17)	7.5(-17)	7.5(-17)
20	8.2(-17)	8.3(-17)	8.3(-17)	8.3(-17)
		X-Π		
12	6.2(-19)	6.4(-19)	6.4(-19)	6.4(-19)
15	7.4(-19)	7.6(-19)	7.7(-19)	7.7(-19)
20	7.2(-19)	7.4(-19)	7.4(-19)	7.5(-19)
		X-E		
12	3.9(-19)	7.9(-19)	8.3(-19)	8.4(-19)
15	8.1(-19)	1.4(-18)	1.4(-18)	1.4(-18)
20	8.0(-19)	1.3(-18)	1.4(-18)	1.4(-18)

[a] Numbers in parentheses are powers of 10.

TABLE D-I. Minimum impact parameters and transition energies.

Transition	b_0 (Å)	$\Delta E_{\alpha_i \alpha_f}$ (eV)
	O_2	
$X \rightarrow B^3\Sigma_u^-$	0.921	8.741
$X \rightarrow E^3\Sigma_u^-$	0.138	10.315
$X \rightarrow 1^3\Pi_u$	0.247	10.403
	S_2	
$X \rightarrow B^3\Sigma_u^-$	0.974	4.700
$X \rightarrow 2^3\Sigma_u^-$	2.424	7.480
$X \rightarrow B''^3\Pi_u$	2.28×10^{-16}	6.429

24. R. Rydberg, Z. Phys. 73, 376 (1931); 80, 514 (1933); O. Klein, Z. Phys. 76, 226 (1932); A. L. G. Rees, Proc. Phys. Soc. London 59, 998 (1947).

25. R. P. Saxon and B. Liu, J. Chem. Phys. 67, 5432 (1977); 73, 870, 876 (1980).

26. L. T. Redmon and R. N. Diffenderfer, submitted to the Journal of Chemical Physics.

27. R. J. Buenker and S. D. Peyerimhoff, Chem. Phys. Lett. 34, 225 (1975); Chem. Phys. 8, 324 (1975).

28. R. J. Buenker, S. D. Peyerimhoff, and M. Peric', Chem. Phys. Lett. 42, 383 (1976).

29. G. D. Brabson and R. L. Volkmar, J. Chem. Phys. 58, 3209 (1973).

30. H. S. Taylor, Adv. Chem. Phys. 17, 91 (1970).

31. W. H. Miller, J. Phys. Chem. 83, 960 (1979).

32. V. E. Bondybey and J. H. English, J. Chem. Phys. 69, 1865 (1978); 72, 3113 (1980).

33. Y. Matsumi, T. Munakata, T. Kasuya, J. Chem. Phys. 81, 1108 (1984).

34. W. C. Swope, Y.-P. Lee, and H. F. Schaefer, III, J. Chem. Phys. 70, 947 (1979).

35. P.J. Flory, J. Chem. Phys., 4, 23 (1936); see also Ref. 16 and references therein.

36. H. F. Schaefer, III and W. H. Miller, J. Chem. Phys. 55, 4107 (1971).

37. J. M. Ricks and R. F. Barrow, C. J. Phys. 47, 2423 (1969).

38. M. Heaven, T. A. Miller, and V. E. Bondyberg, J. Chem. Phys. 80, 51 (1984).

REFERENCES

1. P. H. Krupenie, J. Phys. Chem. Ref. Data 1, 423 (1972).
2. G. M. Lawrence, Phys. Rev. A, 2, 397 (1970).
3. M. J. Mumma and E. C. Zipf, J. Phys. Chem. 55, 1661, (1971).
4. F. Linder and H. Schmidt, Z. Naturforsch. 26a, 1617 (1971).
5. S. Trajmar, D. C. Cartwright, and W. Williams, Phys. Rev. A 4, 1482 (1971).
6. S. Trajmar, W. Williams, and A. Kuppermann, J. Chem. Phys. 56, 3759 (1972).
7. K. Wakiya, J. Phys. B 11, 3913, 3931 (1978).
8. S. Chung and C. C. Lin, Phys. Rev. A 21, 1075 (1980).
9. S. R. Leone and K. G. Kosnik, App. Phys. Lett. 30, 346 (1977).
10. R. F. Barrow and R. P. duParcq in Elemental Sulfur, edited by B. Meyer (Interscience, New York, 1965).
11. A. W. Hazi, Phys. Rev. A 23, 2232 (1981).
12. A. W. Hazi, T. N. Rescigno, and A. E. Orel, Appl. Phys. Lett. 35, 477 (1979).
13. M. J. Redmon, Bruce C. Garrett, L. T. Redmon, and C. W. McCurdy, Phys. Rev. A 00, 0000 (1985), preceding paper.
14. S. P. Khare and B. L. Moiseiwitsch, Proc. Phys. Soc. London 88, 605 (1966).
15. S. P. Khare, Phys. Rev. 157, 107 (1967).
16. K. J. Miller and M. Krauss, J. Chem. Phys. 47, 3754 (1967).
17. M. Inokuti, Rev. Mod. Phys. 43, 297 (1971).
18. D. C. Cartwright, Phys. Rev. A 2, 1331 (1970); 5, 1974 (1972).
19. S. Chung and C. C. Lin, Phys. Rev. A 6, 988 (1972); 9, 1954 (1974).
20. S. Chung, C. C. Lin, and E. T. P. Lee, Phys. Rev. A 12, 1340 (1975).
21. C. W. McCurdy and V. McKoy, J. Chem. Phys. 61, 2820 (1974).
22. T. N. Rescigno, C. F. Bender, and V. McKoy, J. Phys. B 8, L433 (1975).
23. G. P. Arrighini, F. Biondi, C. Guidotti, A. Biagi, and F. Marinelli, Chem. Phys. 52, 133 (1980).

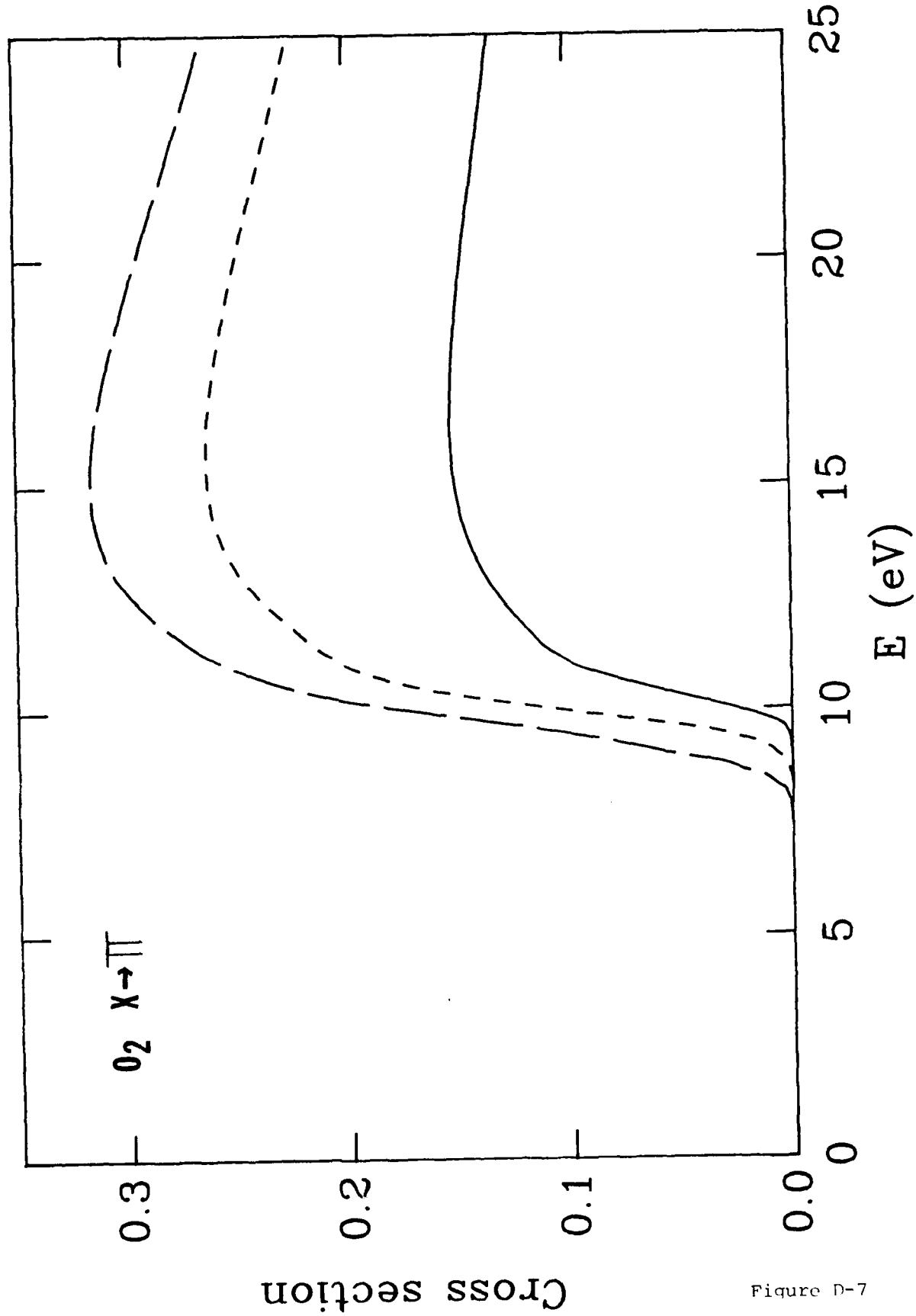

Figure D-7

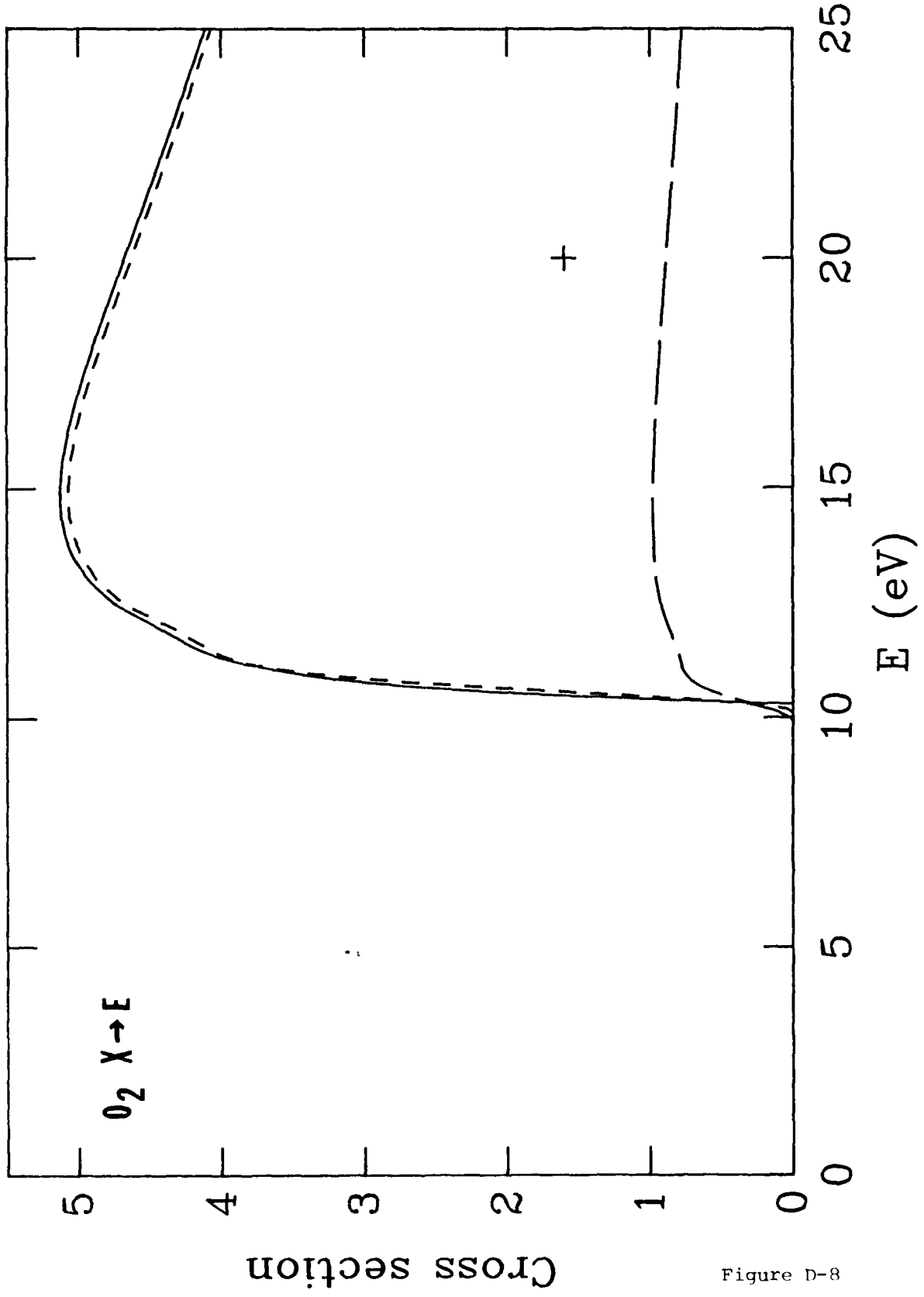

Figure D-8

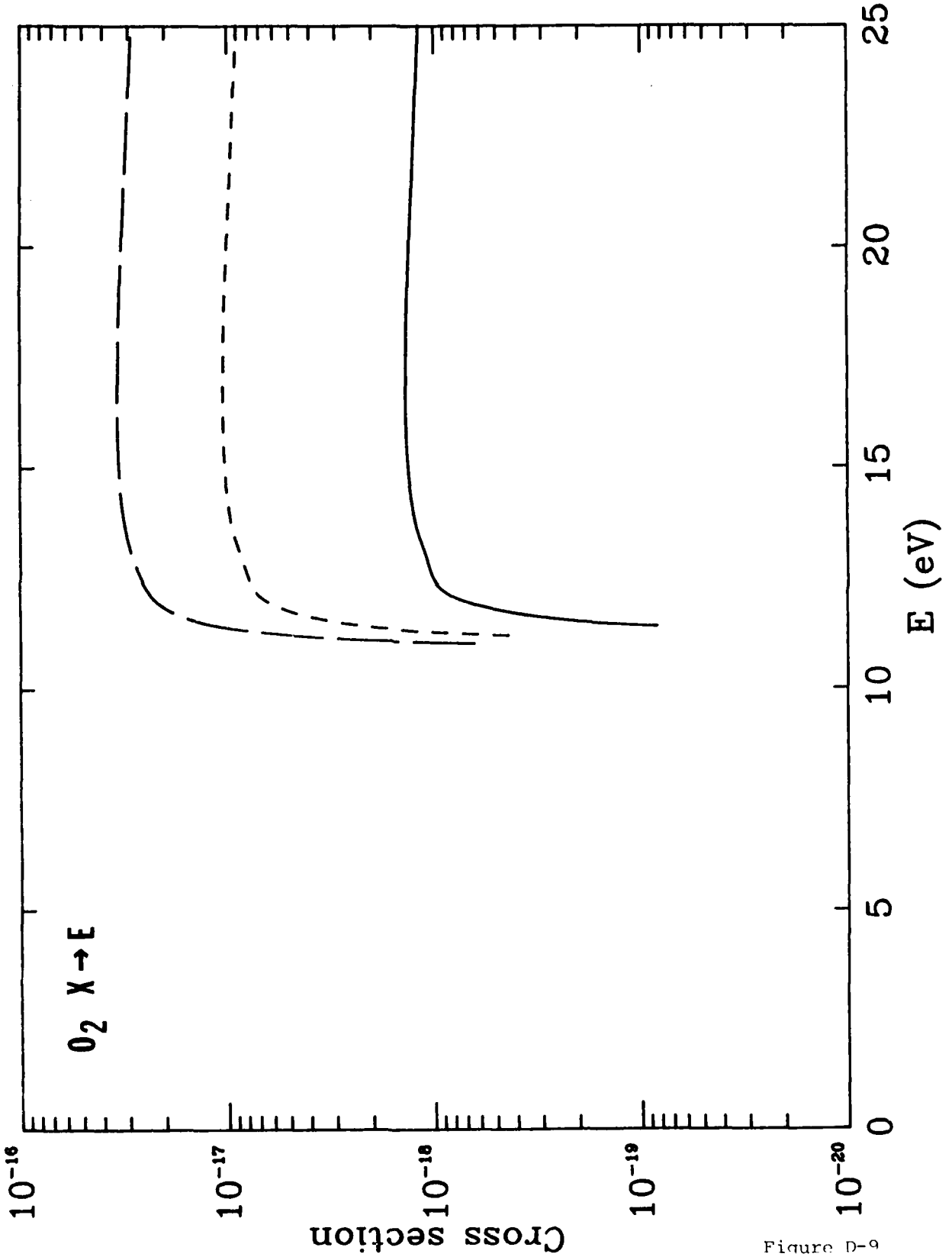

Figure D-9

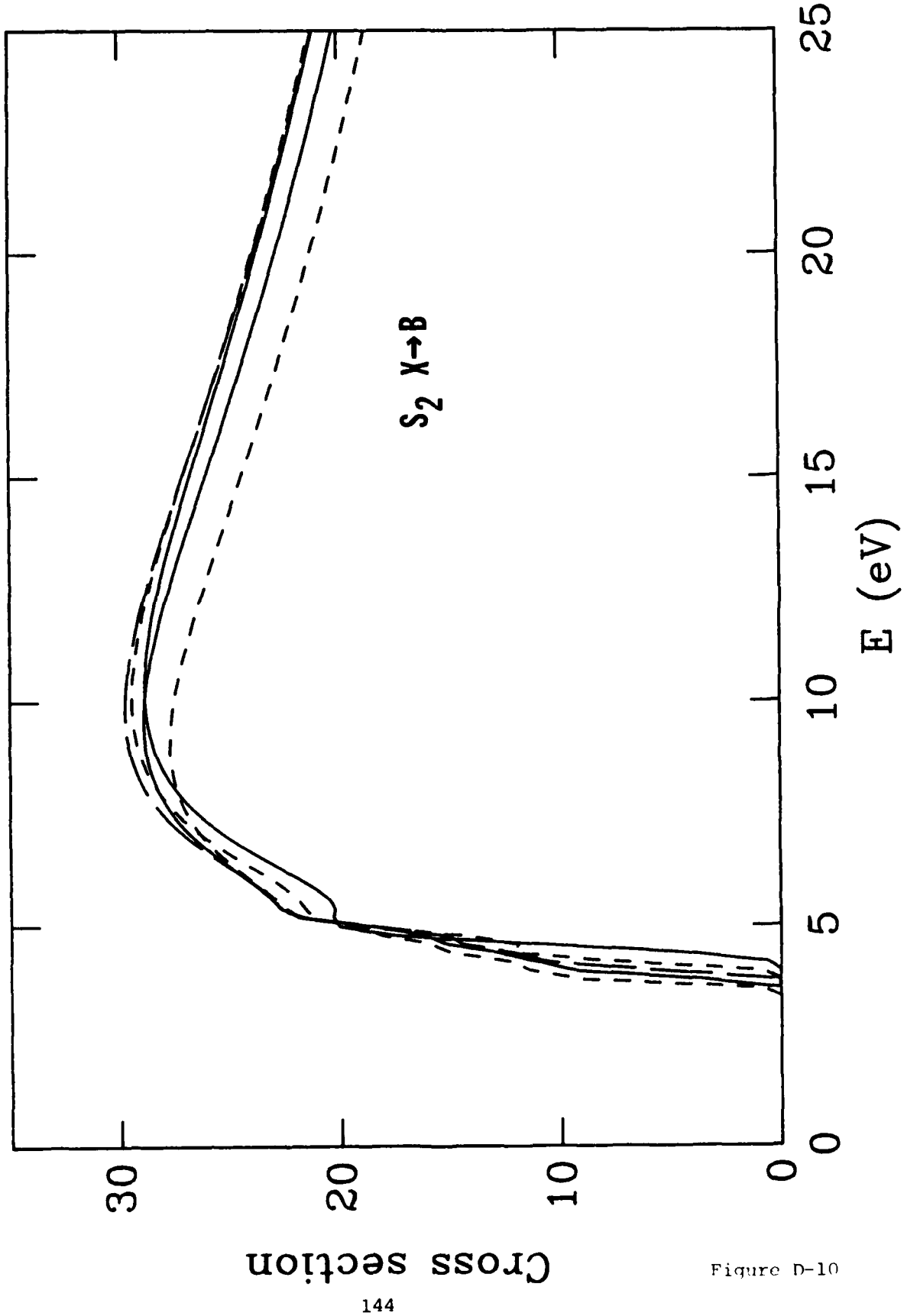

Figure D-10

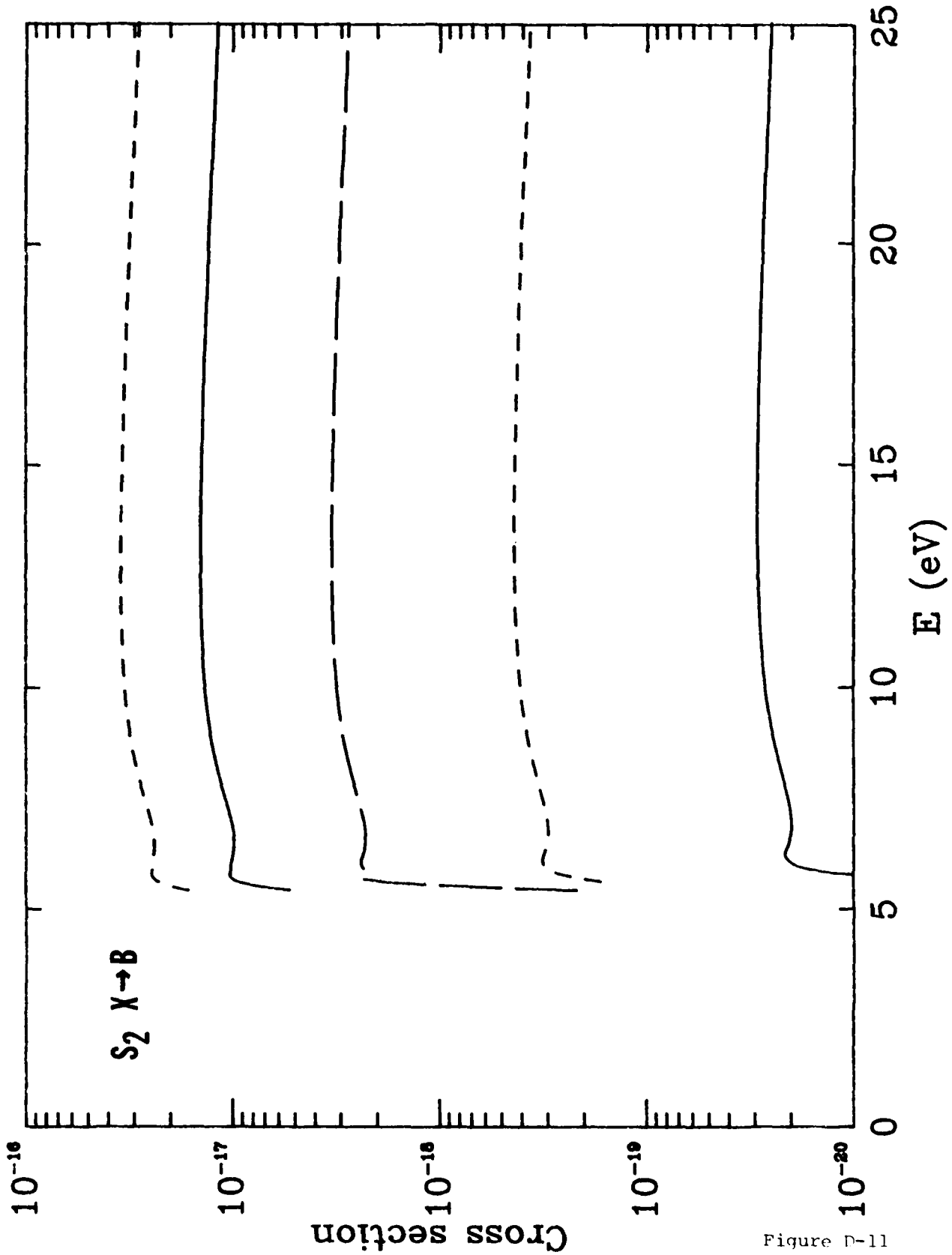

Figure D-11

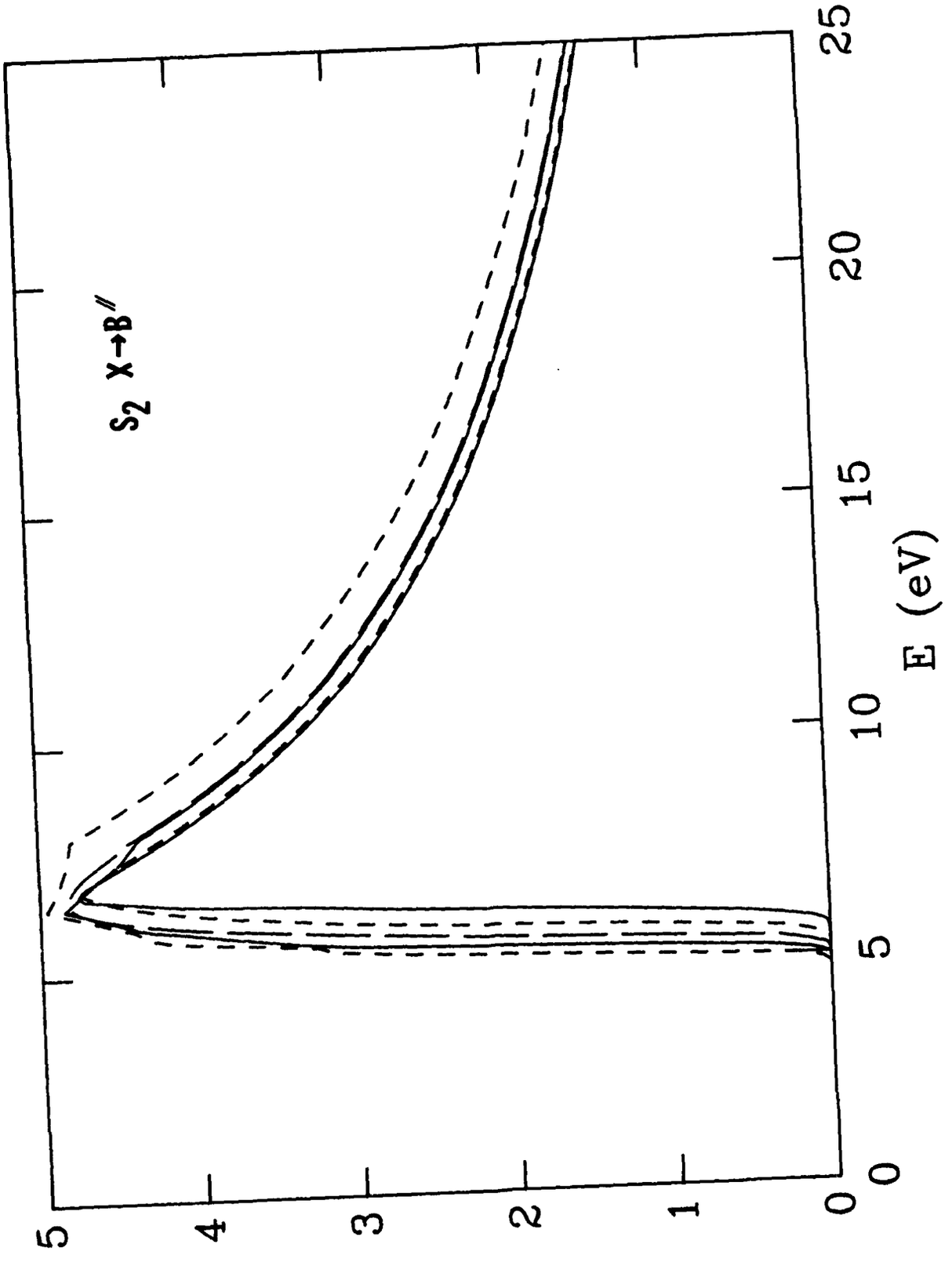

Figure D-12

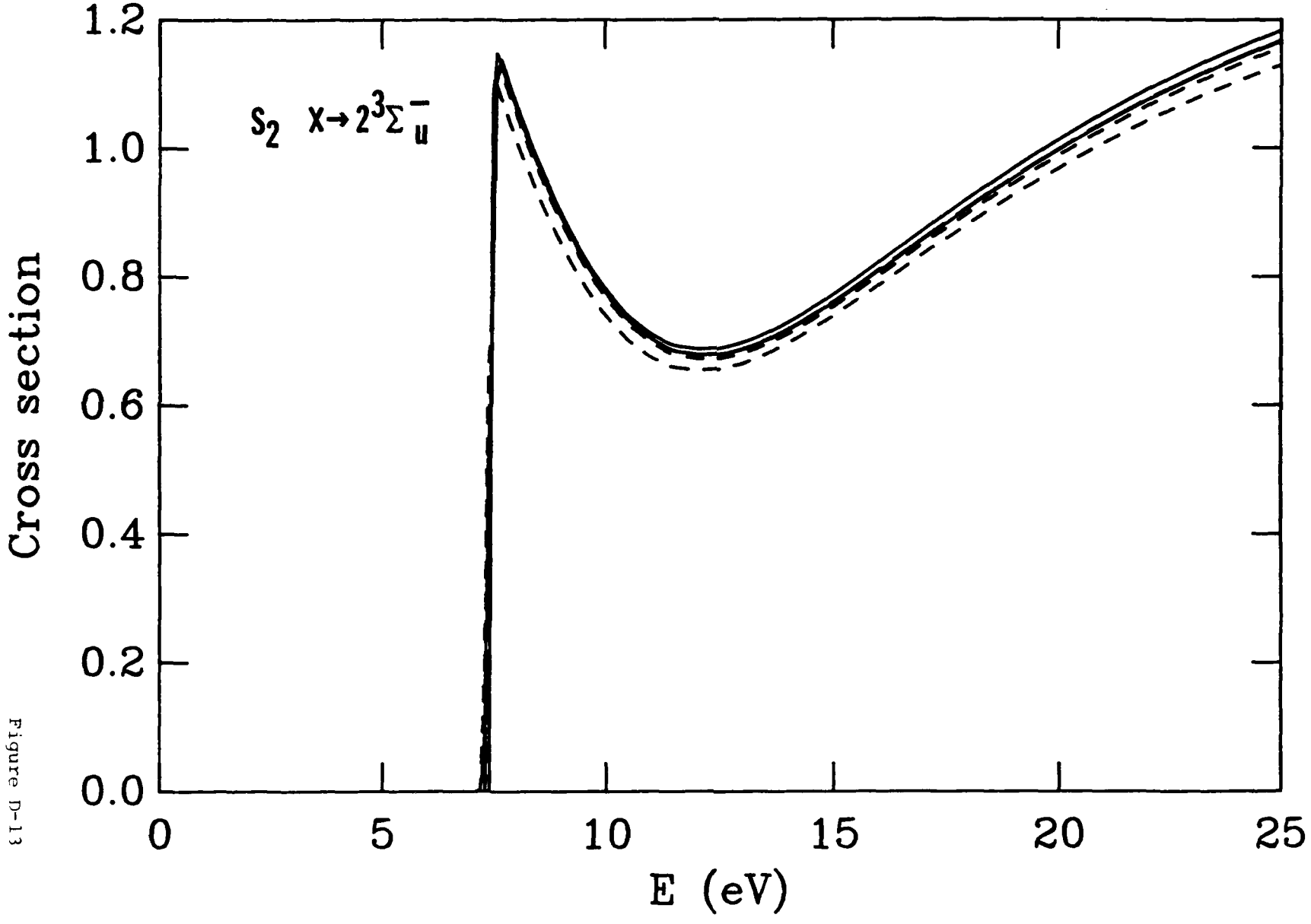
S_2 $X \rightarrow 2^3\Sigma_u^-$
Cross section
E (eV)
0.0
0.2
0.4
0.6
0.8
1.0
1.2
0
5
10
15
20
25

Figure D-13

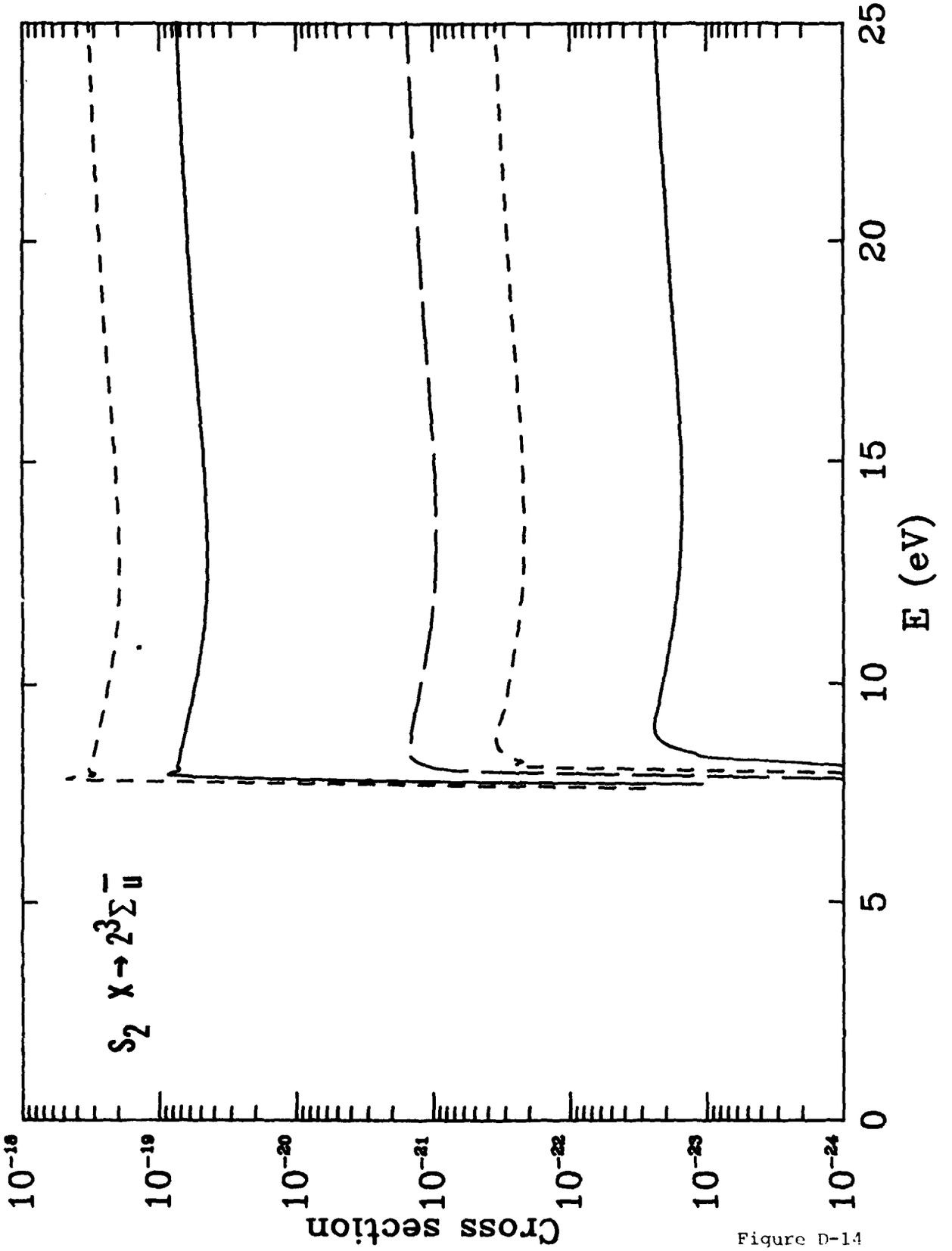
S_2 X → $2^3\Sigma_u^-$
Cross section
10^{-18}
10^{-19}
10^{-20}
10^{-21}
10^{-22}
10^{-23}
10^{-24}
0
5
10
15
20
25
E (eV)

Figure D-14

APPENDIX E

Electron-impact dissociation of HCℓ

by

Bruce C. Garrett, Lynn T. Redmon, and Michael J. Redmon

Chemical Dynamics Corporation
1550 West Henderson Road
Columbus, Ohio 43220

The HCℓ molecule plays an important role in laser plasma systems such as the XeCl laser. Dissociation of HCℓ can have a significant impact on the efficiency of the laser. Stevens and Krauss[1] concluded that photodissociation by UV radiation should not be an important process for this system; however, to date no consideration has been given to the direct dissociation of HCℓ by low-energy electron impact. In this note we report calculations of cross sections for electron-impact dissociation of HCℓ.

The photodissociation of HCℓ by UV radiation is dominated by the transition to the $A^1\Pi$ state. The A state of HCℓ is the lowest energy state that is accessible from the ground electronic state by an optical transition. This state is unbound and the transition from the ground electronic state to it has a large oscillator strength. As evidence of these facts continuous absorption for this transition has been observed experimentally.[2]

Compared to photodissociation, electron-impact dissociation is more complicated because of the possibility of exchange between the incident electron and electrons in the molecule. Even so, electron-impact dissociation of HCℓ will be dominated by optically allowed transitions for electron collisions at sufficiently high energies, for which coulombic repulsive interactions dominate over exchange interactions. At extremely low threshold energies, exchange interactions become more important and spin-forbidden transitions to triplet states can become an important route for dissociation of HCℓ. However, for the low-energy collisions characteristic of the gas-laser

system, electron-impact dissociation of HCℓ will proceed mainly through the A state.

The presence of vibrationally excited states of HCℓ, under the conditions of the gas laser, has been indicated by both experiment[3] and kinetic models of the laser plasma.[4] Therefore, it is important to assess the effect of vibrational excitation of the HCℓ molecule upon the dissociation cross sections.

The impact parameter method for diatomic molecules[5,6] is designed to treat optically allowed transitions. When extended to treat dissociation and to include the effects of vibrational and rotational excitation,[7,8] it is well suited for these studies. A detailed description of the method and our computational procedures are presented in detail elsewhere.[7,8]

As input to the calculations we use RKR data for the potential energy curve for the $X^1\Sigma^+$ state.[9] The potential energy curve for the $A^1\Pi$ state and dipole transition moment for the X to A transition are taken from the ab initio calculations of Stevens and Krauss.[1] These data are shown in Fig. 1. Also needed as input to the calculations is the minimum impact parameter b_0. We computed electronic wavefunctions and the components of the transition density matrix for the X and A states at the equilibrium geometry of the X state, to be used in Born-approximation calculations. A value of the minimum impact parameter of $b_0 = 2.784\ a_0$ was obtained by requiring the original impact parameter method of Hazi[5] to match the Born-approximation calculations at a translational energy of 800 eV. The structure calculations employed a basis set of 46 functions including those appropriate for ionic and Rydberg states. The configuration spaces for the MCSCF calculations consisted of 67 and 57 terms for the X and A states, respectively. The dipole transition moment was also calculated, using the A state optimized orbitals, and the

ılue obtained (0.28507 a.u.) agreed well with the value of Stevens and Krauss.

As a test of the accuracy of the potential energy curve for the A state, : compare calculated oscillator strengths per unit energy (df/dE) with :periment. Experimentally, continuous absorption is observed to begin at ›000 cm^{-1} and to reach a maximum at 65500 cm^{-1}. Our calculated df/dE peaks : approximately 73000 cm^{-1}. If a threshold value for df/dE is defined as hundredth of the maximum value, the threshold energy is approximately 51000 n^{-1}. The shift (above the experimental values) of both the threshold energy ıd the energy at which the absorption is peaked indicates that the A-state ›tential we are using is probably too repulsive. The effect of this on ıe dissociation cross section is a shift to higher energy, but the magnitudes E the cross sections should be essentially correct.

The cross sections for dissociation of HCℓ through the A state are shown ı Fig. 2 for v_i= 0, 1, and 2. As v_i is increased, the threshold is moved › lower energies and there is an enhancement in the cross sections. Figure shows the dependence of the cross section upon initial rotational state. ıe cross sections in Fig. 2 correspond to transitions from the ground ›tational state. In Fig. 3 we present cross sections averaged over Boltzmann ıstributions of rotational states characterized by temperatures of 0, 300,)0, and 1000 K. These cross sections are a monotonically decreasing function E T_{rot}; as T_{rot} is increased from 0 to 300 K the cross sections decrease / about a factor of 2 but further increases in T_{rot} decrease the cross :ctions by less than 5%. Since these cross sections are approximately an :der of magnitude larger than the cross section for photodissociation ılculated by Stevens and Krauss, electron-impact dissociation will play more significant role in laser system containing HCℓ.

ACKNOWLEDGEMENT

This research was supported by the Air Force Wright Aeronautical Laboratories, Aero Propulsion Laboratory, Air Force Systems Command, United States Air Force, under contract no. F33615-82-C-2241.

rences

W. J. Stevens and M. Krauss, J. Chem. Phys. 77, 1368 (1982).

K. P. Huber and G. Herzberg, Molecular Spectra and Molecular Structure IV. Constants of Diatomic Molecules (Van Nostrand Reinhold, New York, 1979).

W. L. Nighan and R. T. Brown, Appl. Phys. Lett. 36, 498 (1980).

R. E. Center, J. H. Jacob, M. Rokui, and Z. Rozenberg, "34th Annual Gaseous Electronics Conference, 1981", p. 51 (abstract).

A. W. Hazi, Phys. Rev. A 23, 2232 (1981).

A. W. Hazi, T. N. Rescigno, and A. E. Orel, Appl. Phys. Lett. 35, 477 (1979).

M. J. Redmon, B. C. Garrett, L. T. Redmon, and C. W. McCurdy, submitted to Phys. Rev. A.

B. C. Garrett, L. T. Redmon, and M. J. Redmon submitted to Phys. Rev. A.

F. G. Smith, J. Quant. Spectrosc. and Radiat. Transfer, 13, 717 (1973).

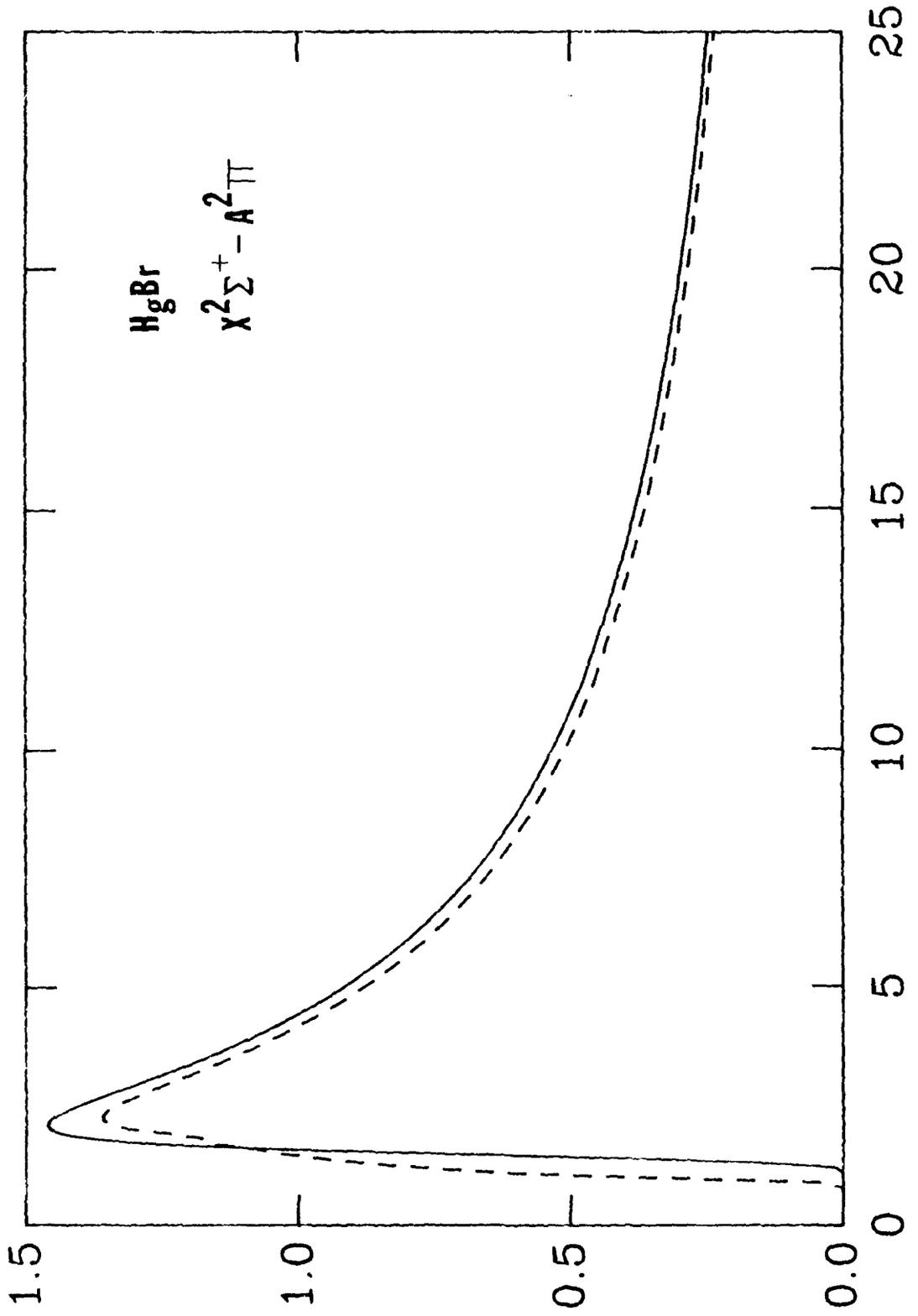

Figure F-3

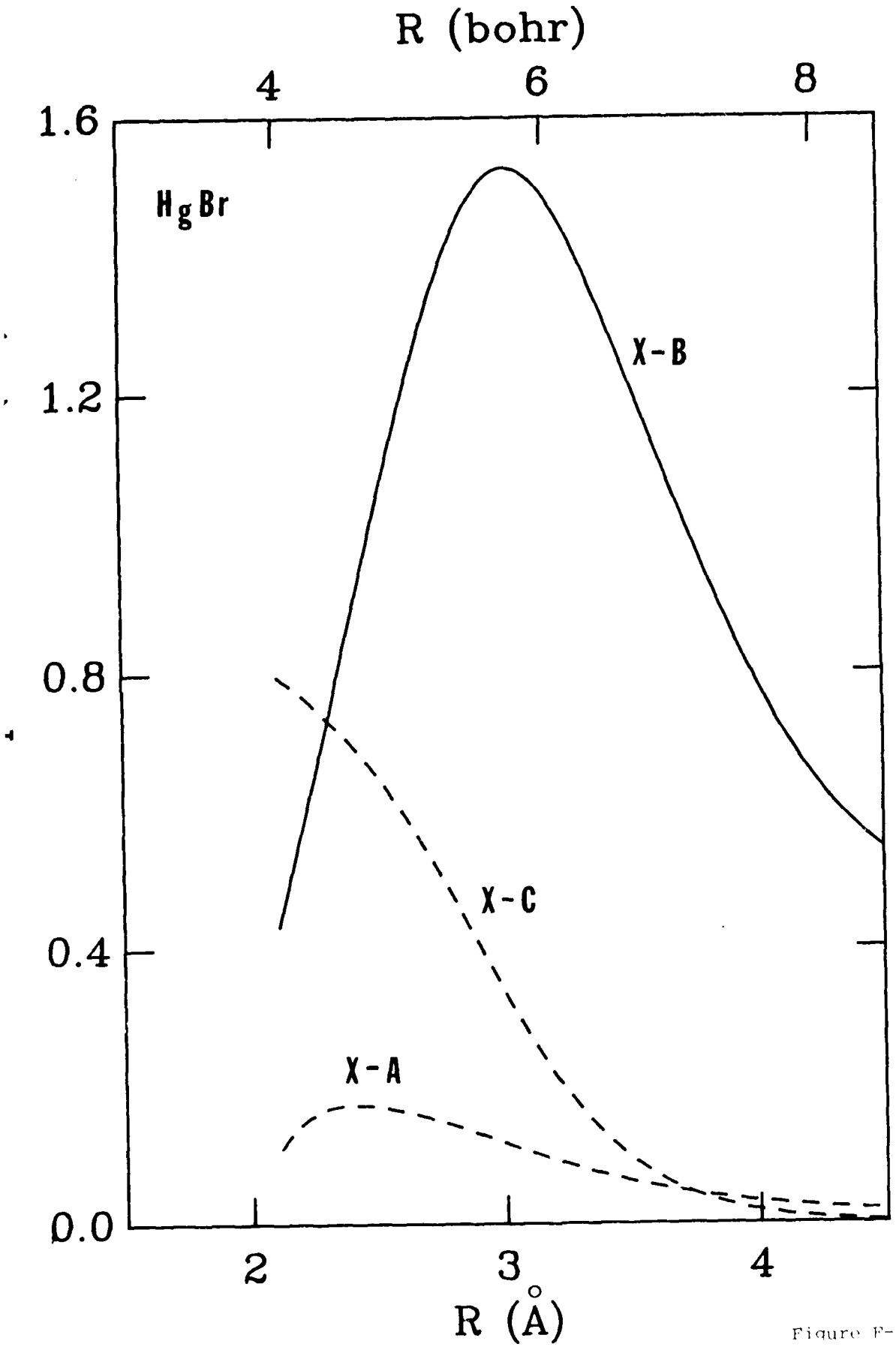

Figure F-2

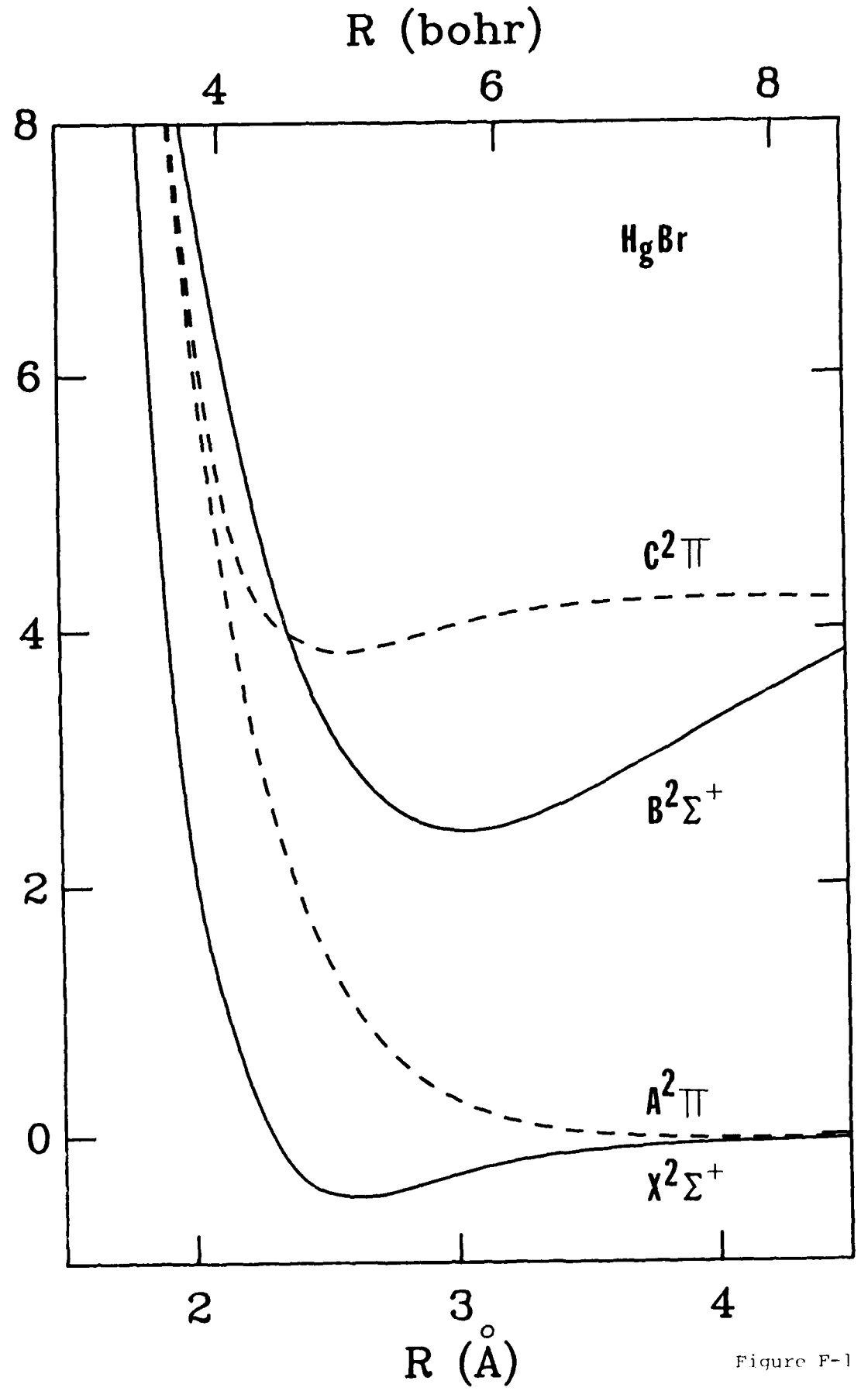

Figure F-1

FIGURE CAPTIONS

1. Potential energy curves (solid lines) for the X and B states and (dashed lines) A and C states of HgBr.
2. Dipole matrix elements for the X-B transition (solid curve), and X-A and X-C transitions (dashed curves) in HgBr. The curves are fits to the data of Wadt (see text).
3. Cross sections multiplied by a factor of 10^{16} in units of cm^2 versus electron translational energy for electron impact dissociation of HgBr through the A state. The solid and dashed curves are for initial vibrational states $v_i = 0$ and 4, respectively.
4. Cross sections multiplied by a factor of 10^{16} in units of cm^2 versus electron translational energy for electron-impact dissociation through the A state of the $v_i = 4$ vibrational state of the X state of HgBr. The solid and dashed curves are for rotational temperatures of 0 and 1000 K, respectively.
5. Cross sections multiplied by a factor of 10^{16} in units of cm^2 versus electron translational energy for electron impact excitation of the B state of HgBr. The solid and dashed curves are for initial vibrational states $v_i = 0$ and 10, respectively.
6. Cross sections multiplied by a factor of 10^{16} in units of cm^2 versus electron translational energy for electron impact excitation of the C state of HgBr. The solid and dashed curves are for initial vibrational states $v_i = 0$ and 10, respectively.

REFERENCES

1. R. Burnham and E. J. Schimitschek, Laser Focus 17, 54 (1981).

2. E. J. Schimitschek, J. E. Celto, and J. A. Tries, Appl. Phys. Lett. 31, 608 (1977).

3. E. J. Schimitschek and J. E. Celto, Opt. Lett. 2, 64 (1978).

4. R. T. Brown and W. L. Nighan, Appl. Phys. Lett. 32, 730 (1978).

5. W. L. Nighan, "Properties of Electron-Beam Controlled XeCl(B-->X) and HgBr(B-->X) Laser Discharges", in Applied Atomic Collision Physics, Vol. 3, E. W. McDaniel and W. L. Nighan, eds. (Academic Press, New York, 1982).

6. A. W. Hazi, Phys. Rev. A 23, 2232 (1981), p. 319.

7. M. J. Redmon, B. C. Garrett, L. T. Redmon, and C. W. McCurdy, Phys. Rev. A, in press.

8. B. C. Garrett, L. T. Redmon, C. W. McCurdy, and M. J. Redmon, Phys. Rev. A, in press.

9. B. C. Garrett, L. T. Redmon, and M. J. Redmon, submitted to Phys. Rev. A.

0. C. W. McCurdy and V. McCoy, Phys. Rev. A 61, 2820 (1974).

1. W. R. Wadt, Appl. Phys. Lett. 34, 658 (1979).

2. L. R. Kahn, P. J. Hay, and R. D. Cowan, J. Chem. Phys. 68, 2386 (1978).

3. R. S. Pitzer, unpublished.

excitation of the B state for initial vibrational levels v_i = 0 and 10. There is at most a 40% enhancement for v_i = 10 over v_i = 0.

In Fig. 6 bound excitation cross sections are shown for the X-C transition, again for v_i = 0 and 10. The enhancement near threshold is caused by the different rate of change with energy of the structural factor (influenced by Franck-Condon factors) and the dynamical factor.[7]

ACKNOWLEDGEMENT

This research was supported by the Air Force Wright Aeronautical Laboratories, Air Force Systems Command, United States Air Force, under Contract No. F33615-82-C-2241.

The author's wish to thank Dr. Willard Wadt for supplying tables of his potential curves and dipole matrix elements to supplement the data in Ref. 11. They also thank Professor Russell Pitzer for the use of his integral program.

and 5.3 Å, and by extrapolation outside of this range.[8] The dipole matrix elements are shown in Fig. 2. These are 4-point Lagrange interpolations of Wadt's data.

The A state is totally repulsive and is expected to be a major contributor to the overall HgBr(X) dissociation cross section. In Fig. 3 we present cross sections for dissociation through the A state from threshold to 25 eV for initial vibrational states v_i equal to 0 and 4. The cross section rises rapidly to a value near 1.5×10^{-16} cm^2 at 2.0 eV and subsequently falls off smoothly with increasing energy. There is only a small effect on the magnitude of the cross section caused by varying initial vibrational energy, although there is some enhancement predicted by the impact parameter model near threshold.

In Fig. 4 the effect of initial rotational temperature is presented. The rotational effect was examined for initial vibrational states from $v_i = 0$ to 4. The same quantitative trends were observed for all v_i and we report only those for $v_i = 4$. The decrease of a factor of two observed in going from $T_{rot} = 0$ to 1000 K is somewhat of an anomaly compared to what we have seen in other systems[7-9] and results from the fact that, for $T_{rot} = 0$, only $j_i = 0$ contributes to the cross section, while for $T_{rot} > 0$, other angular momentum states contribute.[7] The contributions from various angular momentum components are weighted by different symmetry factors (for Σ to Π transitions only) which results in a low temperature enhancement of the cross section.

For the X-B and X-C transitions from initial vibrational states 0 to 4 the dissociation cross sections are extremely small, being less than 10^{-28} cm^2 for the X-B transition. This is reflected in the fact that the sum of Franck-Condon factors for transitions to bound vibrational levels of the B and C states is unity to within the accuracy of the calculations (approximately six significant figures). In Fig. 5 we present cross sections for bound

formulation is presently restricted to optically-allowed transitions. However, vibrational and rotational degrees of freedom can be treated explicitly.[7]

The impact-parameter method requires as input potential energy curves and dipole transition matrix elements. In addition, a value for the lower bound of an integral over the impact parameter (the minimum impact parameter b_0) is required.[6] This is obtained by requiring the impact-parameter cross section to equal the cross section obtained from the Born approximation[10] at high energies. For the Born calculation we require the one-electron density matrix from the electronic structure calculation.

For HgBr we used the potential curves and dipole matrix elements from the ab initio calculations of Wadt.[11] These calculations employed relativistic pseudopotentials[12] within the configuration interaction (CI) method, and included spin-orbit effects through a semiempirical scheme. The basis set was of double-zeta plus polarization quality. To obtain the one-electron density matrices required by the Born approximation calculation (to fix b_0) we performed multiconfiguration self-consistent-field (MCSCF) calculations using Wadt's basis set and pseudopotential parameters. The one-electron integrals were obtained with the new integral package of Pitzer.[13] MCSCF calculations were performed for all four states at the experimental equilibrium geometry of the X state using various configuration spaces having from one to 264 terms. We had difficulty obtaining a single set of orbitals that described the ground and excited states equally well, so we chose the set that best reproduced the transition dipole matrix elements of Wadt[11] for these transitions. This set was used to determine the density matrices for the Born calculation. The computed minimum impact parameters for the X-to-A, X-to-B, and X-to-C transitions were 0.64 a_0, 2.1 a_0, and 1.9 a_0, respectively.

The potential energy curves used in the calculations are shown in Fig. 1. They are represented by spline interpolation of Wadt's data between 2.1

Electron impact dissociation of HgBr is investigated using a modified impact-parameter method. Cross sections are calculated for dissociation through the $B(^2\Sigma^+)$, $A(^2\Pi^+)$ and $C(^2\Sigma^+)$ states. The X-A transition is found to dominate the dissociation process. There is only a small enhancement of the cross section due to molecular vibrational energy, and no rotational enhancement. Cross sections are also presented for nondissociative excitation.

The mercury bromide (B-->X) electronic dissociation laser has recently received considerable attention because of its high efficiency, scalability, and blue/green wavelength (502 nm).[1] The B state of HgBr can be obtained from $HgBr_2$ by photodissociation,[2] by discharge techniques,[3] or by electron beam pumping.[4] A recent review of the properties of e-beam controlled HgBr discharges is provided by Nighan, along with extensive references.[5] In this report we are concerned with electron impact excitation and dissociation processes for the X to $B(^2\Sigma^+)$, $A(^2\Pi^+)$ and $C(^2\Sigma^+)$ states of HgBr because of their possible importance to closed-flow, repetitive-pulse HgBr laser kinetics.

We have applied a modified impact-parameter method[6,7] that is well suited for the calculation of post-threshold electron impact cross sections in diatomic molecules. The method has previously been applied to the study of electronic excitation and dissociation processes in O_2 and S_2,[8] and in HCl.[9] In this method, the cross section is expressed as the product of an electronic structure factor and a dynamical factor. The former is obtained from an ab initio electronic structure calculation and the latter, representing the dynamics of the scattered electron, is expressable in terms of simple functions.[6] The

APPENDIX F

Electronic Excitation and Dissociation of HgBr by Electron Impact

by

Michael J. Redmon, Bruce C. Garrett, and Lynn T. Redmon

Chemical Dynamics Corporation
1550 West Henderson Road
Columbus, Ohio 43220

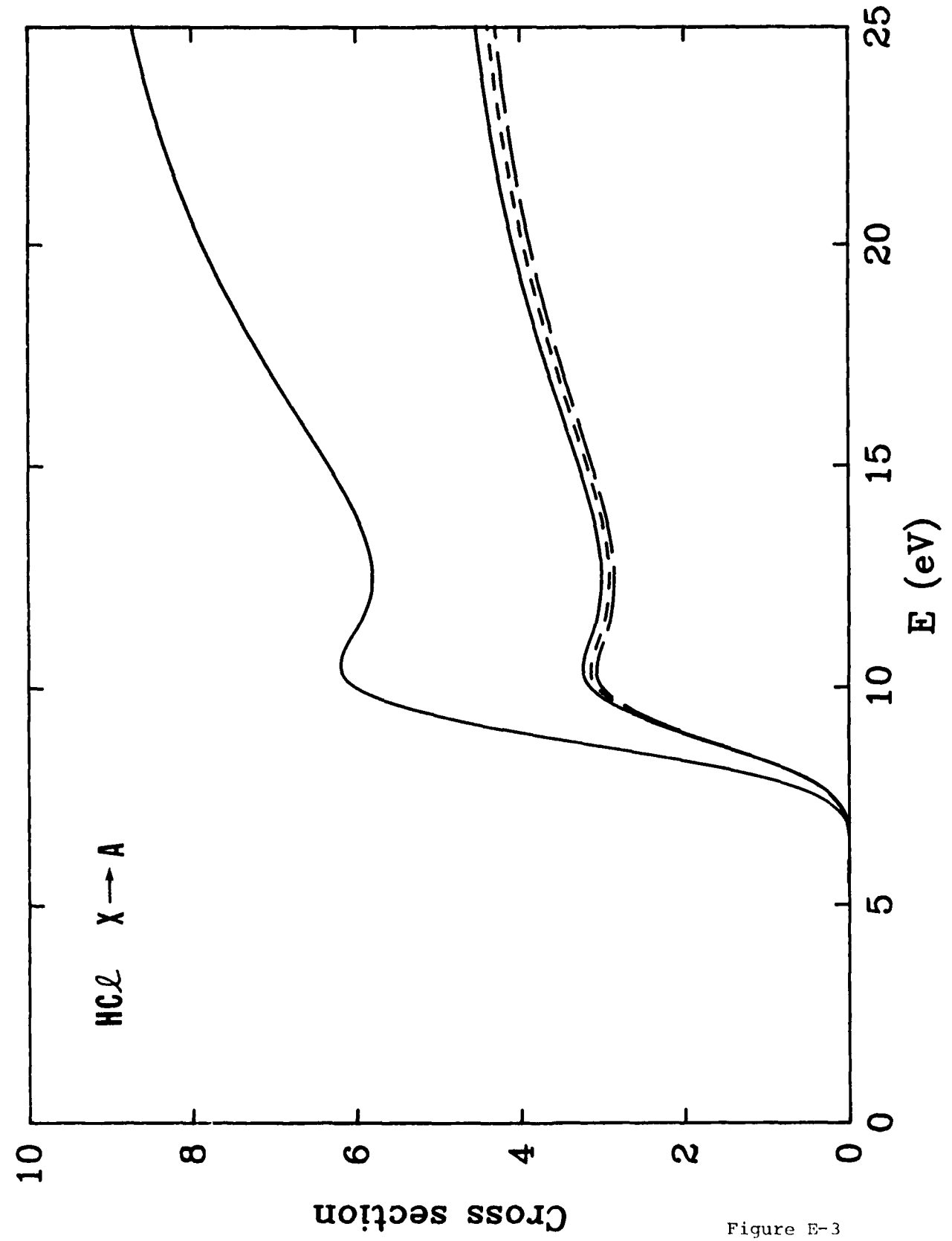

Figure E-3

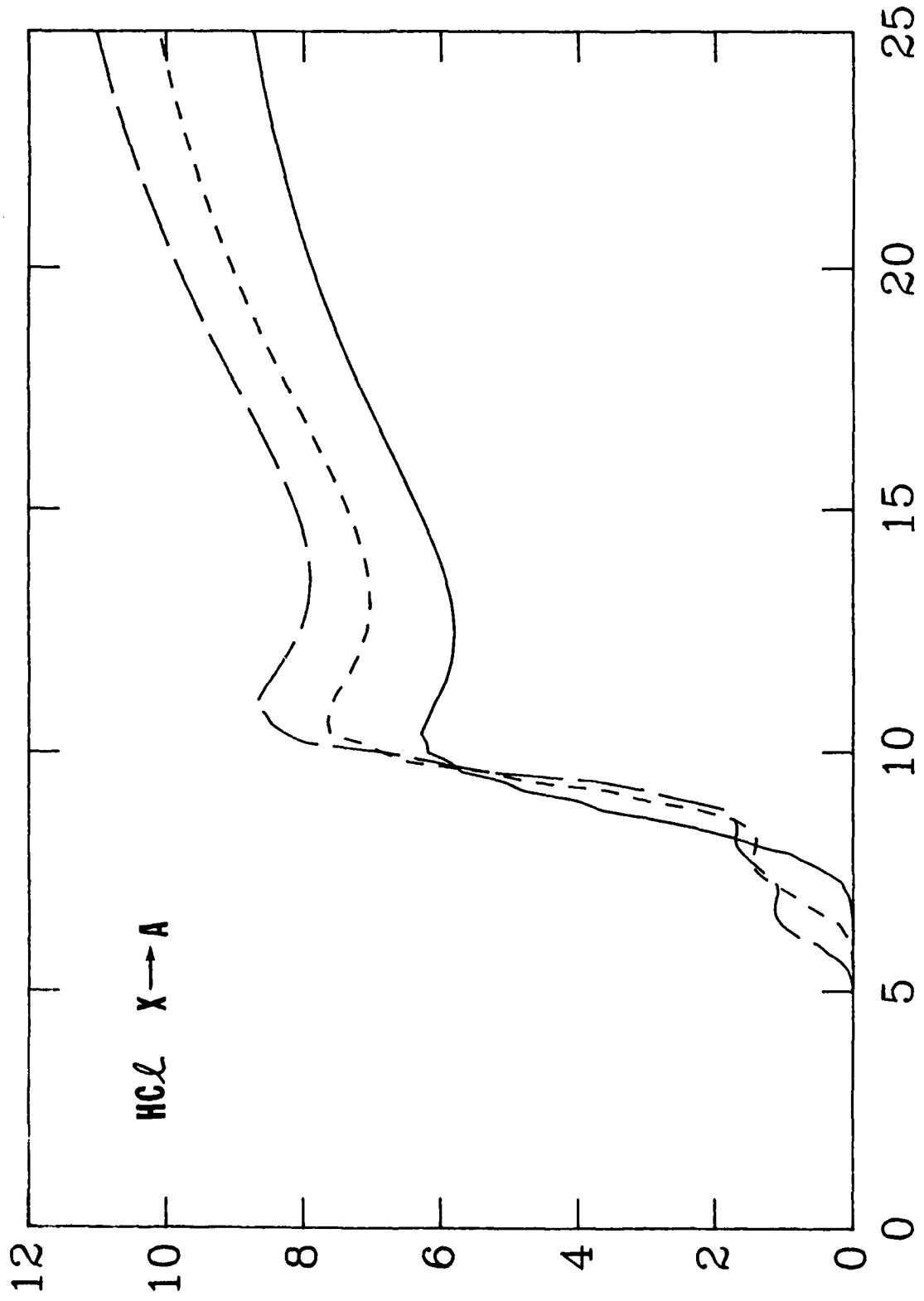

Figure E-2

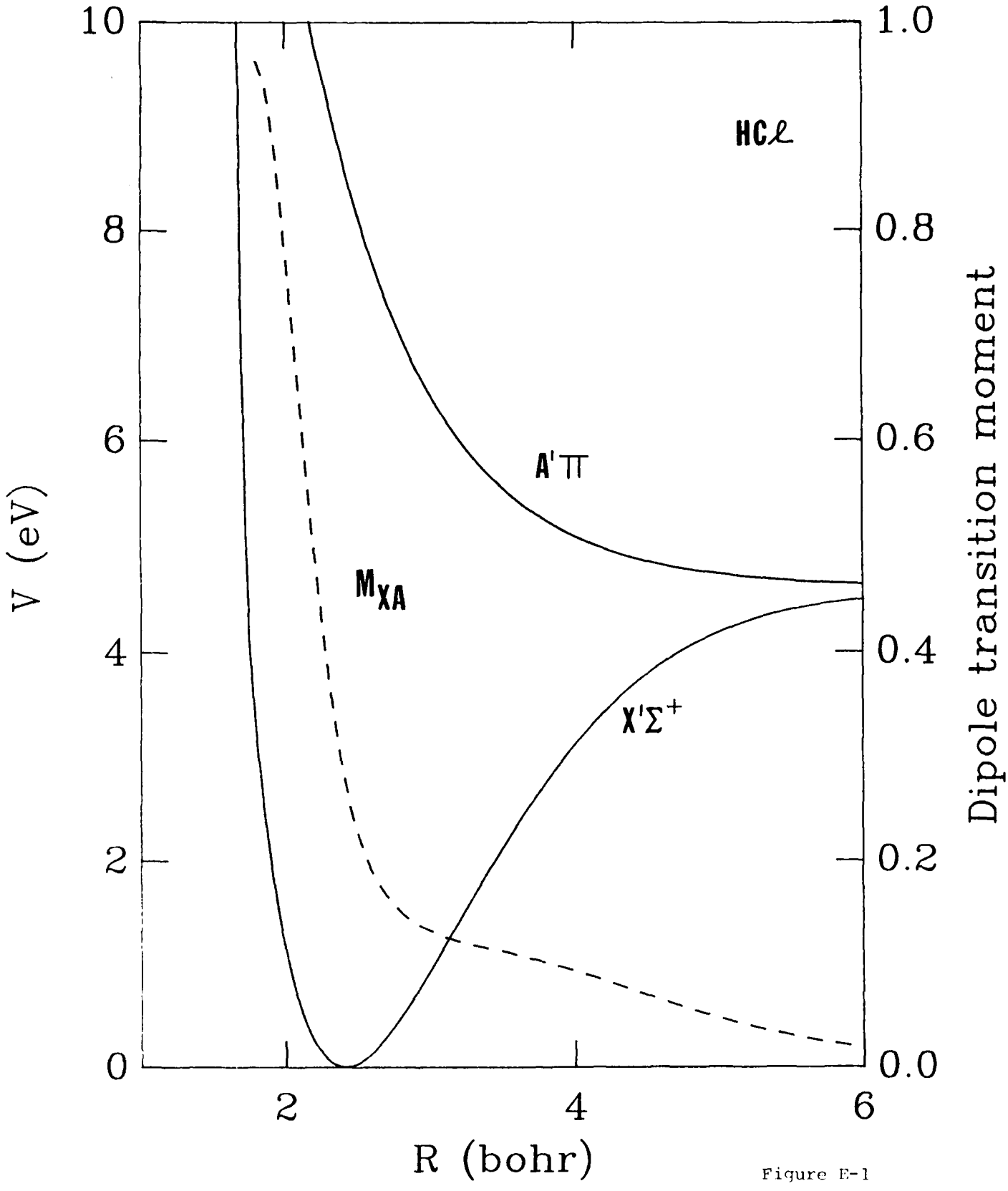
10
8
6
4
2
0
V (eV)
1.0
0.8
0.6
0.4
0.2
0.0
Dipole transition moment
HCℓ
A'Π
M_{XA}
X'Σ+
2
4
6
R (bohr)

Figure E-1

Figure Captions

1. Potential energy curves (solid lines) for the X and A states of HCℓ and the dipole transition moment (dashed line, in atomic units) for the X to A transition.
2. Cross sections multiplied by a factor of 10^{18} in units of cm^2 versus electron translational energy for electron-impact dissociation of HCℓ through the A state. The solid, short-dashed, and long-dashed curves are for initial vibrational states v_i = 0, 1, and 2, respectively.
3. Cross sections multiplied by a factor of 10^{18} in units of cm^2 versus electron translational energy for electron-impact dissociation of HCℓ through the A state. The highest solid curve is for a rotational temperature of 0 K, the next solid curves, short-dashed and long dashed curves are for 300, 600, and 1000 K respectively. All cross sections are for v_i=0.

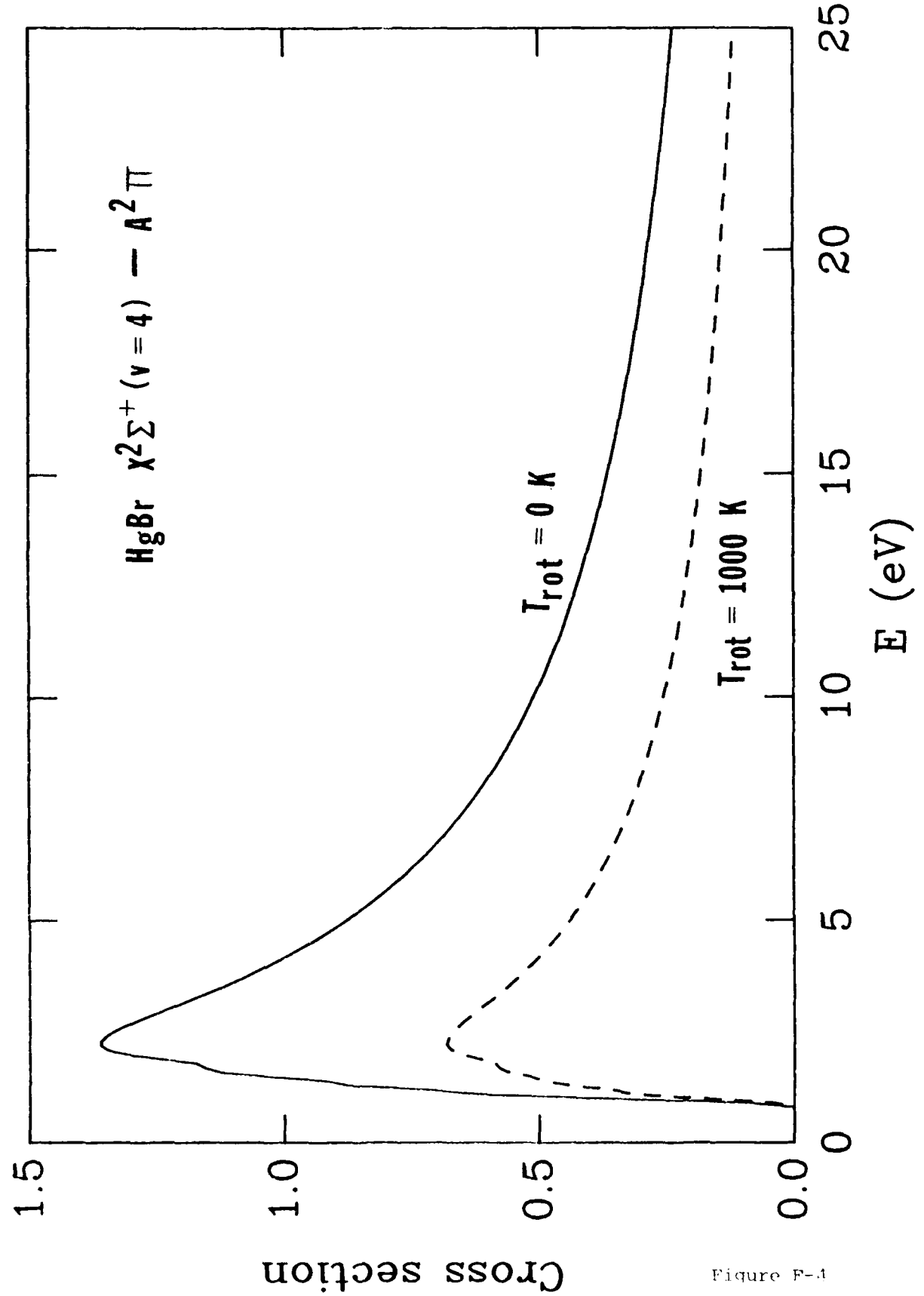
HgBr $X^2\Sigma^+ (v=4) - A^2\Pi$
T_{rot} = 0 K
T_{rot} = 1000 K
Cross section
E (eV)
0.0
0.5
1.0
1.5
0
5
10
15
20
25

Figure F-4

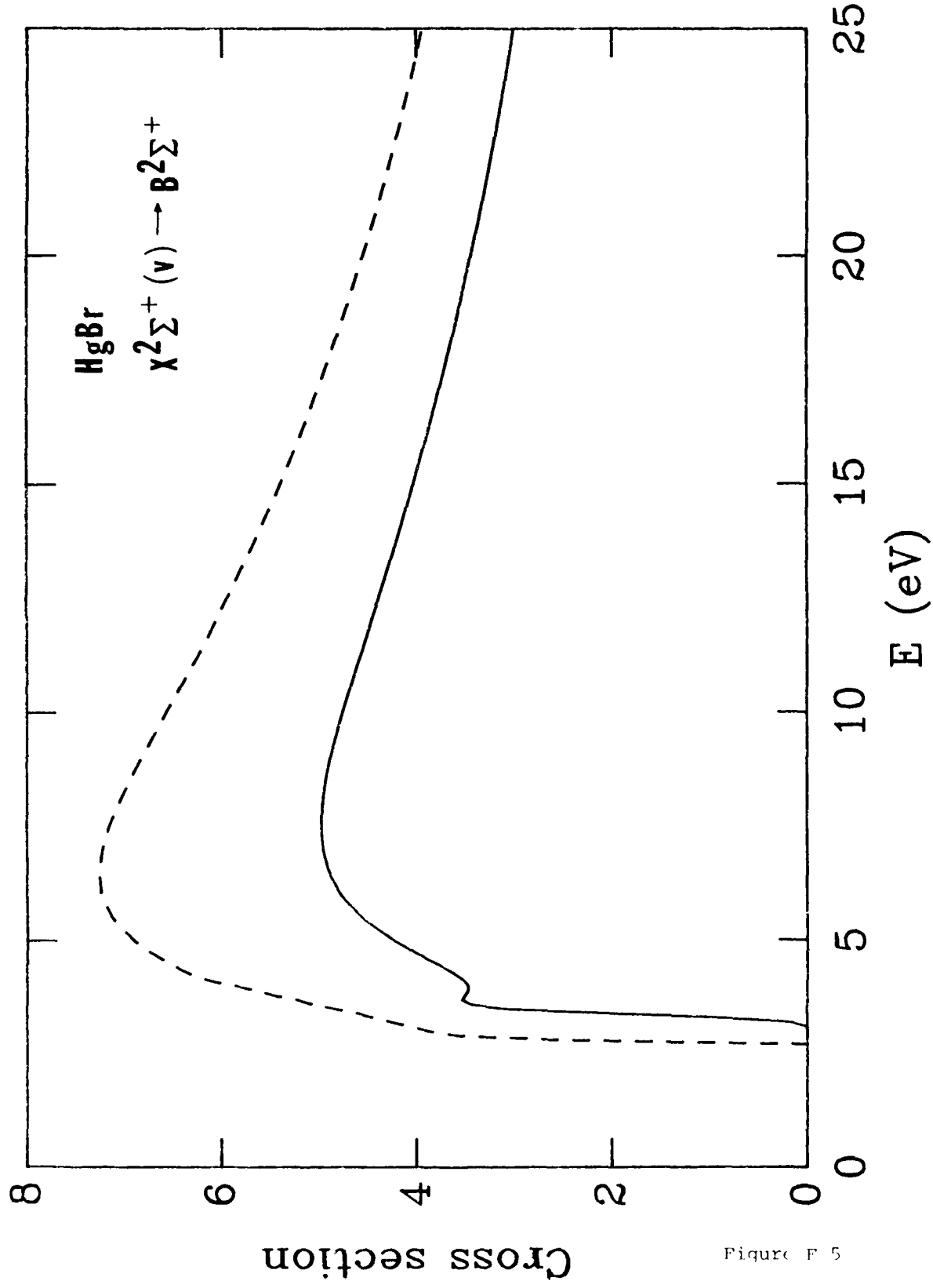
HgBr
$X^2\Sigma^+ (v) \rightarrow B^2\Sigma^+$
Cross section
0
2
4
6
8
0
5
10
15
20
25
E (eV)

Figure F 5

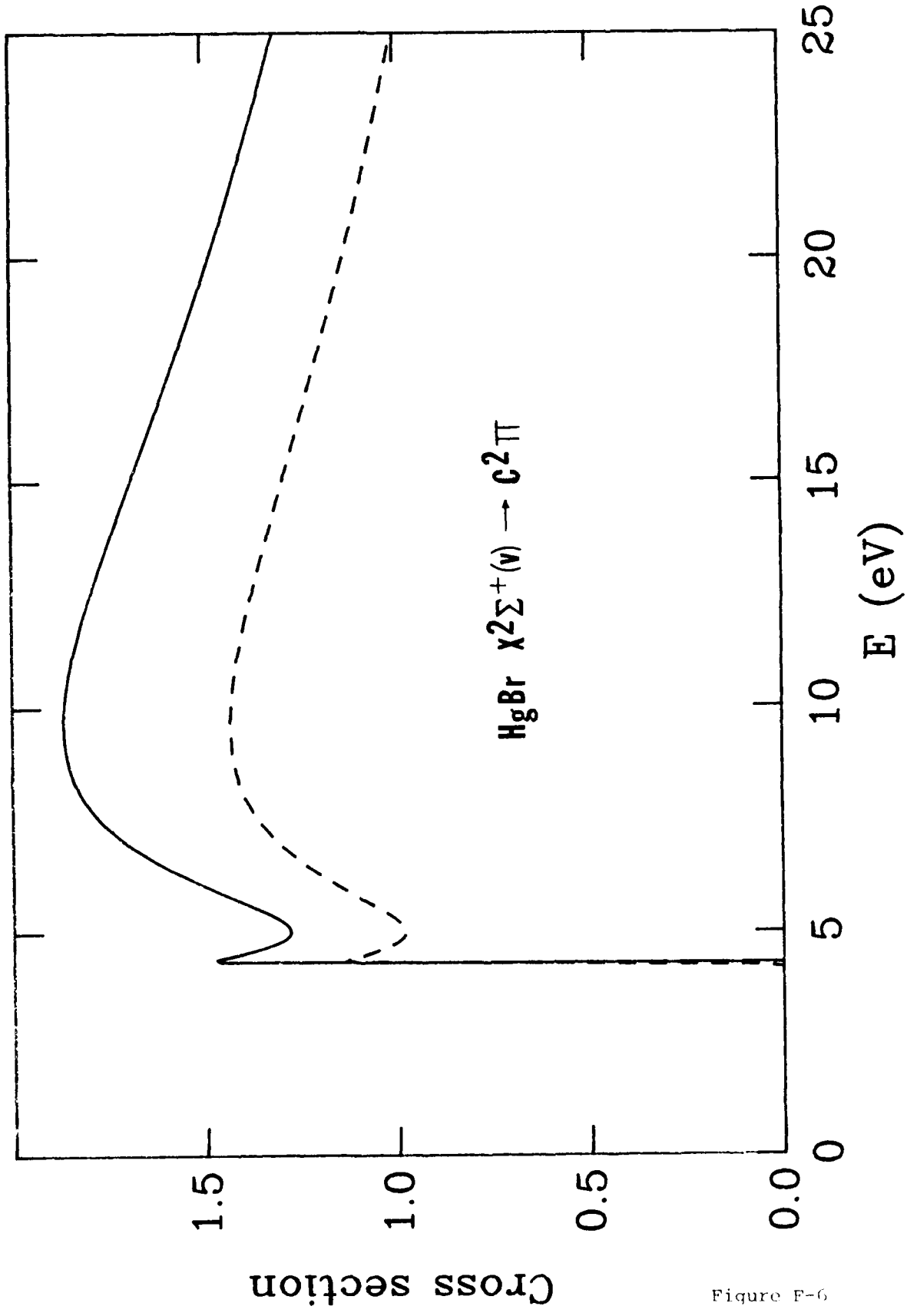
Cross section
1.5
1.0
0.5
0.0
0
5
10
15
20
25
E (eV)
HgBr $X^2\Sigma^+(v) \rightarrow C^2\Pi$

Figure F-6

APPENDIX G

Program Flowcharts

Impact Parameter Method

Program IP

Description: Compute cross sections for electronic excitation of diatomic molecules by electron impact using the impact parameter method of Hazi. Vibrations and rotations are treated as being degenerate and the fixed-nuclei approximation and Franck-Condon approximations are used. Cross sections correspond to those summed over final rovibrational states.

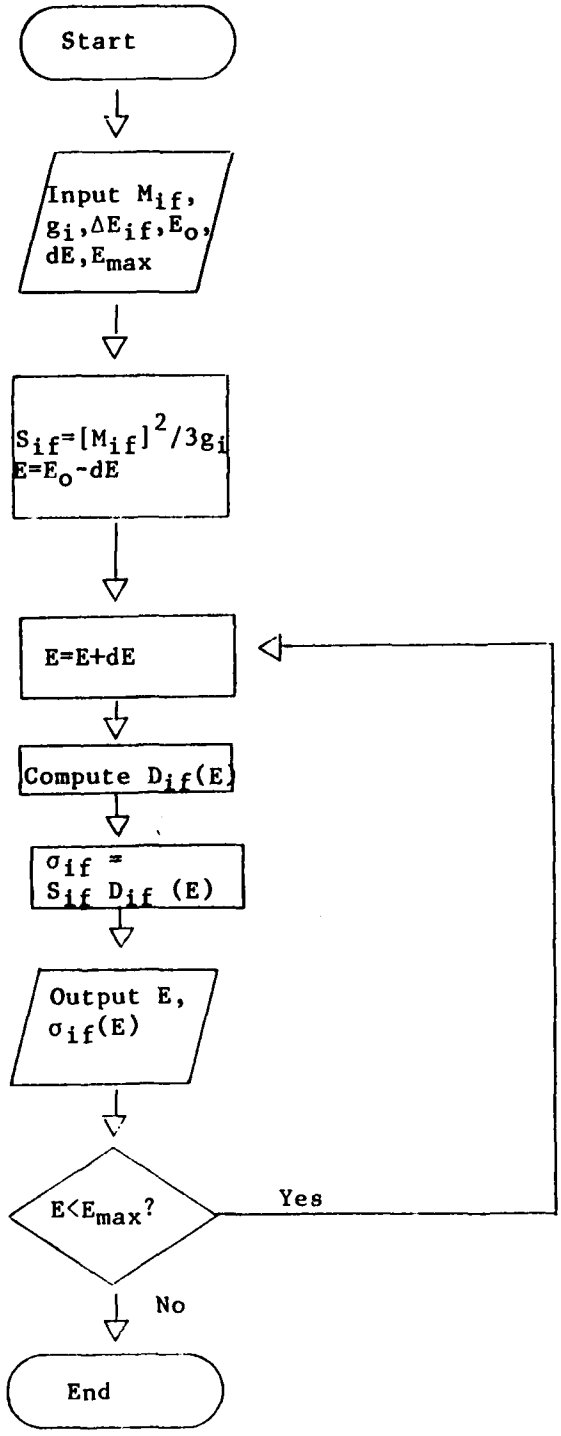

Program IPV

Description: Compute cross sections for electronic excitation of diatomic molecules to bound vibrational states by electron impact using the impact parameter method. Vibrations are treated explicitly within the fixed-nuclei approximation and rotations are treated as being degenerate. Cross sections are summed over final vibrational states, dissociative states are excluded.

Flowchart:

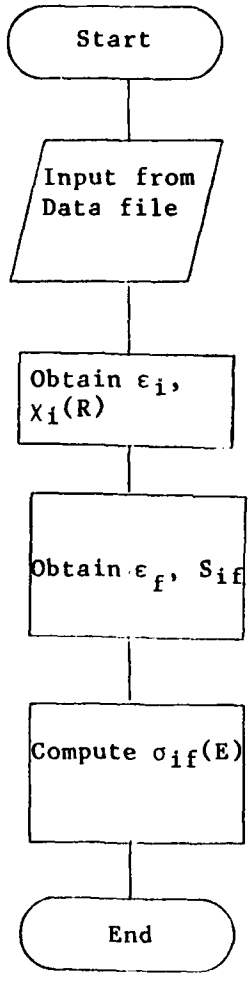

Program IPV (INPUT from data file)

Flowchart:

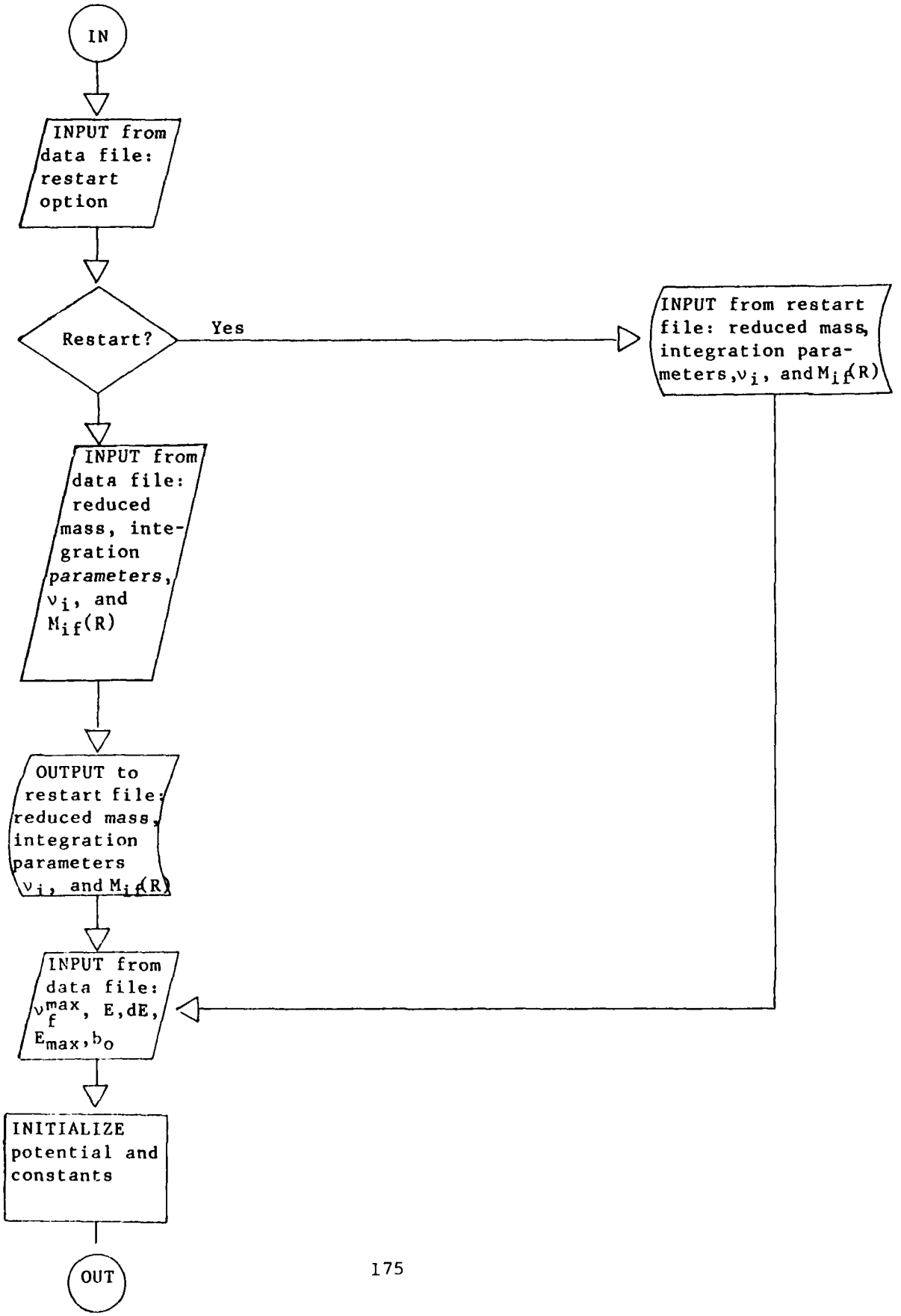

Program IPV (Obtain ε_i, $\chi_i(R)$)

Flowchart:

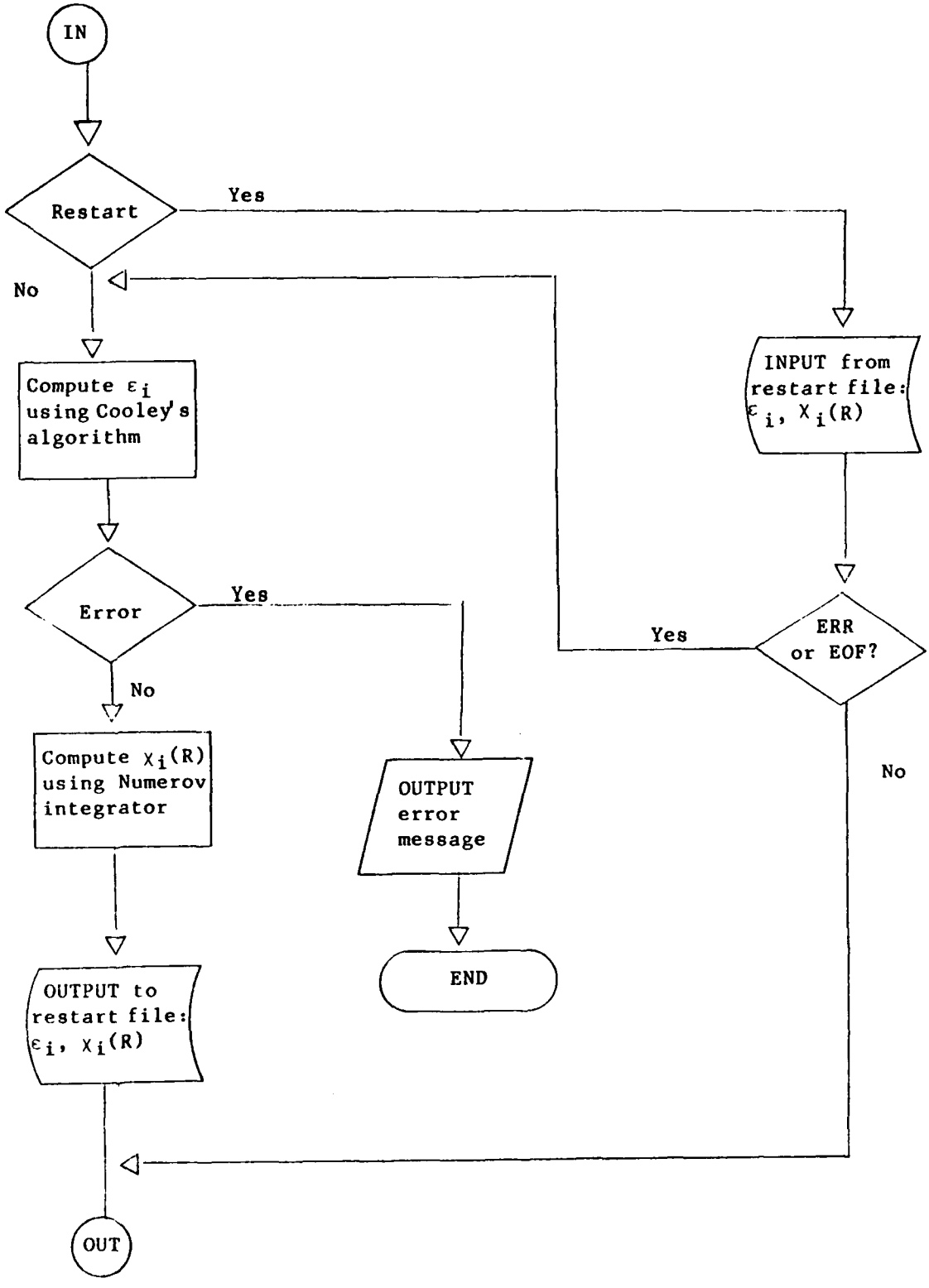

Program IPV (Obtain ε_f, S_{if})

Flowchart:

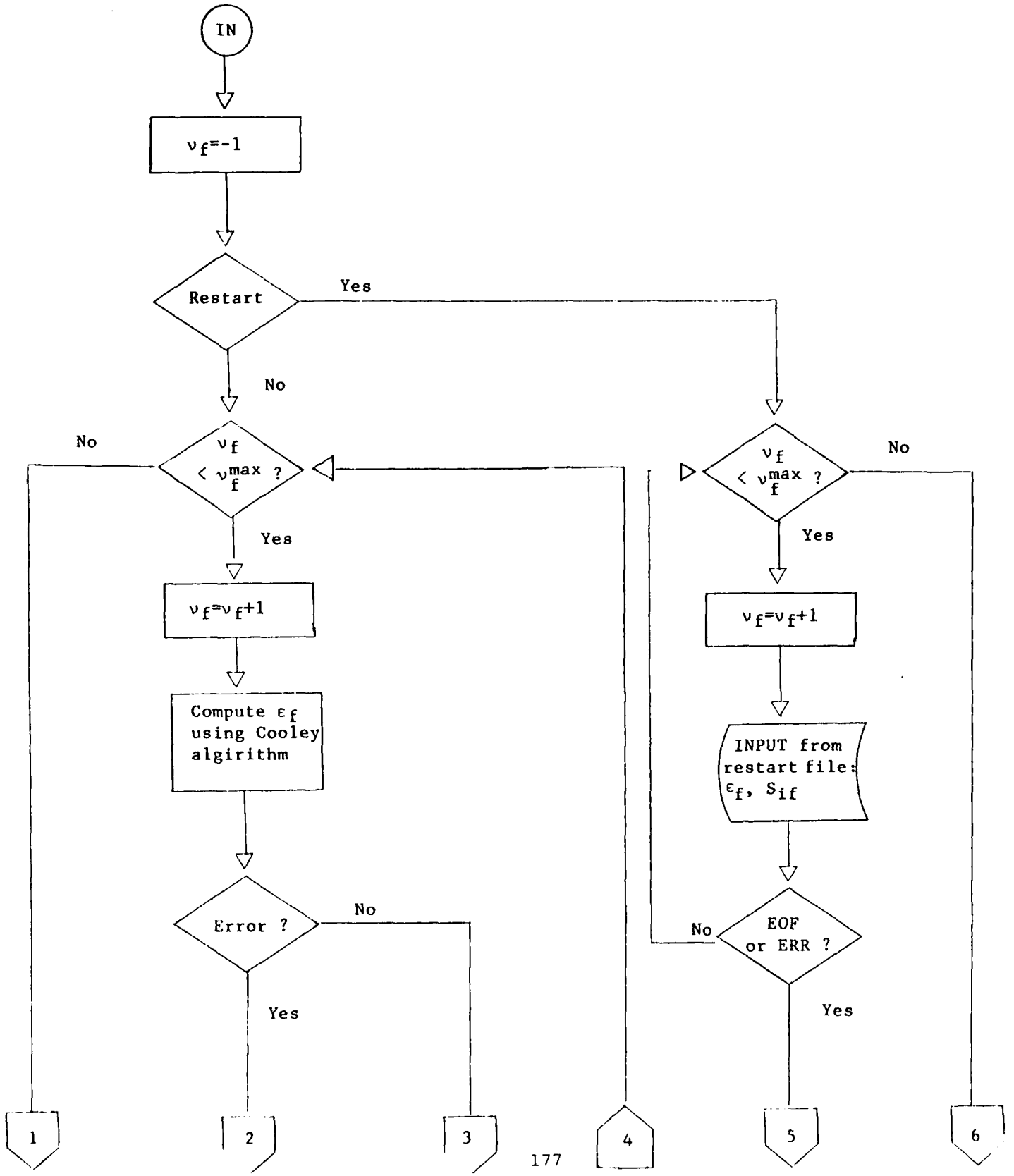

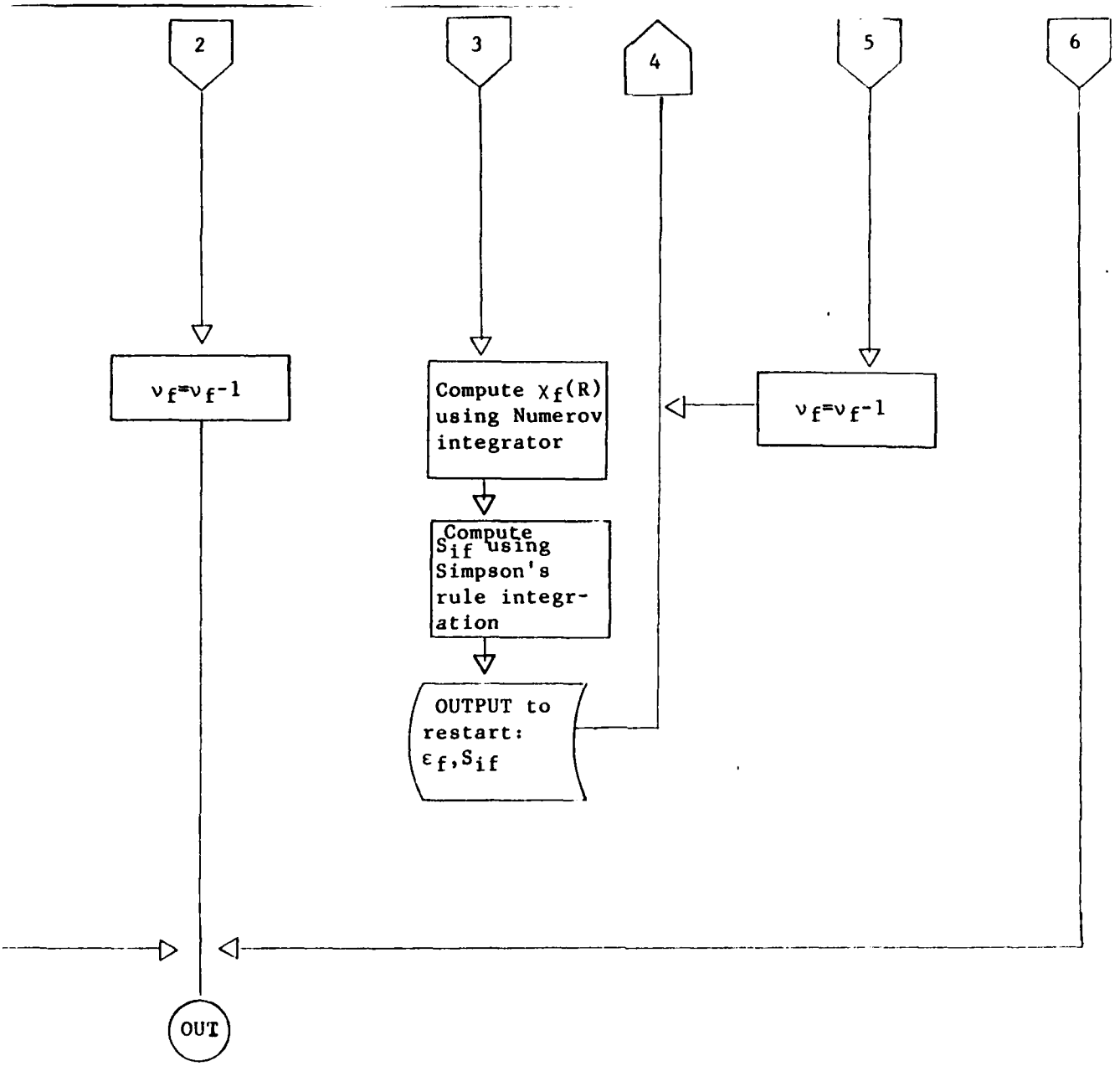
2
3
4
5
6
$\nu_f=\nu_f-1$
Compute $\chi_f(R)$ using Numerov integrator
Compute S_{if} using Simpson's rule integration
OUTPUT to restart: ε_f, S_{if}
$\nu_f=\nu_f-1$
OUT

Program IPV (Compute $\sigma_{if}(E)$)

Flowchart:

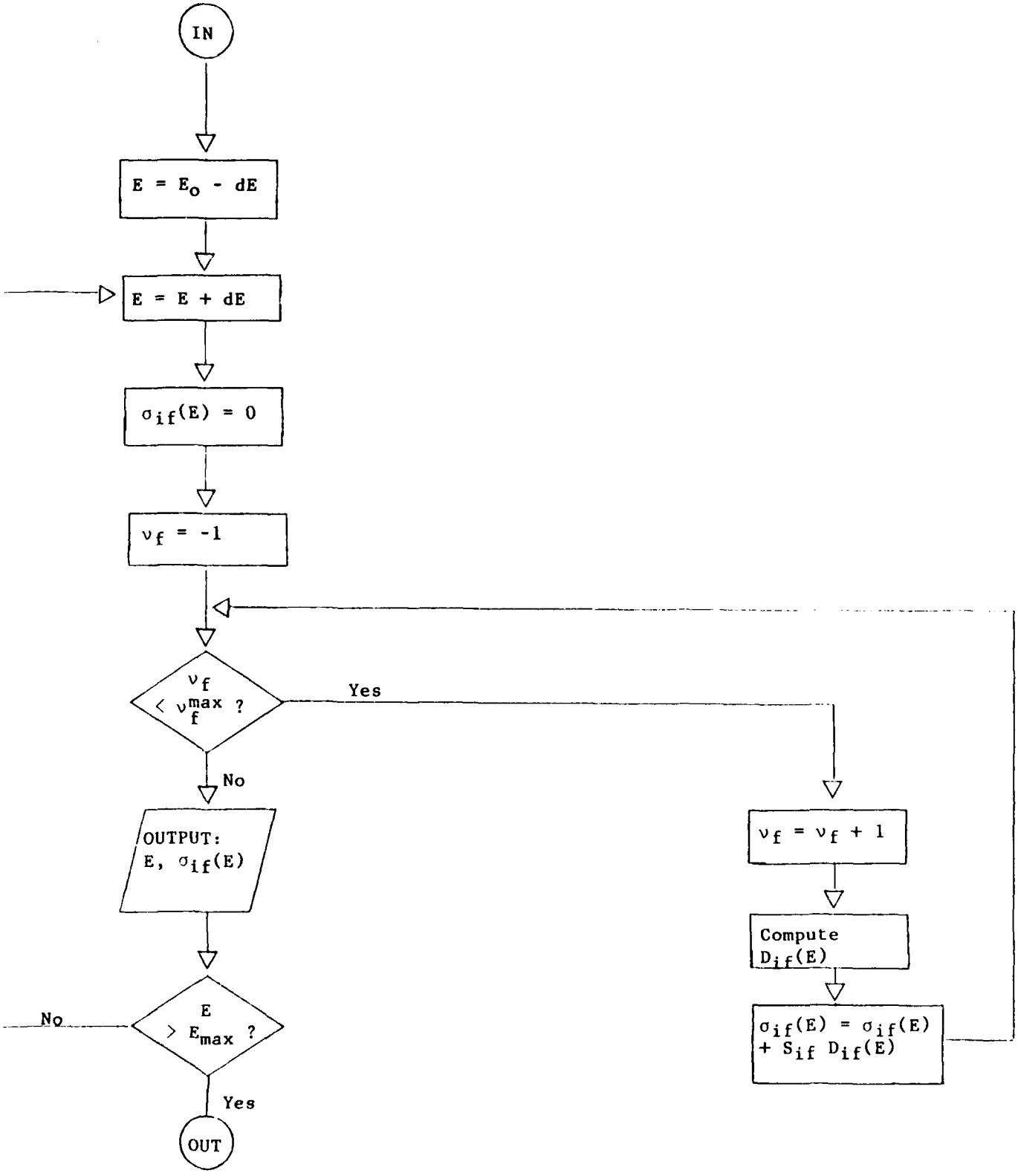

:am IPVR

:iption: Compute cross sections for electronic excitation of diatomic :ules to bound vibrational states by electron impact using the impact neter method of Hazi. Vibrations and rotations are treated explicitly in the fixed-nuclei approximation. Cross sections are summed over final ɔrational states, dissociative states are excluded.

:hart:

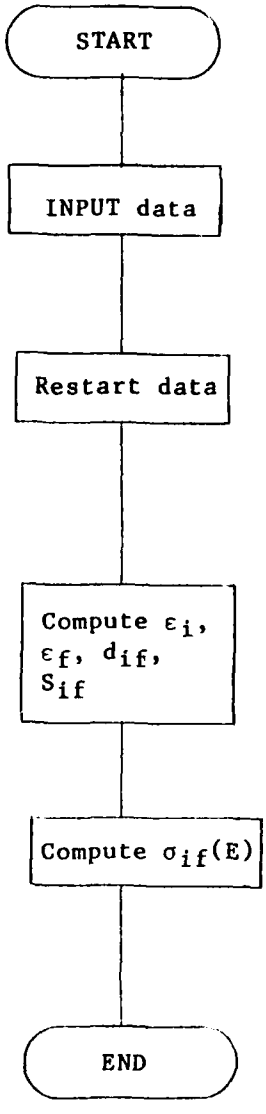

Program IPVR (INPUT data)

Flowchart:

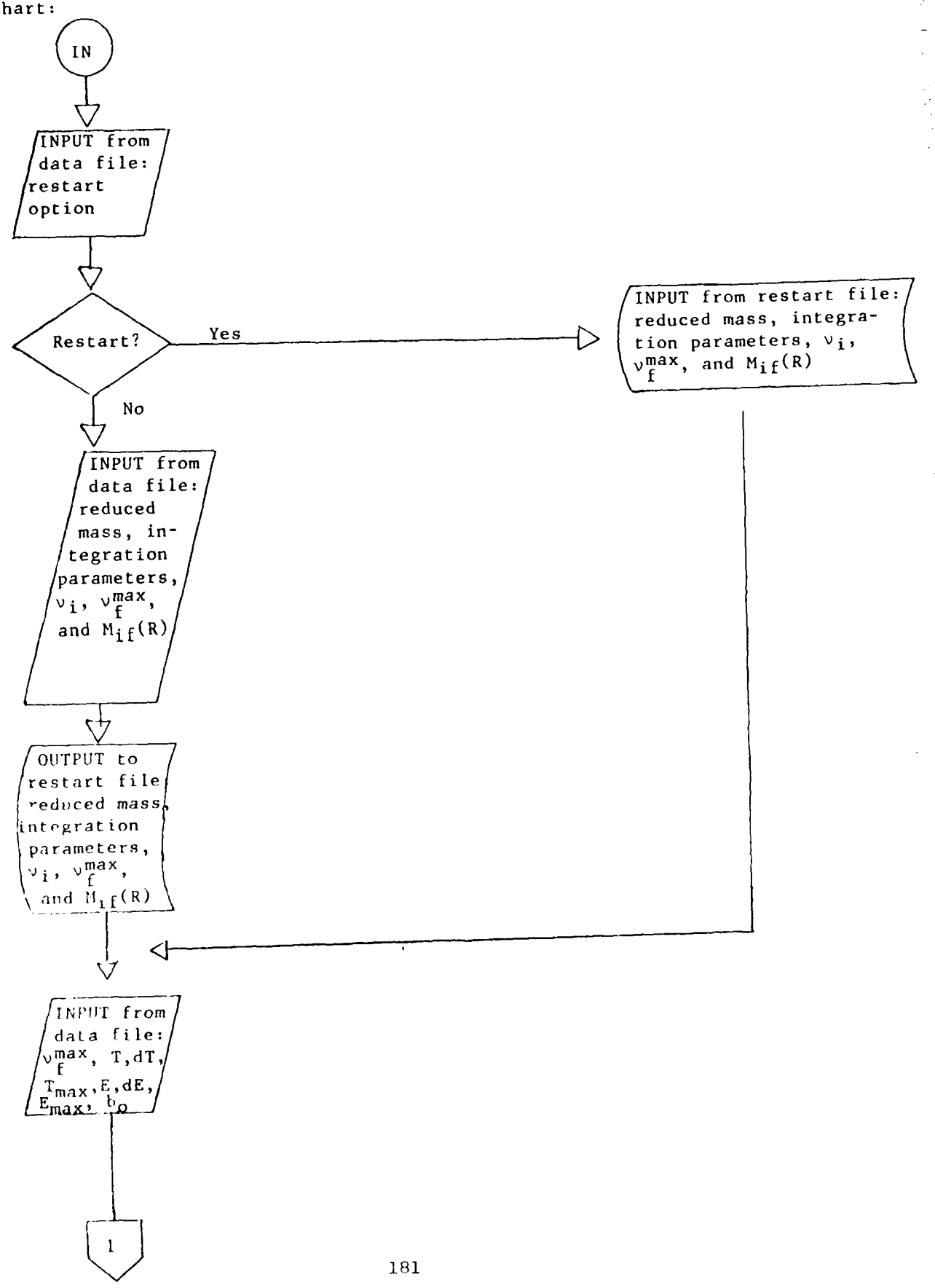

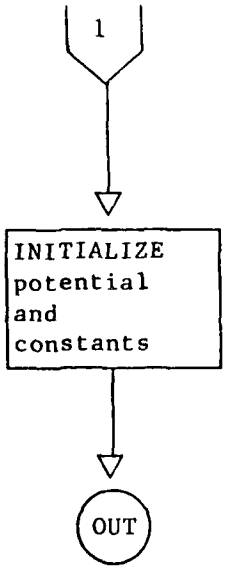
1
INITIALIZE
potential
and
constants
OUT

AD-A154 827 VIBRATIONALLY ENHANCED DISSOCIATION OF DIATOMIC MOLECULES(U) CHEMICAL DYNAMICS CORP COLUMBUS OH B C GARRETT ET AL. MAY 85 CDTR-85-1 AFWAL-TR-85-2020 3/3

UNCLASSIFIED F33615-82-C-2241 F/G 7/4 NL

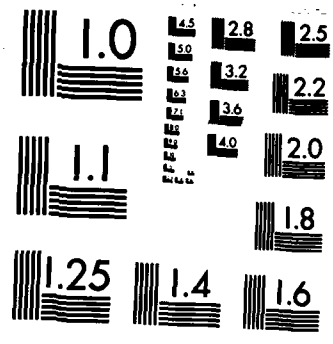

Program IPVR (Restart)

Flowchart:

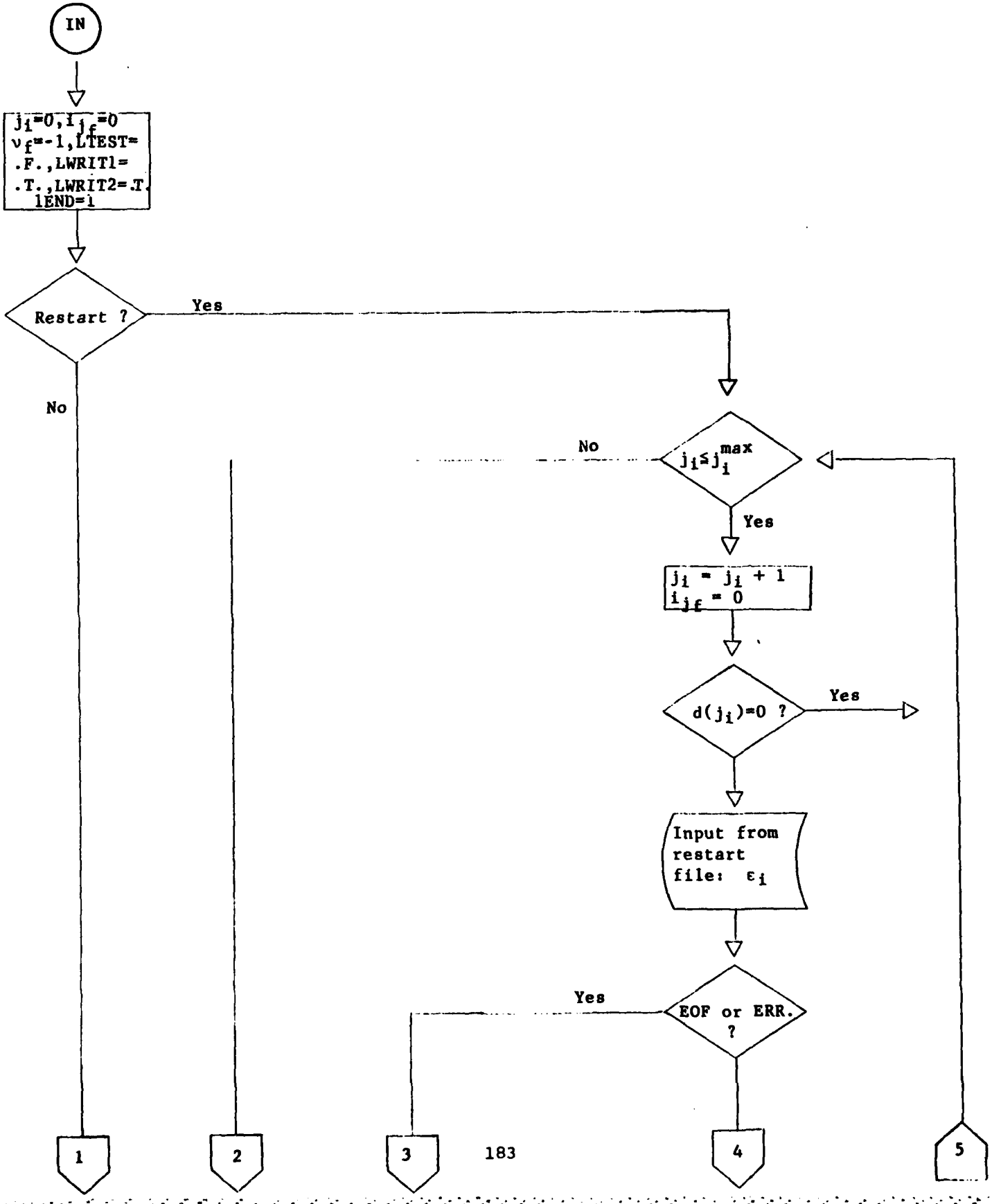

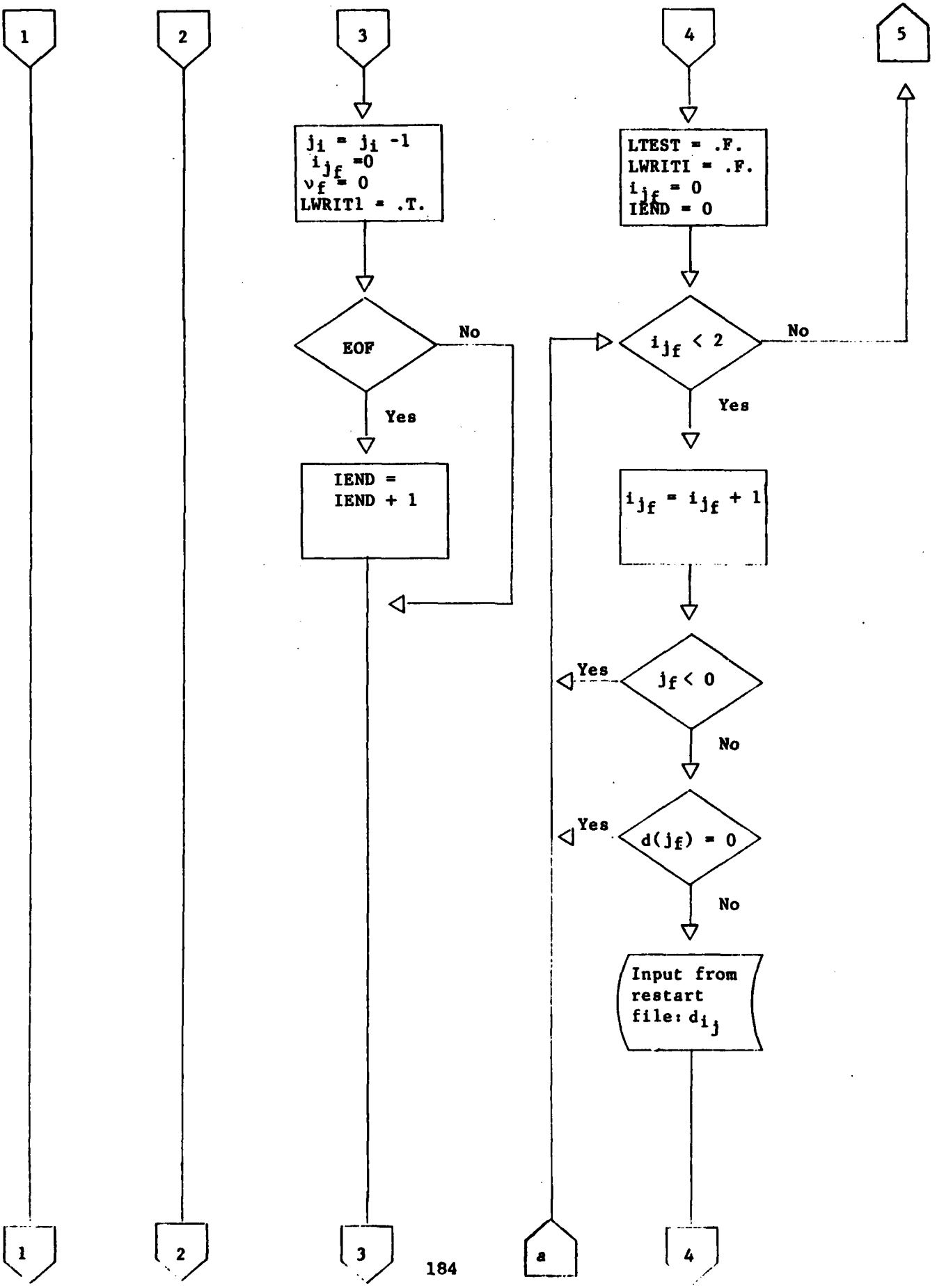
1
2
3
4
5
$j_i = j_i - 1$
$i_{j_f} = 0$
$\nu_f = 0$
LWRIT1 = .T.
EOF
No
Yes
IEND = IEND + 1
LTEST = .F.
LWRITI = .F.
$i_{j_f} = 0$
IEND = 0
$i_{j_f} < 2$
No
Yes
$i_{j_f} = i_{j_f} + 1$
$j_f < 0$
Yes
No
$d(j_f) = 0$
Yes
No
Input from restart file: d_{i_j}
a
1
2
3
4

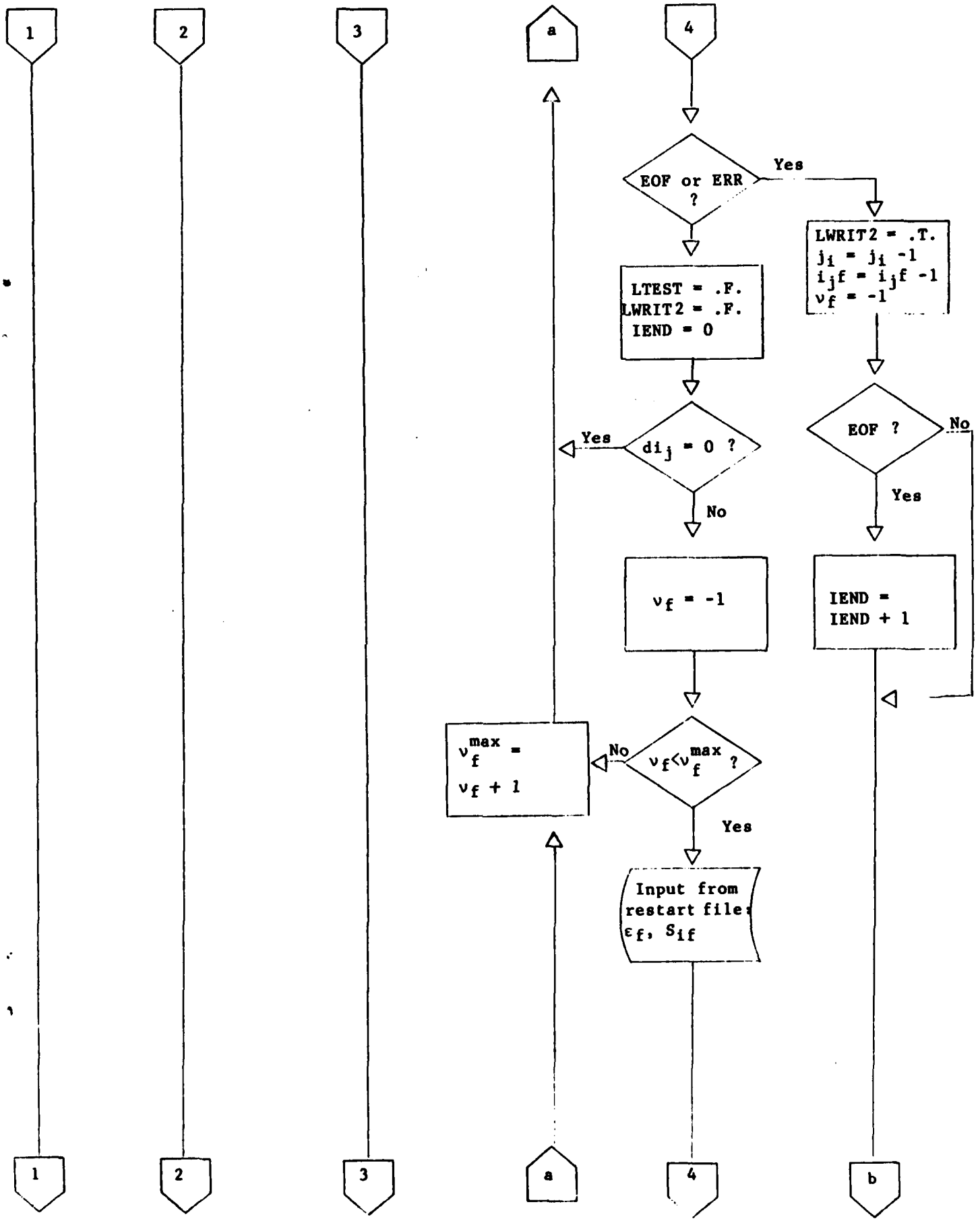
1
2
3
a
4
EOF or ERR ?
Yes
LWRIT2 = .T.
$j_i = j_i - 1$
$i_{jf} = i_{jf} - 1$
$\nu_f = -1$
LTEST = .F.
LWRIT2 = .F.
IEND = 0
EOF ?
No
Yes
$di_j = 0$?
Yes
No
$\nu_f = -1$
IEND = IEND + 1
$\nu_f^{max} = \nu_f + 1$
No
$\nu_f < \nu_f^{max}$?
Yes
Input from restart file: ε_f, S_{if}
1
2
3
a
4
b

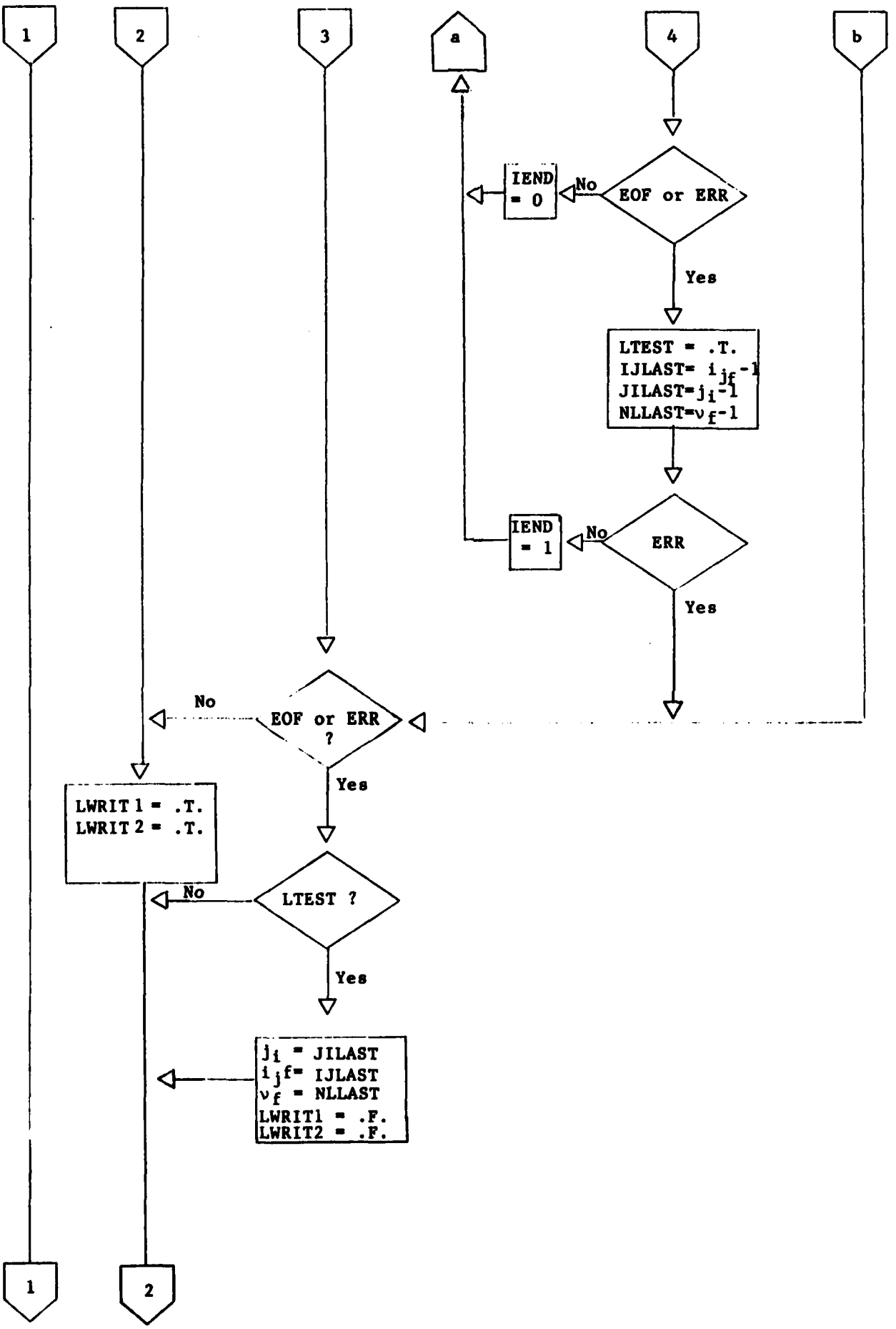
1
2
3
a
4
b
IEND = 0
No
EOF or ERR
Yes
LTEST = .T.
IJLAST= i_{jf}-1
JILAST=j_i-1
NLLAST=ν_f-1
IEND = 1
No
ERR
Yes
No
EOF or ERR ?
Yes
LWRIT 1 = .T.
LWRIT 2 = .T.
No
LTEST ?
Yes
j_i = JILAST
i_{jf}= IJLAST
ν_f = NLLAST
LWRIT1 = .F.
LWRIT2 = .F.
1
2

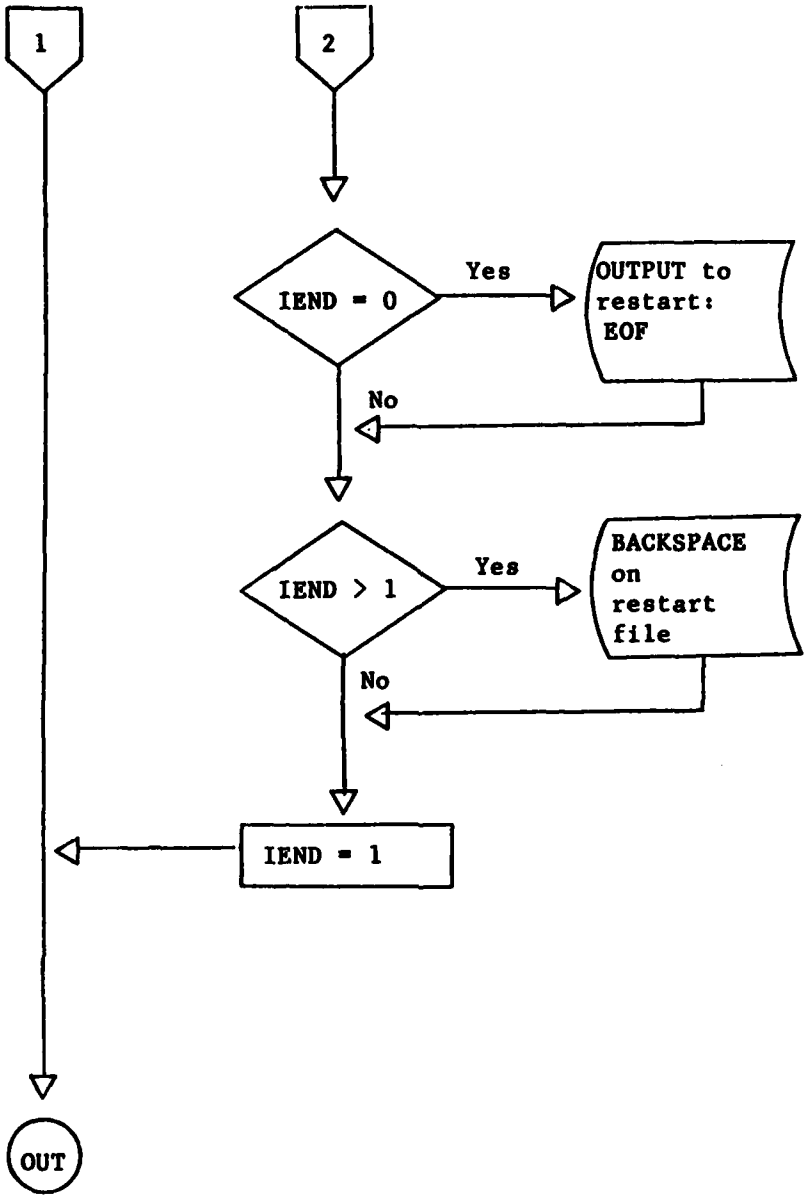

*U.S.Government Printing Office: 1985 — 559-065/20777

END

FILMED

7-85

DTIC